SEASONAL HYDROLOGIC DYNAMICS UNDER CHANGING CLIMATE, LAND USE-LAND COVER AND HUMAN INFLUENCE

BY

NAMRATA BATRA

DISSERTATION

Submitted in partial fulfillment of the requirements
for the degree of Doctor of Philosophy in Civil Engineering
in the Graduate College of the
University of Illinois at Urbana-Champaign, 2010

Urbana, Illinois

Doctoral Committee:

Professor Praveen Kumar, Chair
Professor Albert J. Valocchi
Professor Murugesu Sivapalan
Professor Ximing Cai
Professor Upmanu Lall

Abstract

Climatic changes along with the land use-land cover changes (LULCC) and human impacts significantly modify the hydrologic flow regime of the river basins, affecting water resources and environment from regional to global scale. Aided by satellite data, modeling and understanding of the interactions between physical and human systems, more reliable regional LULCC and climate change projections are now available. However, resulting quantitative projection of changes on the hydrologic components at the seasonal time scale are sparse. This study attempts to quantify the hydrologic response in different hydro-climatic regions of the world at the seasonal time scale in the context of the projected LULCC and climate change assessed through Intergovernmental Panel on Climate Change (IPCC) A1B emission scenario. The Common Land Model (CLM) is used as the hydrologic model for the study since it incorporates detailed physical process representation, uses physical parameterization without the need for calibration and can be run at relatively high spatial and temporal resolutions. A coupled modeling framework is applied to assess human water use impact on hydrologic discharge at the river basin scale by coupling of CLM to the Water Availability and Supply Model (WASM).

A consistent global GIS based dataset is constructed for the Surface Boundary Conditions (SBCs) and meteorological forcing of the model. European Center for Medium Range Weather Forecasts (ECMWF) reanalysis data at 6-hour time step for the period 1976 through 2000 is used for meteorological forcing. The model results are validated using the observed discharge data from Global Runoff Distribution Center (GRDC). The ability of the hydro-

logic model to capture the dominant runoff processes at multiple time scales of interaction of the processes is explored using wavelet analysis. Future climate change projections are derived from the Fourth Assessment Report of IPCC based on the multi-model ensembles of projections. An Integrated Model to Assess the Global Environment (IMAGE), developed by the Netherlands Environmental Assessment Agency is used for LULCC data.

The study is performed over nine river basins selected from Asia, Africa and North America to represent the broad climatic, landscape and human controls on the seasonal hydrological dynamics, and to assess how these controls differ for basins lying in different hydro-climatic regions. It is observed for all the study basins that small changes in the precipitation lead to much larger changes in the runoff response. The analysis reveals that certain regions (Orange and Volta basins in Africa) have seasons which are highly likely to experience significant reduction in future runoff while there are other regions (Ganges, Krishna and Huai basins in Asia) which have seasons very likely to experience increased runoff. These seasonal differences reflect the changes in water availability, which may not be known through annual estimates. Moreover, different aspects of human interferences are observed over each of the study basins. Comparison and quantification of such differences in the hydrologic components are of particular importance for the water resource managers and policy makers.

To my family and friends.

Acknowledgments

Attaining the three magic letters of "Ph.D." always felt like a dream to me, and I kept going with the saying that "All things are possible with faith". I owe my deepest gratitude to my advisor Prof. Praveen Kumar, for his faith in me and for all of his guidance, encouragement, and advice throughout my Ph.D. program. I would like to express my earnest appreciation to the members of my thesis committee: Prof. Valocchi, Prof. Sivapalan, Prof. Cai, and Prof. Lall, for their guidance, encouragement and insightful comments.

I would like to acknowledge International Water Management Institute (IWMI), NOAA (Grant COM NA06OAR4310053), NSF (Grant ATM 06-28687) and NASA Graduate Student Fellowship Program for supporting this research. Computational support was provided by National Center for Supercomputing Application (NCSA), Illinois. My sincere thanks to Weddy Jackson from NCSA for his technical assistance. I would like to thank my colleague Ethan Yang for his valuable contribution in processing of data used in the study and for his analysis on the role of human influence on hydrologic dynamics. One of the chapters in the thesis is included as a joint work with him. Many thanks to the Netherlands Environmental Assessment Agency and Aminul Islam from IWMI, for assisting with the synthesis of the projected land use-land cover maps used in the study. I would like to express my sincere thanks to my senior lab mates Choi, Francina, Amenu, Paik, Srinivas, Ricky and Ben, for their words of encouragement and helpful guidance at all times. I would also like to thank Darren, Venkat, Juan, Ciaran and Satish for being wonderful lab mates. I can think of so many other friendly faces, walking across the corridor of Hydro-Lab to be thankful to, as

my one day of absence from the lab would be their big concern. Thanks for being there at any time of the day or night.

I would like to express my sincere gratitude to my family for having their deepest faith in me. My father's heartfelt words of encouragement and his confidence in me led me to this direction and kept me motivated. I am very grateful for my mom, of her sacrifices, efforts and that extra push which made this thesis possible. My heartiest thanks to my sister Shalini, without her support, I would never have continued with my endeavor. It gives me a great sense of satisfaction to have been able to live up to their expectations. Many thanks to my roommate Sruthi and Debashree with whom I shared all my struggles and happy times. And, many thanks to all my other wonderful friends who made my graduate life in UIUC such a memorable experience.

Table of Contents

List of Tables

List of Figures

Chapter 1

Introduction

1.1 Research Objectives

Water is indispensable for all forms of life but both climatic and non-climatic factors pose a threat to future water availability. Water is one of the resources that will be most severely affected by climate change and land use land cover change (LULCC) in the 21st century [6, 7, 8, 9]. Water management and design practices face new challenges under climate change conditions, which require a better quantitative understanding of the potential changes, especially changes in the seasonal patterns of water availability in order to meet present and emerging water demands. Several studies [10, 11, 12] have shown that small perturbations in precipitation will have a significant impact on the river basin hydrology and hence on water availability.

In addition to climatic variables, LULCC bring alterations to the hydrologic response by altering moisture and energy fluxes. There are important connections between the land surface characteristics and the hydrologic cycle. LULCC results in changes in the vegetation cover, rooting depth, surface roughness and albedo characteristics of the surface. These changes tend to affect the hydrologic processes in terms of degree of infiltration, runoff, evapotranspiration (ET) and precipitation patterns. Moreover, there are different aspects of direct human interferences, such as reservoir operation [13] groundwater pumping [14], water withdrawals and return flows [15], which alter the natural hydrologic processes. Human interventions in the water cycle contribute to future changes in the seasonal hydrologic

dynamics [16]. In a number of river basins, the growing abstraction of water by individual users and state-initiated projects has approached or even exceeded the threshold of renewable water resources [17, 18]. Water shortages and conflicts have increased accordingly [17].

Under climate change conditions, developing countries face both persisting and new water resource challenges. Most of their hydraulic infrastructure use hydrologic design parameters based on assumptions about historical climatic and geographical conditions which have changed in the recent years. Given the limited resources and capacity to regulate flows in rivers and streams, these regions are very vulnerable to any shift in the climatic variability. For example, the hydrology of southern region in Africa is projected to be most affected by climate change since the accelerating hydrologic cycle will further decrease the scarce water resources of this region [19]. Several studies have shown that semi-arid and arid basins will be the most vulnerable basins with respect to water stress in the late 21st century ([19, 20, 21, 22]). In certain basins, rapid deforestation has reduced the amount of water lost by plants resulting in an increase in the overland flow and flash floods with heavy rainfall [23]. Probability of flooding will increase for many river basins in the Northern Hemisphere as the frequency of heavy rainfall events is likely to increase with the intensification of the hydrologic cycle [24]. Any alteration in the hydrologic response of the basin leads to substantial change in the seasonal timing of water availability, which requires costly adjustments and often results in conflicts among different interest groups [25]. Thus, it is important to identify the key issues and challenges which an expected LULCC and climate change will bring in the hydrology of a given region. In order to understand and predict the changes in water availability, it is important to analyze the uncertainties involved in the projections and the challenges involved in reducing the uncertainties.

1.2 Literature Review

Available water supplies are under great stress as a result of population growth, unsustainable consumption patterns and poor management practices. It is very likely that hydrologic impact of climate change and LULCC will cause further stress on an already stressed system. Changes in water availability in the 21st century as a result of climate change and LULCC are evident from a number of studies ([19, 20, 26, 27, 28]). Manabe et al. (2004) [27] report that the reduction of soil moisture in many semiarid regions of the world will become increasingly noticeable under climate change conditions leading to severe shortage of water. In contrast, an increasingly excessive amount of water is likely to be available in water-rich regions in high northern latitudes. Nohara et al. (2006) [26] investigated the projections of river discharge during the 21st century and determined an increase in the annual mean precipitation, evaporation, and runoff in high latitudes of the Northern Hemisphere, southern to eastern Asia, and central Africa. On the other hand, a decrease is reported in the Mediterranean region, southern Africa, southern North America, and Central America. Though, there are a number of studies which have evaluated the impact of future LULCC and climate change on hydrological responses in major river basins of the world, they have typically focused on averages of river discharge at the annual scale and very few studies show global projections of seasonal differences in the river discharge. Global warming is very likely to accelerate global hydrological cycles, where wet seasons are likely to become wetter and dry seasons will become dryer in the 21st century [8]. There are seasonal differences which may not be explained simply by changes in annual precipitation, heavy precipitation, or differences between precipitation and evapotranspiration. The implied amplification of existing differences in water availability between different regions and over different seasons present a profound challenge to the water-resources managers of the world.

1.2.1 Uncertainties in Projections and Response

There are uncertainties associated with future emissions of greenhouse gases, uncertainties about the response of the climate system to these changes at global and local scales, and uncertainties associated with climate models and the spatial and temporal distributions of impacts. Climate change projections such as changes in temperature, precipitation and corresponding moisture and energy fluxes are therefore characterized by major uncertainties regarding their magnitude, timing and spatial distribution. These uncertainties pose major challenges for planners taking decisions on adaptation measures.

Numerous studies have been conducted at scales ranging from small watersheds to the entire globe to assess the impacts of LULCC and climate change on hydrologic systems. More than 80 studies have been listed by Arnell et al. (2004) [20] in which climate change impacts for one or more watersheds were analyzed using an approach that coupled climate models with hydrologic models. Arora et al. (2001) [29] lists four different approaches which have been widely used to assess climate change impacts on river basins, which include "(1) estimates obtained by applying arbitrary changes in climate input to hydrological models, (2) spatial analogue techniques, (3) temporal analogue techniques, and (4) the use of results from General Circulation Models (GCMs), either directly or by downscaling to the appropriate scale". They concluded that of the four options, GCM-derived results present the best choice for hydrologic model inputs, although the application of a GCM to regional or smaller scales presents incompatibilities between model scales.

Fowler et al. (2007) [30] and Prudhomme et al. (2002) [31] use large-scale atmospheric variables output from GCMs to downscale to basin scale hydrologic variables through statistical relationships. The potential hydrological impacts of climate change estimated by changing the climate inputs to hydrological models are studied by a number of researchers

including Chiew et al. (1995) [32], Avila et al.(1996) [33], and Singh and Kumar (1997) [34]. They apply a range of changes in temperature and precipitation to a rainfall-runoff model to study the sensitivity of runoff and soil moisture. Arora and Boer (2001) [29] analyze the hydrology of 23 major river basins as atmospheric CO2 concentrations increase by 1% per year from the present until 2100. They report a decrease in runoff in the major river basins, though the changes in runoff are not uniform. Hirabayashi et al. (2008) [35] discussed the impact of climate change on river discharge of major river basins at shorter time scales i.e., flood and drought, with the highest spatial resolution coupled ocean-atmosphere-land GCM (MIROC). They showed an increase in the frequency of summer flood in Asian basins, and an increase in the frequency of drought in North America and South Africa. Moreover, several regions were projected to have increases in both flood and drought frequency. Several regions show shifts in the flood season from springtime snowmelt to the summer period of heavy precipitation. Manabe et al. (2004) [27] report an increase of wet-season river discharge in the South Asia region and the increase of summer drought in North America. In regions of positive runoff change, such as high northern latitudes, the increase obtained by Arnell (2003) [36] is smaller than that of Manabe et al. (2004) [27]. While in the region of negative change, the reduction is larger for Arnell et al. (2003) [36]. This characterization of differences between the results of different studies is based on the differences in models employed and the climate projections used in the study.

Recently, many studies have attempted to quantify the uncertainty associated with climate change projections. A typical method of evaluating effects of climate change on flow regime is to use an ensemble of GCMs, scenarios and statistical downscaling to provide inputs to a hydrological model, and examine the range of effects on the modeled flows. Horton et al. (2006) [37] assessed the uncertainty in climate change impacts on alpine discharge regimes and determined that for the glacierized catchments, variability in the temperature range is very critical as it leads to significant differences in the snow accumulation and melting

processes. Uncertainty analysis on the range of seasonal variability will provide new insights for the hydrologic response under climate change scenario.

1.2.2 Challenges and Limitations in Projecting Response

Model and Data

The biggest challenge for climate change impact assessment studies lie in the suitability of model and data. Although, there are a number of land surface models (LSMs) that can be used to assess the LULCC and climate change dynamics on the hydrologic response, there are differences in model structures, complexity, economy-of-physics and details of model parameters among different LSMs [38]. Most of the hydrologic studies dealing with climate change assessment use models with simplified dynamical representations. The development and use of more advanced hydrologic models, in terms of theory and physical processes, decrease the predictive uncertainty, and this leads to better adaptive measures [39]. Models with physically interpreted parameters can better predict responses under different circumstances than those models that require calibration, and hence are more suitable for prediction studies [39].

In recent years, based on the improvements in observational capability that provide better higher resolution input data and model structure that are capable of exploiting this data, hydrologic models have also improved in the capability of addressing the impacts of LULCC on hydrologic processes. There are a large number of studies which address the impacts of LULCC on hydrologic processes in different regions of the world [40, 41, 42]. Many of the existing hydrologic models use soil as a single layer and lack the influence of vertical heterogeneity and the impact of related land cover changes. Major existing hydrologic models for global analysis include Water Balance Model (WBM) [43], WaterGAP Global Hydrology Model (WGHM) [44], and Hydra [45]. These models have a soil-hydrology and surface energy balance scheme which is not able to capture the near surface soil moisture dynamics [41].

Since the hydrology of any basin is characterized by multiple time scales of interaction of processes, it is important to assess the ability of the model to capture the variability of governing processes. Several studies have shown that examining time series data in time frequency space leads to a better understanding of the underlying processes [46, 47, 48]. The Fourier transform and spectral analysis have been used consistently for many years as a method of pattern analysis and signal processing [49, 50]. Kumar (1997) [51] presents an extensive discussion on the application of wavelets to understand the time scales of hydrologic fluxes. Several studies demonstrate that use of a wavelet spectrum based performance measure contributes to model diagnosis and improve the calibration of hydrologic models. Kang et al. (2007) [52] used wavelet analysis to analyze temporal patterns of precipitation, river discharge, and well water level for three different periods: 15 years, 3 year, and a hydrological year, and noticed strong seasonal patterns of river discharge and well water level for relative short time periods. Nakken at al. (1999) [53] utilised wavelet analysis to identify and isolate the natural climatic components of the hydrologic record, and to distinguish the influence of anthropogenic land use changes on runoff records over time. Study by Labat et al.(2005) [47] applied wavelet transforms to provide physical explanations for time scale dependant relationships for the Atlantic river discharges to long term climatic indexes: the Southern Oscillation and the North Atlantic Oscillation. Identification of the dominant runoff processes in different hydro-climatic regions (for example, semi-arid vs. humid) is not yet explored using the time scale variability of precipitation and runoff. The identification of the dominant runoff process allows detailed insights in the runoff generation process of a basin and how it may change under climate change conditions. Thus, wavelet analysis serves as an important tool to understand the time scales of hydrologic dynamics which has not yet been extensively used for climate change studies. Besides understanding the natural hydrologic processes, it is important to account for human influence as human interferences significantly affect hydrologic processes in many hydrologic systems around the world. For

those hydrologic systems, quantification of the impact of human interference would be more appropriate for prediction and process understanding.

Human Influence

Besides indirect human influence in terms of LULCC, there is direct influence on the hydrologic system such as reservoir release, water withdrawal, irrigation, return flow, etc. While the impacts of LULCC on hydrologic cycle have been extensively modeled, direct human interferences are normally ignored. Hejazi et al. (2008) [13] presented a methodology to incorporate reservoir operation into hydrologic modeling for improved flow assessments. Water consumption for irrigation use plays a significant role in the hydrologic cycle of a given region. Many studies have identified dramatic changes to local and regional hydrology due to expansion of agricultural land and cropland irrigation [54, 55]. Water use in irrigation alters the hydrologic cycle in several ways: by reducing base flow to rivers, by increasing physical evaporation and transpiration, through changes in vegetation distributions, surface albedo and roughness, and by subsequent feedbacks to precipitation, and alterations to the soil moisture, runoff and ground water storage. Claessens et al. (2006) [14] showed that not accounting for diversions (groundwater pumping) result in overestimated water budget components; and without a detailed account of water budget components, inferences regarding streamflow or ET response under climate and LULCC could be invalid. Moreover, it is important to note that some basins may show an increase in net diversions while others may show reduced diversions under seasonal variability of precipitation change [56]. Significant reductions in water supply would make irrigation more difficult or impossible in certain regions, while increases in precipitation could allow marginal lands to support agricultural production or reductions in actual demands for irrigation water [54]. Increases in precipitation could also have negative consequences for agriculture if they come in the form of damaging storms that erode soils and flood the land [54]. Currently, a lot of effort is being made to incorporate various aspects of direct human interferences into hydrologic simulation

models, such as reservoir operation [13], groundwater pumping [14], and irrigation [57, 38]. A number of studies have combined water supply and demand assessments based on datasets and models at a global scale [58, 59]. However, few of these modeling studies simulate detailed hydrologic processes at all, and when they do, they do not implement it in a way that allows modifications from human water use on natural hydrologic processes to be detected.

Land Use-Land Cover Change (LULCC) and Climate Change Projections

For assessing the impact of LULCC on hydrologic processes, projection of future LULCC involves a lot of uncertainties [60]. Though remote sensing can provide quick and comparatively inexpensive information about LULCC for the current conditions, population growth, technological advances, economic, social, cultural and political factors all play important roles in the generation of future land cover maps. Over the last decades, a range of models projecting LULCC have been developed based on gross amount of land use types and observed changes or based on the spatial distribution, proximity of land use, socio-economic factors, national policy, etc. Different modeling approaches have been adopted in the study of LULCC with a wide range of assumptions [61, 62, 63, 64]. Predictive models based on future scenario are considered more suitable for designing sustainable development [65, 66, 67]. Several experiments and modeling studies demonstrate that river discharge has increased as a consequence of deforestation [68, 69, 42]. There are differences in projections of hydrologic response resulting from the uncertainties in model and LULCC projections. For example, Rost et al. (2008) [70] found that the net effect of land cover conversion and irrigation leads to increase in discharge (4%) and decrease in land evapotranspiration (0.9%) at the global scale; while Gordon et al. (2005) [69] found that these effects cancel each other.

As discussed, many studies have addressed climate change impacts on water resources using GCMs [71, 72, 30, 73, 74]. However, these studies use data from only a limited number of GCMs. Often only one GCM model is used [71, 72]. Several studies run their impact

models using two or three different GCMs [75, 76], leading to a wide range of outcomes and even opposing conclusions [75]. There are several reasons which restrict the use of all GCM predictions. Often the access to GCM data is an important issue. Though, advanced downscaling models such as regional climate models are likely to provide better predictions for small scale processes, they are often only implemented for a limited number of GCMs. Finally, practical issues such as computational demands is another limitation. It should be noted that GCMs contain large errors, due to simplification of climate representation, potentially wrong assumptions about climate processes, limited spatial and temporal resolution, and errors in the forcing data [77, 78, 9]. Arnell (1999) [79] projected the global river discharge simulated by the Hadley Centre climate model and suggested that the annual runoff increases in high-latitude regions, equatorial Africa, and Southeast Asia, but it decreases in mid-latitudes and most subtropical regions. However, Arora and Boer (2001) [29] have shown that the annual river discharge decreases in equatorial Africa and Southeast Asia. Therefore, the projection of runoff is greatly dependent on GCM characteristics, which are still difficult to validate against appropriate observations. Ensemble simulations capture the uncertainties owing to boundary conditions, initial conditions, different model structures and process representations. In Multi Model Dataset (MMD-A1B), all models are assumed to be equally valid and no weighing factors are used. There are several studies which evaluate model performances in order to provide more emphasis to those models which simulate variables or processes of interest for a given region ([80, 81]).

Inter-comparison of hydrologic response of basins in different climatic regimes helps develop an improved understanding of the impact of climate change on the hydrologic dynamics. Comparative studies have been carried out in different climate-soil vegetation regions in small domains [82]. For example, many of the studies have compared the results for watersheds in the western section of the United States, including the Colorado River Basin [83, 84, 18, 85], the Columbia River Basin [86, 87, 85, 88], and the Missouri River Basin

[89, 87, 85]. However, very few have presented a comparative analysis of basins across the globe to represent a wide range of climatic zones [82]. Moreover, very few studies have quantified the combined effects of future climate and LULCC on basin hydrology [90].

1.3 Research Contributions

This thesis integrates contemporary assessments of LULCC and regional climate change, with distributed hydrologic modeling, meteorological forcing, and IPCC projections, to evaluate anticipated changes in the hydrologic cycle at seasonal time scale. Diverse hydro-climatic regions from across the world are assessed to evaluate how the climate and LULCC factors interplay to alter seasonal hydrologic dynamics. For each of the different factors altering hydrologic response, the influence of change is independently assessed on the overall hydrologic response. The set of simulations include human influence, LULCC, climate change, latest multi-model outputs of IPCC-AR4 climate models, and analysis in time-frequency domain which provide a sequence of original contributions. These contributions are organized into three categories, each of which is a chapter in this thesis described as:

Understanding Time Scales of Hydrologic Dynamics: Wavelet Analysis Approach [Chapter 3]

Multiple time scales of interaction for the hydrologic processes are evaluated using wavelets to extract information regarding the originating mechanisms of hydrologic signals and the underlying geophysical processes. The ability of the hydrologic model to capture the dominant processes in different hydro-climatic regions (such as semi-arid vs. humid) is assessed using this approch. It assists us in developing a predictive understanding of the possible alteration of hydrologic processes under LULCC and climate change scenarios.

- Several factors like soil permeability, topography, vegetation cover, interacting at multiple time scales are identified to affect the hydrologic response. High frequency runoff peaks are attributed to fast runoff processes resulting from the hortonian overland flow in semi-arid basins.

Assessing Water Use Effects on Hydrologic Discharges at the River Basin Scale: [Chapter 4]

A coupled hydrologic and water management modeling framework is applied to model the impact of human influence on river basin discharge. A diverse range of indices are used to explore the different aspects of human interferences with natural hydrologic processes.

- The extent to which human interferences impact natural flow discharge is quantified using indices derived from basic mass balance equations as well as through water use regimes and Budyko curve.

- Seasonal water consumption is evaluated using monthly water withdrawal and return flows for the selected basins. The impact of human interferences is found strongest during the summer season for Asian basins.

- It is analyzed that not accounting for direct human interferences, in terms of groundwater pumping, irrigation use, reservoir regulations, etc. in hydrological studies will lead to overestimated water budget components under climate change scenario.

Seasonal Hydrologic Dynamics under Climate and Land Use-Land Cover Change in Different Hydro-climatic Regions: [Chapter 5]

The potential impacts of climate and LULCC on the hydrologic response for major regions of the world are analyzed using a distributed hydrologic model, meteorological forcing, and

landscape information at the seasonal scale. Important contributions in this regard include the following:

- A consistent global GIS based dataset is constructed for the Surface Boundary Conditions from highest quality datasets available. Meteorological forcing dataset is constructed from European Center for Medium Range Weather Forecasts (ECMWF) reanalysis data at 6-hour time step for the period 1976 through 2000.

- The broad climatic and landscape controls on the seasonal hydrologic dynamics are presented over several basins from diverse hydro-climatic regions from Asia, Africa and North America. Future changes in water availability are presented based upon changes in the volume and seasonality of precipitation, runoff and evapotranspiration. Severe reduction in streamflow is projected to occur in certain seasons which may not be revealed through annual estimates of analysis.

- The range of uncertainty analysis show the translation of precipitation to runoff response varies for each season depending upon antecedent moisture conditions and hydrogeologic characteristics of the basin. The basins in humid zone have a higher uncertainty range resulting from an increase in precipitation while the basins in semi-arid zone present a higher uncertainty range with a reduction in precipitation.

- Precipitation change amongst the LULCC and climate change is identified as the dominant driving force in effecting the future runoff response in all the study basins. LULCC is found to be the dominant factor governing ET response in humid basins while precipitation change is found to be the dominant ET control in arid basins.

1.4 Dissertation Organization

This thesis is organized in six chapters. In Chapter 2, the model and the datasets prepared in the study are described along with the description of study basins. A comparative overview of the time scales of hydrologic dynamics is explored for the selected basins in humid, mediterranean and semi-arid regions using the continuous wavelet analysis in Chapter 3. In Chapter 4, the human influence on each basin is evaluated using a coupled hydrologic water management model. In Chapter 5, seasonal hydrologic dynamics under LULCC and climate change is then explored for each basin. Chapter 6 concludes with summary and research contributions of this thesis, including a discussion of open questions that can be addressed in future work. An overview of IPCC scenarios and IMAGE model used for LULCC projections is given in Appendix A. The comparison of meteorological forcing data (ERA-40) to other observational records is given in Appendix B.

Chapter 2

Model and Data Description

The literature review from the previous chapter discussed the models and data used in earlier studies along with their limitations. This chapter describes the models and data used to meet our research objectives and their suitability and limitations. An elaborative description of Common Land Model (CLM) is given in this chapter with a focus on land bio-geophysical and hydrological processes simulated by the model. The model is designed to handle a variety of data sources and hence can use the most current datasets available for defining land surface type, soil and vegetation parameters, model initialization, and atmospheric boundary conditions. The input data requirement of CLM is considered as a limitation by many of the studies. In this study, a consistent global GIS based dataset is constructed for the Surface Boundary Conditions (SBCs) from highest quality datasets available. Meteorological forcing dataset is constructed from European Center for Medium Range Weather Forecasts (ECMWF) reanalysis data. Data synthesis of SBCs (surface elevation, bedrock depth, fractional vegetation cover, land cover, soil sand and clay fraction profiles) is described in detail along with the information of source, source resolution and projection. A discussion on the limitations with reanalysis data and ECMWF biases as reported by others is included.

A comprehensive description is given for the nine selected river basins from different hydroclimatic regions of the world. For example, Ohio, Volta and Huai river basins are selected from the humid zone while WGM, Orange and Krishna river basins are selected from the semi-arid zone for a comparative study. The climate, land cover, hydrologic characteristics, expected changes and the role of human influence are described for each of the selected basin.

2.1 Common Land Model

The Common Land Model (CLM) is a community developed land surface model which combines and advances the features of well documented and modular land models; the NCAR Land Surface Model (LSM) [91], the Biosphere Atmosphere Transfer Scheme (BATS) [92], and the snow model from IAP94 (the 1994 version of the Chinese Academy of Sciences Institute of Atmospheric Physics Land Surface Model [93]). Model incorporates detailed physical process representation and uses community accepted standardized parameterizations to establish a physically based soil-vegetation-atmosphere transfer scheme model.

The major characteristics of CLM include ten unevenly spaced vertical layers for soil temperature and soil moisture; a multilayer parameterization scheme of snow process; an explicit treatment of the mass of liquid water and ice water and their phase change within the snow and soil system; a runoff parameterization following the Topography-based Runoff Prediction Model (TOPMODEL); a canopy photosynthesis-conductance model; high-resolution geographic distributions of land cover, vegetation, and root and soil properties. The biogeochemical processes simulated by the model include photosynthesis, plant and microbial respiration, and net primary production. Figure 2.1 shows the land biogeophysical processes which consist of computation of albedo, radiation fluxes through the canopy, and heat and momentum fluxes at the land-atmosphere interface. Important processes include: vegetation composition, structure, and phenology; absorption, reflection, and transmittance of solar radiation; absorption and emission of longwave radiation; momentum, sensible heat (ground and canopy), and latent heat (ground evaporation, canopy evaporation, transpiration) fluxes; heat transfer in soil and snow including phase change; canopy hydrology (interception, throughfall, and drip); snow hydrology (snow accumulation and melt, compaction, water transfer between snow layers) and soil hydrology (surface runoff, infiltration, sub-surface drainage, redistribution of water within the column).

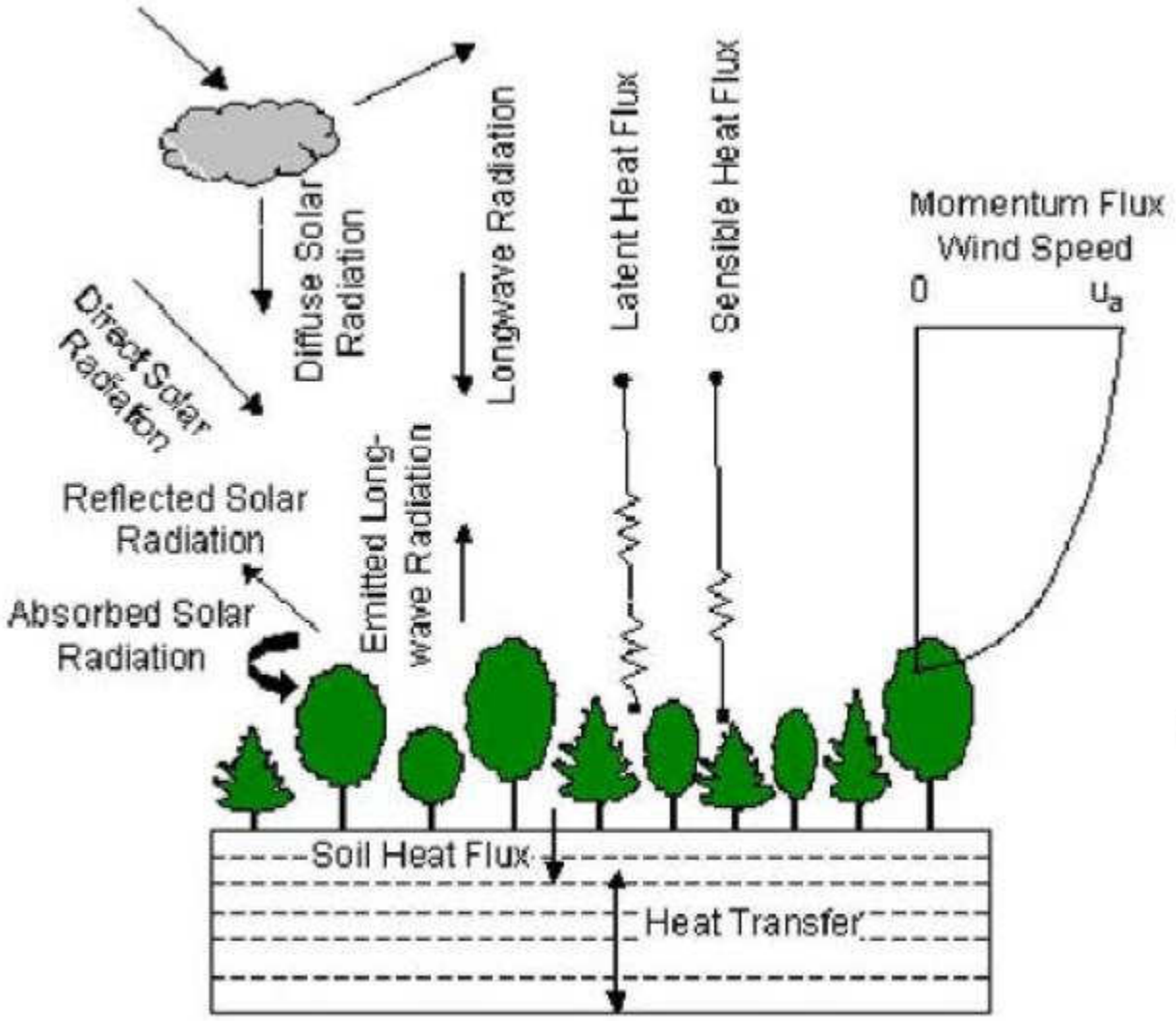

Figure 2.1: Land biogeophysical processes simulated by CLM. Adapted from Bonan (2002) [1]

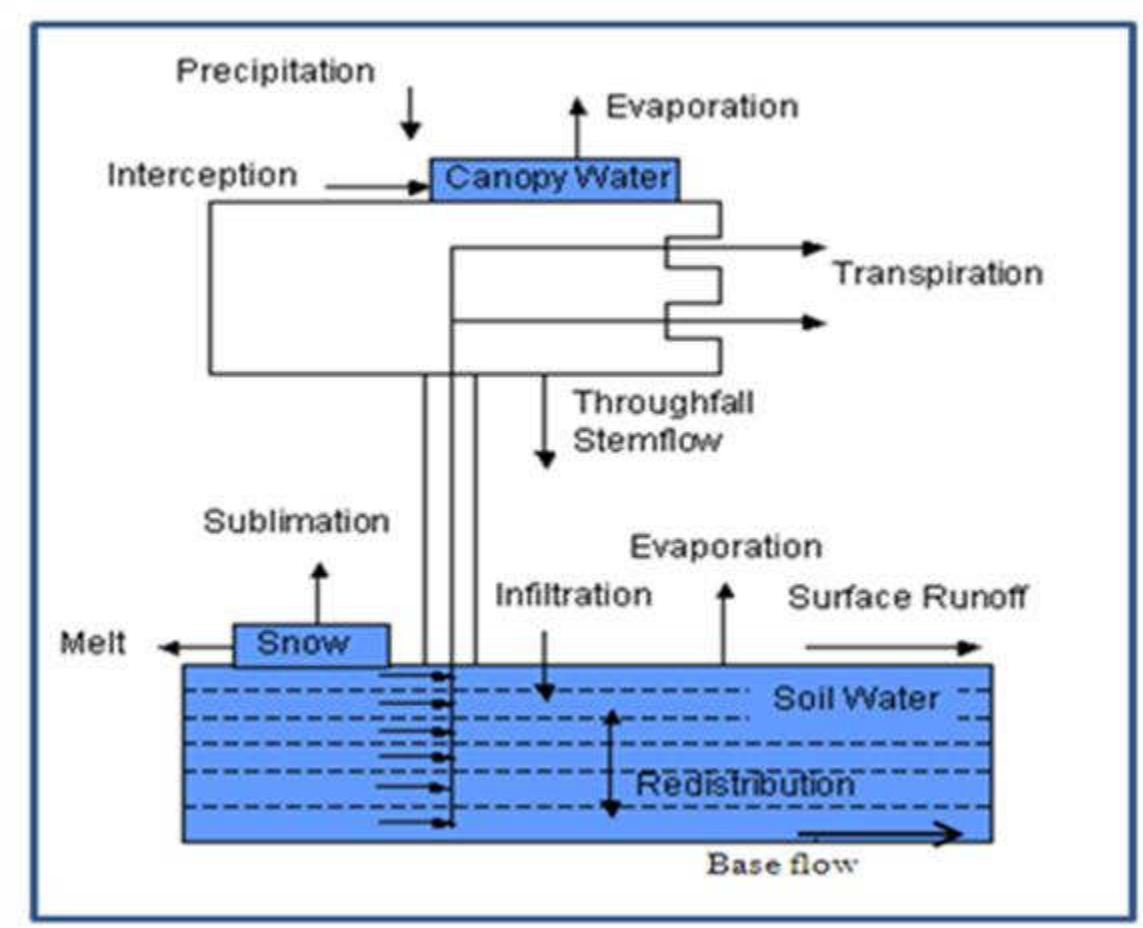

Figure 2.2: Land hydrological processes simulated by CLM. Adapted from Bonan (2002) [1]

Figure 2.2 presents the land surface hydrologic cycle in CLM, from Bonan (2002) [1]. The hydrologic processes include interception, throughfall, stemflow, snow accumulation and melt, infiltration and runoff. Model runoff includes surface and base flow, both of which are computed over saturated and unsaturated areas separately. The fraction of the saturated area depends on the soil moisture state, computed as a function of water table depth and topographic features. Runoff parameterization follows the TOPMODEL concept, where the local hydraulic gradient is assumed to be equal to the local surface slope and all points with the same value of the topographic index (a/tan B) respond with similar hydrologic behavior. The topographic index is derived from the basin topography, where "a" is the drained area per unit contour length and "tan B" is the slope of the ground surface at the location. The model makes calculations for representative values of the index and the results are mapped back into space by knowledge of the pattern of the index derived from a topographic analysis. Surface runoff is parameterized as a combination of saturation excess runoff in the saturated fraction and BATS-type [92] surface runoff in the unsaturated fraction. The formation of base flow contains three different mechanisms: bottom drainage, saturation excess, and lateral subsurface runoff due to local slopes. The soil thermal and hydraulic parameters are produced by soil texture. Soil textural classes are determined uniquely by a combination of three variables, the percent of total masses of clay, silt and sand of soil. The hydraulic conductivity and soil matrix potential are parameterized following Clapp and Hornberger (1978) [94] and Cosby et al. (1984) [95]. No spatially explicit scheme for routing of runoff is used. Basin discharge is computed as the aggregated runoff response over the basin. Evapotranspiration (ET) consists of evaporation from wetted stems and leaves, transpiration through the canopy and evaporation from the ground. The detailed technical description of the model can be found in Dai et al. (2003) [96].

The CLM is designed for coupling to atmospheric numerical models. It provides surface albedos (direct beam and diffuse for visible and near-infrared wavebands), upward longwave

radiation, sensible heat flux, latent heat flux, water vapor flux, and zonal and meridional surface stresses required by atmospheric models. These are regulated in part by many ecological and hydrological processes, and the model simulates processes such as leaf phenology, stomatal physiology, and the hydrologic cycle. Spin up strategy is used to simulate the model over a period of time so that initial conditions reach the equilibrium state and equilibrium state variables then serve as the initial values. The model state variables that require initialization include canopy temperature, canopy interception water storage, temperature at the nodes of soil and snow layers, mass of water within the layer of soil and snow, mass of ice within the layer of soil and snow, and snow layer thickness.

Energy and water balance calculations are performed over each grid cell at every time step, and each grid maintains its own prognostic variables. The model applies finite difference spatial discretization methods and a fully implicit time integration scheme to numerically integrate the governing equations. The overall structure of CLM includes three elements: 1) the core single-column soil-snow-vegetation biophysical code, 2) the land boundary data, and 3) the scaling procedures required to interface atmospheric model grid-square inputs to land single-column processes. The model is structured in a way to allow the best science for each of these elements, and ensures that the core model can be tested with single-point field data, and that the satellite remote sensing and global field survey datasets can be incorporated. The CLM has been evaluated extensively in standalone mode with field measurements [96], indicating realistic simulations of state variables (soil moisture, soil temperature, and snow water equivalent) and flux terms (net radiation, latent and sensible heat fluxes, and runoff).

CLM is chosen as the hydrologic model for our study because this study required a model to assess LULCC and climate change impact on the hydrologic dynamics of different hydroclimatic regions. Since LULCC processes are critically dependent on modeling the near surface soil moisture, a model with multiple soil layers capturing soil moisture dynamics at

different levels is needed for better assessment. For climate change assessment, a model with physically based process representations and with the capability of being driven by climatic variables at a higher temporal resolution is required. Moreover, a comparative study of future hydrologic response across the world requires a model with no calibration or correction factor. CLM is designed to handle a variety of data sources and hence can use the most current datasets available for defining land surface type, soil and vegetation parameters, model initialization, and atmospheric boundary conditions. CLM incorporates advanced physical complexity, theory and processes; uses physical process representations without the need for calibration and can be run at high spatial and temporal resolutions; thus serving all the above mentioned objectives to be used as the hydrologic model of our study. Model is structured in a way to capture the relevant processes significant for understanding the impact of climate and land use-land cover change on the hydrologic dynamics.

2.2 Data Description

2.2.1 Surface and Sub-surface Characteristics

The CLM model requires specification of surface boundary conditions (SBC) to define surface and sub-surface characteristics of the study domain. One of the critical requirements in the construction of SBC's is that each field must be defined over the whole study domain with no missing values and should have physical consistency across all relevant parameters [97]. The primary SBC's include surface elevation; land cover category; soil, sand and clay fraction profiles; depth of the bedrock; fractional vegetation cover; leaf and stem area index. Amongst all, leaf and stem area indices are not time invariant and vary over the season. Time varying vegetation parameters Leaf Area Index (LAI) and Stem Area Index (SAI) are derived from the dynamic empirical vegetation model inherent in CLM [96].

For different parameters, we use databases that result in data in varied resolutions, finer or coarser than the model grid, a wide range of map projections and complex data formats. This presents significant challenges and requires labor intensive efforts to process the data on model grid mesh. Criteria for filling up the missing value also differ with each parameter. Geographic Information System (GIS) software application tools, Arc/Info and Arc/Map, from Environmental Systems Research Institute, Inc. are used to obtain the suitable input data format. The basic steps for each parameter include data processing with ArcGIS involving the conversion of image file (ASCII, BIL) to raster grid by generating a corresponding header file. The downloaded data is then projected to model domain projection and overlaid over the model grid mesh. The processed SBCs for the model along with the information of source data and source resolution is given in Table 2.1. All the model data are converted to 30km by 30km spatial resolution in Lambert Azimuth Equal Area projection.

Table 2.1: The list of the processed surface and sub-surface characteristics along with the information of source data and source resolution over the global domain.

Surface Boundary Attribute	Source	Resolution
Digital Elevation Model	USGS GTOPO30 (http://edcdaac.usgs.gov/gtopo30/hydro/)	1 Km
Fractional Vegetation Cover	USGS Global Land Cover Classification (http://edcsns17.cr.usgs.gov/glcc/)	1 Km
Sand and Clay Fraction Profile	FAO-UNESCO (http://hydrolab.arsusda.gov/soils/)	10 Km
Bedrock Depth	FAO-UNESCO (http://www.lib.berkeley.edu/EART/fao.html)	10 Km
Land Cover Category	Netherlands Agency (http://www.pbl.nl/en/themasites/image/)	50 Km

Topographical data sets are constructed from the U.S. Geological Survey 30-arc-second digital elevation model of the world (GTOPO30) provided by HYDRO1K. The Digital Elevation Model (DEM) data is available in the band interleaved by line (BIL) image format (http://edcdaac.usgs.gov/gtopo30/hydro/index.html) in the Lambert Azimuth Equal Area projection. Raw DEM data was downloaded for all the continents as image files with a suitable header file at 1 km resolution and then converted to 30 km spatial resolution (Fig. 2.3).

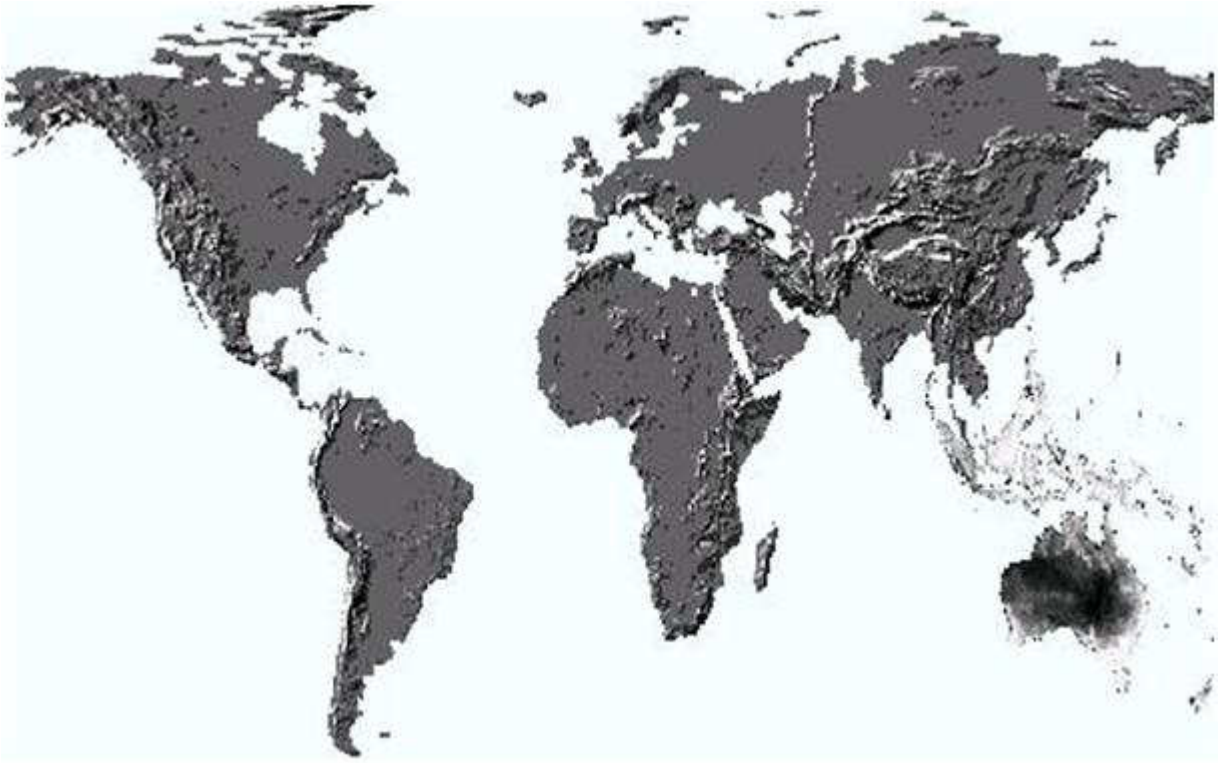

Figure 2.3: Digital elevation representation, derived from USGS 30 arc-second digital elevation model of the world (GTOPO30).

Fractional vegetation cover (FVC) is an ecological parameter that determines the contribution partitioning between bare soil and vegetation for surface evapotranspiration, photosynthesis, albedo, and other fluxes crucial to land-atmosphere interactions. It is assumed to be time invariant and is derived following the approach presented in Zeng et al. (2002) [98]. The Normalized Difference Vegetation Index (NDVI) is used from AVHRR from the

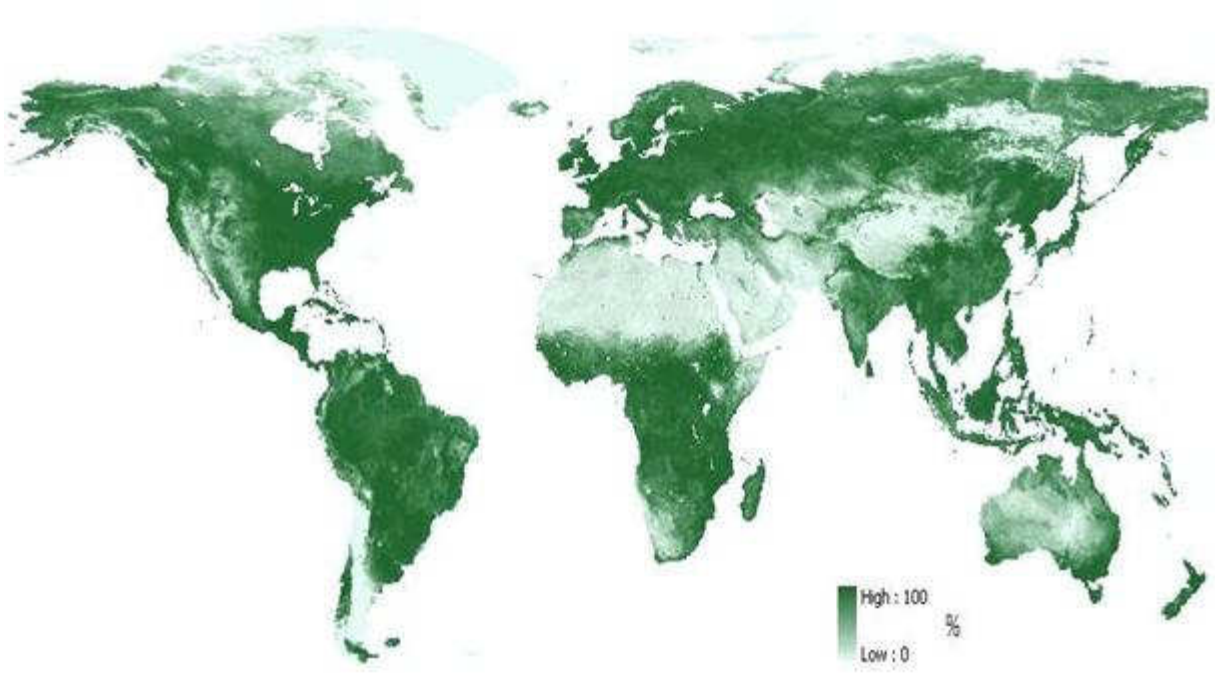

Figure 2.4: The geographic distribution of Fractional Vegetation Cover (FVC)

same global 1-km AVHRR satellite product as for Land Cover Category (LCC). The 10 day (April 1992-March 1993) composites are used to determine the annual maximum NDVI (Np,max) for each LCC. For each pixel, the vegetation cover is computed by using a coefficient Cv which equals the ratio of (Np,max-Ns) to (Ncv-Ns), where Ncv is the NDVI value for a complete coverage of a specific USGS LCC over the pixel and Ns is the NDVI value for bare soil. The resultant Cv point data at 1 km resolution is converted to polygon coverage data, remapped onto the model projection, and intersected with the model grid mesh. The fractional area of each pixel contributing to the grid is extracted. The final FVC is obtained by the area-weighted averaging of Cv values for all pixels within each model grid. The geographic distribution of FVC is shown in Fig. 2.4.

Clay and sand fraction in each soil layer of CLM is derived from the top and sub layers as outlined in Liang et al. (2005) to parameterize the thermal and hydraulic properties of soil for the model layers following Cosby et al. (1984) [95]. Food and Agriculture Organization of the United Educational, Scientific, and Cultural Organization (FAO-UNESCO) soil maps of the

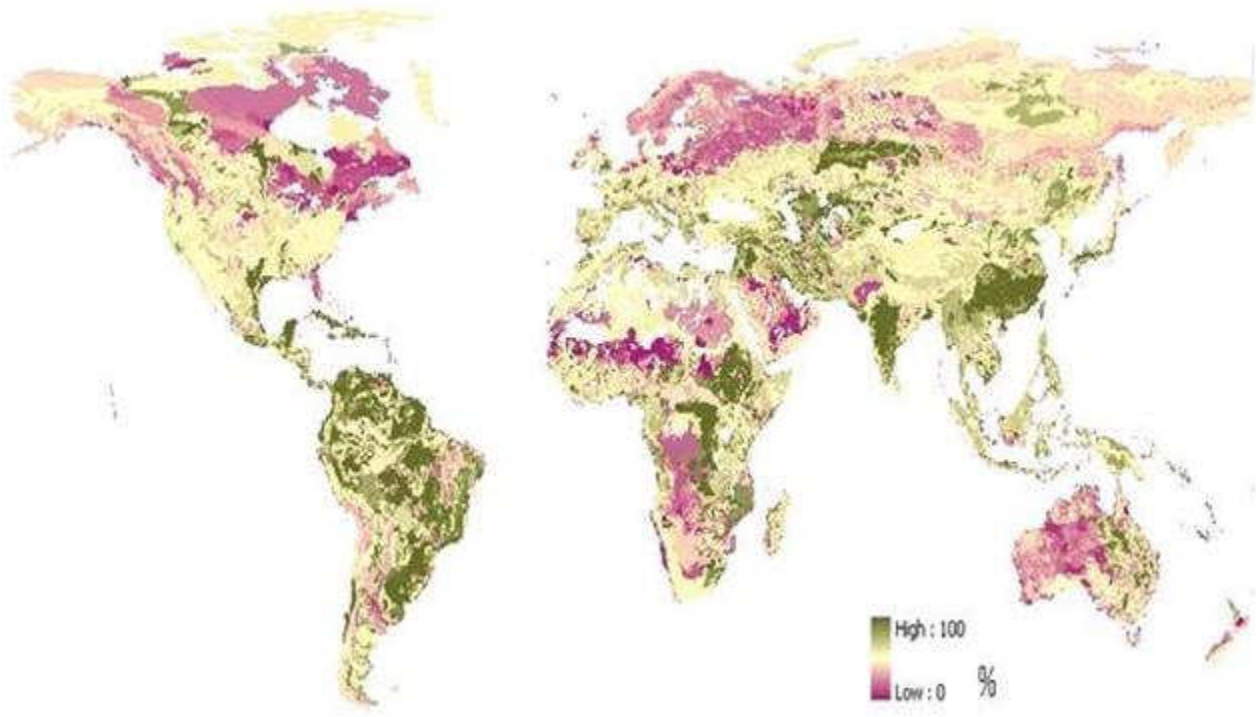

(a) The geographic distribution of % Clay cover in top (0-30 cm) layer

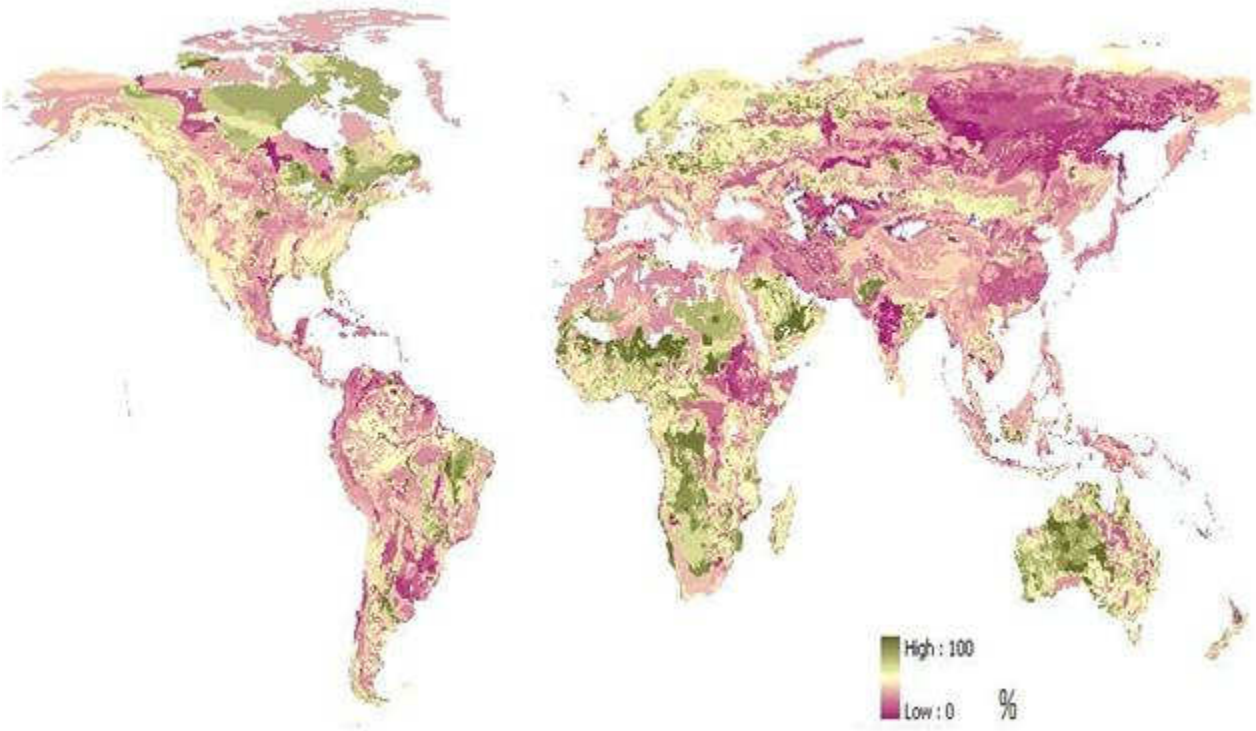

(b) The geographic distribution of % Sand cover in top (0-30 cm) layer

Figure 2.5: The geographic distribution of % Clay and Sand cover in top (0-30 cm) soil layer.

world at 5 min resolution in geographic projection are used to obtain clay and sand % profiles in top (0-30 cm) and sub (30-100 cm) layers (http://hydrolab.arsusda.gov/soils/start.htm). The top layer data are uniformly assigned for the top five layers above 28.91 cm, while the sub layer values are assigned for the remaining six layers above 6m depth as outlined in [99]. After processing of image to a raster grid, the data is clipped to get the continental coverage and converted to model projection. Fig. 2.5 shows the geographic distribution of % clay and sand cover in top layer.

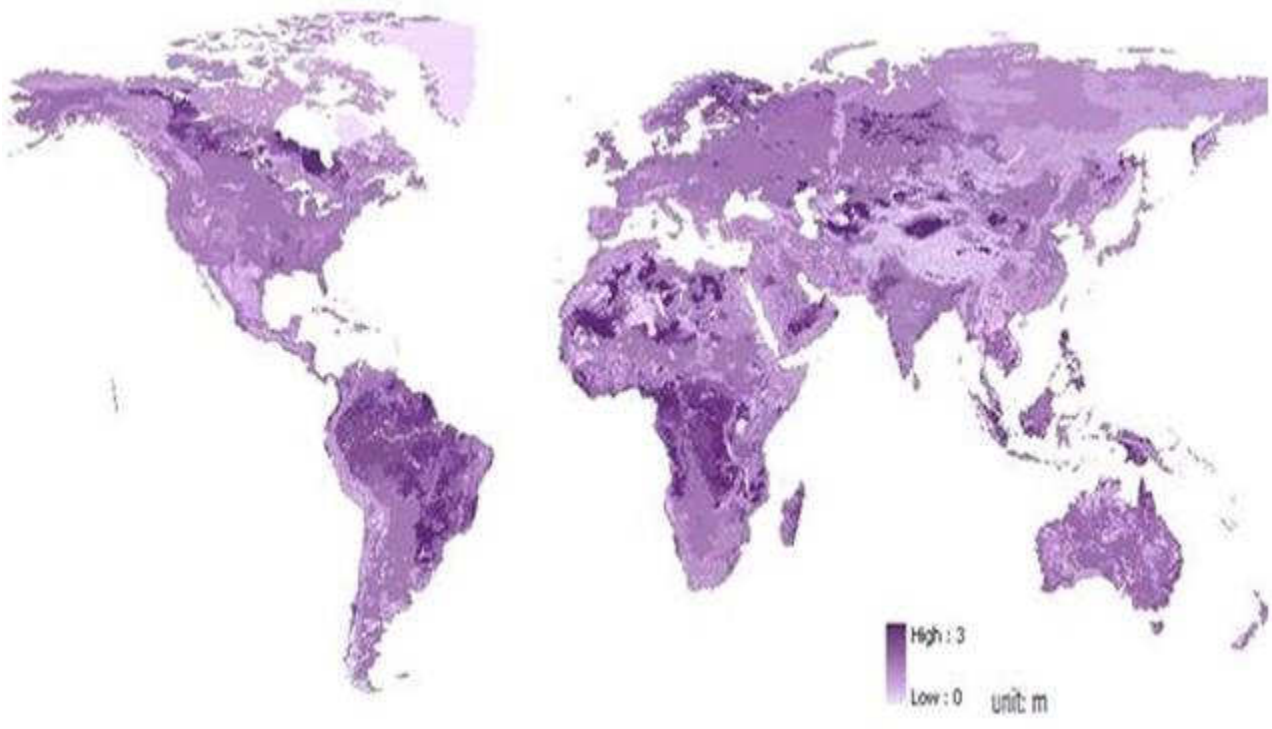

Figure 2.6: The geographic distribution of Bedrock depth

Bedrock depth is defined as the depth of soil between the land surface and the geologic substratum (Miller and White, 1998). Data is obtained from Food and Agriculture Organization of the United Educational, Scientific, and Cultural Organization (FAO-UNESCO) soil map of the world (http://www.lib.berkeley.edu/EART/fao.html) at 5 min resolution in geographic projection (2.6).

Although very high resolution land use-land cover data are available for current conditions, a consistent source of present and future land use-land cover data is used here in order to assess the impact of land use-land cover change on hydrologic dynamics of different hydro-climatic regions. Projections of land use-land cover are derived using an Integrated Model to Assess the Global Environment (IMAGE) developed by Netherlands Environmental Assessment Agency (MNP). IMAGE is an ecological environmental framework which explores the long-term dynamics of global change as a result of interacting demographic, technologic, economic, social, cultural and political factors. An overview of IMAGE model is provided in Appendix A.

Since the Common Land Model uses USGS classification of land cover category to define the soil thermal and hydraulic parameters. The derived land cover maps are required in USGS classification. The maps obtained from MNP are in IGBP classification which were converted to USGS classification. First, the projected as well as historical time series maps from IMAGE were compared to satellite derived land cover map of USGS. Each continent was clipped out from global coverage for each year as it was found that there are some spatial inconsistency of land cover classes between USGS map and projected map at global level. A single class matched well in one part of the world but not in the other part. The projected classes were recoded into USGS classes on a continental basis, which minimizes the global inconsistency. To determine the degree of inconsistency and to assign a USGS class to a particular class of projected map, the number of pixels of USGS classes falling under each class of projected map was calculated. Afterwards the maximum number of pixels were counted to identify the dominant land cover of USGS map under each MNP maps class. Visual interpretation technique was then applied to see if dominant land cover is consistent spatially considering its distribution. More details about the land use-land cover change projection data and the projected change in study basins is given in the fifth chapter.

2.2.2 Meteorological Data

Most of the climate change assessment studies use weather station data at a specific location and are not sufficiently dense to capture the spatial heterogeneity of climate variability prevailing in the region. Several reanalysis data sets have recently been produced and made available for climate and weather prediction studies, for example the European Centre for Medium Range Weather Forecasts (ECMWF) 15 and 40 year reanalysis (ERA-15, ERA-40) [100]; the National Center for Environmental Prediction, National Center for Atmospheric Research (NCEP/NCAR) reanalysis [101] and the NASA Goddard Earth Observing System 1 (GEOS1) reanalysis [102]. The ECMWF 40-year reanalysis project (ERA-40) is the most recent comprehensive reanalysis from September 1957 to August 2002 which complements the NCEP/NCAR 50-year and ECMWF 15-year reanalysis (ERA-15). General aspects of ERA-40 are described in Uppala et al. (2004)[103].

The ERA-40 hydrological cycle has changed in several respects compared to the previous ERA-15 reanalysis. The hydrologic cycle over land has improved [5]. These improvements comprise the eliminated cold biases in winter, the reduced occurrence of negative P-E (precipitation minus evapotranspiration) values, the removed dry bias in winter over Europe, and an improved representation of the snowpack. However, the ERA-40 hydrologic cycle also has several deficiencies. The largest one being the unbalanced global water budget, P-E over the ocean is positive (and not negative as it should be) in the long term mean for the satellite (1989-2001) and transition (1973-1988) periods [5]. The quality of the hydrologic cycle differs between the periods as the biases in the hydrologic cycle are strongly influenced by the different observing systems such as the periods with satellite data or with no satellite data.

The validation of ERA-40 precipitation over land is done by using gridded observational datasets based on gauge measurements. The datasets comprise CRU (Climate Research Unit; [104], GPCC (Global Precipitation Climatology Centre; [105] and GPCP (Global Precipitation Climatology Project) data. CRU and GPCC data are not corrected for the systematic undercatch of precipitation gauges, which is especially significant for snowfall. For GPCP data, a correction has been applied by a factor of about 2 [105] so that the actual precipitation amounts are expected to be in between the corrected and uncorrected data. It is to be noted that gridded precipitation datasets derived from gauge measurements bear some uncertainties due to different systematic errors [105]. Differences between the ERA-40 and GPCP precipitation are typically about 2-7 mm/day in the tropical oceans. A wet bias in excess of 5 mm/day is present over Africa (between 10S and 10N longitude). The excessive precipitation in the tropical regions, particularly after 1991, is seen as the most serious drawback of the ERA-40 reanalyses. This drawback stems from weaknesses of the humidity scheme utilised in the assimilation system [106]. Biases in the ERA-40 precipitation may be related to the fact that several different observing systems for water vapor are used in ERA-40 data assimilation. Refer to Appendix B for comparison of ERA-40 to other observation datasets.

The monthly-mean ERA-40 and NCEP/NCAR analyses of two-metre temperature have been compared with the CRU dataset of surface air temperature anomalies of [107]. CRU data uses all available monthly station averages of mean temperature from land regions of the world. It is found that the overall warming trends are smaller for ERA-40 than for CRU. Over the northern hemisphere, and for Europe and North America separately, the ERA-40 trend is about 30% smaller than the CRU trend for the full period, but within 10% of the CRU trend for 1979 to 2001. The trends for 1979-2001 from ERA-40 are in closer agreement with CRU than are the corresponding trends from NCEP/NCAR. Part of the reason ERA-40 performs better is its use of observations of surface air temperature [106].

ERA-40 data at 6-hour time interval (0, 6, 12, 18 UTC) for 1976-2000 is processed to derive the required meteorological data for the model which includes incoming longwave and shortwave radiation, total and convective rainfall, total and convective snowfall, air temperature, pressure, wind components, boundary layer height and specific humidity. Data is downloaded in netcdf format and then processed to Ascii format using supercomputer which uses Netcdf library, Fortran and C compilers. Ascii data is then converted to GIS grid format and changed to model projection i.e. Lambert Azimuth Equal Area projection and resampled to 30 Km resolution.

2.3 Study Basins

The distribution of selected basins for the study, widely located in different climatic zones is shown in Figure 2.7. For example, Ohio, Volta and Huai river basins are selected from the humid zone while Western Gulf of Mexico (WGM), Orange and Krishna river basins are selected from the semiarid zone for a comparative study. The boundaries of the selected river basins are as described in Cai et al. (2002)[16] to enable coupling of the hydrologic model with the water management model. A comprehensive description of the selected basins, their hydrologic characteristics and expected changes is given below.

California Basins

California basins located on the west coast of the United States have a mediterranean climate, with cool rainy winters and dry summers. Nearly all precipitation occurs during December through March. Precipitation during the summer is infrequent, and rainless periods of several months are common. The two most prominent rivers within the basin are the Sacramento and the San Joaquin, which drain the Central Valley and flow to the Pacific Ocean through the San Francisco Bay. The climate and water of the basin are described in

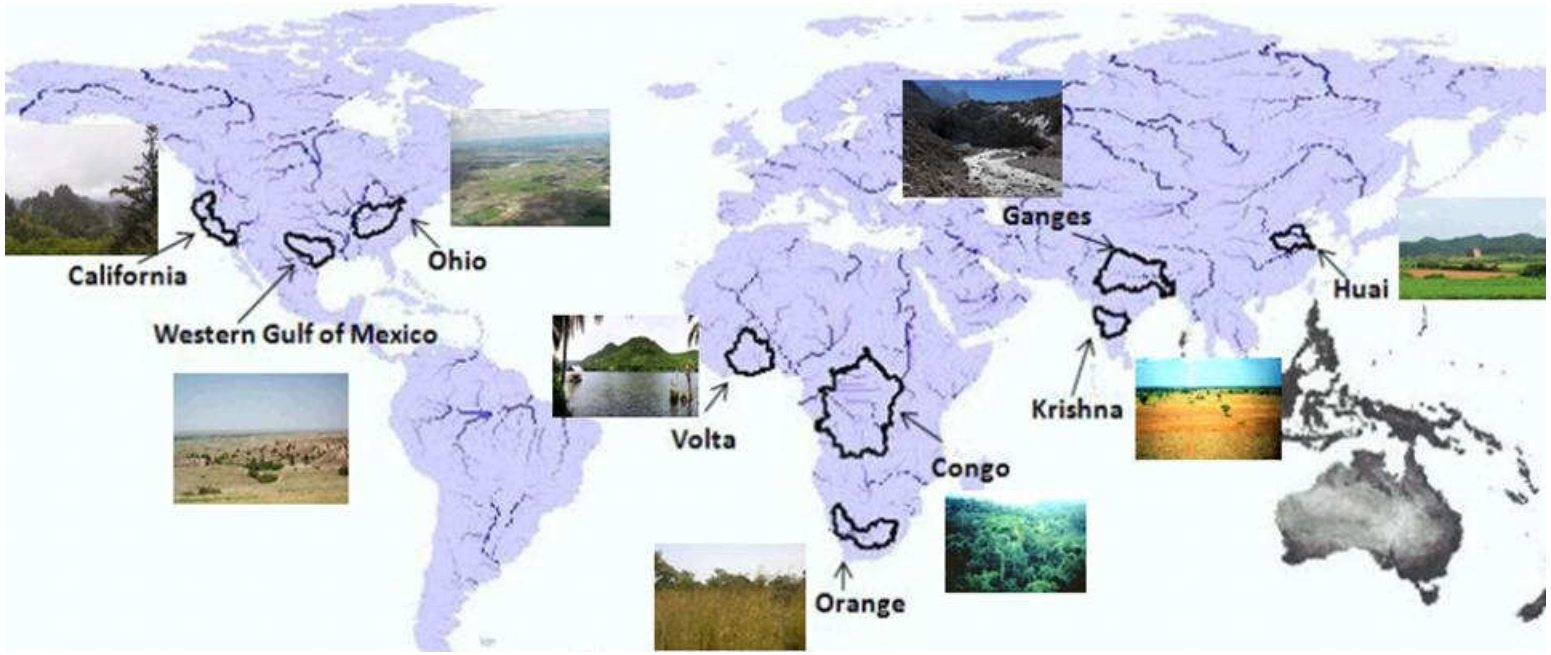

Figure 2.7: The distribution of the selected river basins in different hydro-climatic regions of the world.

more detail in the California water atlas [108].

The principal vegetative cover of the upper mountain areas consists of various species of brush and shrubs. In mountain areas, the steep canyon slopes and stream channel gradients are conducive to rapid concentration of storm runoff quantities. The soils are classified as having moderately low infiltration rates and result in moderately high runoff rates. In highly developed areas, runoff volumes have increased as the soil surface has become covered by impervious materials, natural ponding areas have been eliminated, and flood control facilities have been constructed. Water quality has degraded from runoff by land use conversions and combined sewer outflows.

These basins have more than six rivers and creeks with drainage areas smaller than 60,000 km^2, which together with water diversion from the Colorado River support densely populated regions of the state. Water is the most precious resource upon which California's ecosystems and economic vitality depends. Over the past 50 years, water managers in California have developed an extensive network of water storage and conveyance facilities, have promoted groundwater development and improved water use efficiency to meet the rising demands. In the Western United States, 60% of the climate related trends of streamflow, winter air temperature and snowpack that occurred between 1950 and 1999 were human-induced [22]. Sufficiency of water supplies in view of projected population increase and potential climate change is a challenging threat for the next century. How the existing system of dams, reservoirs and levees will change in the coming decades is not known.

Ohio Basin

The climate of Ohio basin in the United States is classified as humid continental, warm summer type [109]. There are large annual and daily temperature variations. The average annual temperature is 51.7 degrees Fahrenheit F with a few days over 100 degrees F

and an average of 5 days below 0 degrees F [109]. Precipitation is normally abundant and well-distributed throughout the year with fall being the driest season. Major floods in this area occur during the winter and spring months when runoff is accelerated by snowmelt and frozen ground conditions.

The topography has been greatly affected by the advances and retreats of glaciers. Most of Ohio's terrain is relatively flat, representative of glaciated landscape. The soils range from well-drained to the poorly drained soils of old glacial lake beds, soils are deep to moderaltely deep. ET from plant and soil surfaces is relatively high in summer and early autumn and relatively low in winter and early spring. LULCC projections estimate that by 2100, a major fraction of the deciduous broadleaf forest in the basin would be converted to dryland, cropland and pasture.

The Ohio River is the largest tributary of the Mississippi River by volume. During the last century, urbanization in the Ohio River Valley has increased both the peak and average annual runoff. Water withdrawals, of which about 75% is used by thermal power plants, comprise only a small fraction of the streamflow (less than 1%, according to the data from Ohio Development of Natural Resources and United States Geological Survey).

Western Gulf of Mexico Basin

The Western Gulf of Mexico (WGM) basin is located in the south-central part of the United States. It has a highly variable weather - humid subtropical climate on the east and temperate semi-arid steppe climate on the northwest. The easternmost basin is covered by piney woods and as the climate gradually becomes more arid towards west, turns into prairie and desert. Precipitation is relatively light and well distributed throughout the year, with the heaviest amounts occurring during May and September. While most of the winter precipitation occurs as light rain or drizzle, precipitation from April to September usually occurs

as thunderstorms with fairly large amounts of precipitation falling in short periods of time. This region has a long history of both floods and droughts as intense storms result in flash flooding.

The soils of the basin reflect the geographic diversity of the topographic cover. Soils are brown to reddish, mostly deep clay loams, sandy loams, and sands. The rural areas consist mostly of farms. Livestock, mainly beef and cattle, and grain crops of corn and sorghum provide major source of agricultural income. Development is proceeding rapidly with the population growth and farms and ranches are being converted into suburban commuter areas.

The current water supplies are from three primary sources: surface water (40%), groundwater (59%), and wastewater reuse (1%). The annual groundwater supply is projected to decrease by 32% during the same period due to over pumping from the Ogallala and Gulf Coast aquifers [23]. Local planners have tried to reduce water use through conservation programs and have turned to wastewater reuse and desalinization to increase their supply [23].

Congo Basin

The Congo basin located in the western central Africa has the second largest rain forest area in the world, after the Amazon. The Congo basin located in the western central Africa has the second largest rain forest area in the world, after the Amazon. It is also the second largest drainage system in the world, covering approximately 3.8 million Km^2. The major part of Congo lies within the inner humid tropical climatic region extending five degrees north and ten degrees south of the equator, characterized by heavy rainfall, high temperatures and humidity. Rainfall is spread almost uniformly throughout the year. Humid and seasonally invariant weather creates a relatively consistent streamflow in the Congo Basin.

The basin is surrounded by plateaus merging into savannas in the south, mountainous terraces and grassland in the west and mountainous glaciers in the east. Agricultural and municipal water use is relatively low as compared to other selected basins. Recently, a project to build the world's largest hydroelectric dam at a bend in the Congo River, called the Grand Inga, has been proposed. The dam will produce electricity (40,000 megawatts per year) to serve more than 500 million Africans who currently live without any electricity.

Currently, deforestation is the most visible anthropogenic influence in the Congo basin. Tropical deforestation over the last few decades is known to have contributed to increasing CO2 concentration. Typical of tropical forest, the Congo forest has a mean albedo of 0.13, which may change upto 0.20 if converted to grassland. Estimates indicate that the biomass of this moist tropical forest may contain about 24.79 Peta grams of carbon which can significantly effect the climate upon deforestation [Forest Resources, FAO]. Moreover, the changing demography and socio economic issues in the region directly impact land use practices with accompanying climatic feedbacks.

Orange Basin

The Orange basin, located in Southern Africa spreads over four countries: Botswana, Namibia, Lesotho and South Africa covering an area of 425,610 km ^{2}. The Orange river flows across the central landscape of the basin from the highlands in the east through the Kalahari depression in the west to drain into the South Atlantic Ocean. The basin receives less than 500 mm rain on average and is characterized by extremely variable distribution of rainfall and dry conditions. The majority of the rainfall occurs during the wet season (Nov-Apr) with very little rainfall in the dry season (May-Oct).

The region is covered by grassland and shrubland with very sparse vegetation towards west. Projected changes in land cover are dominated by the conversion of forest cover to cropland

and increased urbanisation (FAO, 2001). Both the population and demand for the waters of the Orange River have been increasing. Limited observational data gives rise to considerable uncertainty in broad statistics of freshwater availability and withdrawals. Much of the basin is experiencing some degree of water stress. Climate change, despite uncertainty about the detail of its impacts on water resources, is likely to exacerbate many of the challenges. In the Fourth Assessment Report, the Intergovernmental Panel for Climate Change (IPCC) projects that the basin will be affected by severe dry conditions.

Volta Basin

The Volta basin covers the subhumid to semiarid West African Savanna zone. Natural vegetation is characterized by a mosaic of small patches of grassland, woody grassland, forest, cropped fields, short and long fallow fields and wetlands. The major land use of the basin is agriculture with extensive bush fallow cultivation under food crops. The northern savannah contain much less organic matter and are lower in nutrient than the forest soils. The soils consist mainly of savannah ochrosols and groundwater laterites formed over granite and Voltain shales.

Land use land cover change is projected to result in a gradual shift from savanna to cropped fields. It will alter the biogeophysical and biogeochemical feedbacks between the vegetation and atmosphere by increasing surface albedo and reducing near surface momentum and ET. Studies agree that water availability will be further reduced by higher temperatures and increased evapo-transpiration. The overwhelming majority of the population of the Volta basin depends on rain-fed farming for their livelihoods. However, climate change makes rain-fed agriculture increasingly unreliable. Throughout the Volta Basin this will lead to an expansion of irrigated agriculture. The decreasing rainfall in April and an increased duration of the dry season render rain-fed agriculture less reliable. It becomes difficult for farmers to predict the onset of the rainy season and therefore the right time to plant crops. Greater

variability and a general shortening of the rainy season may cause the loss or even failure of crops.

A dominating feature of the basin is Lake Volta, which is the largest man-made lake in the world in terms of surface area. The lake was created to generate hydropower at Akosombo and Kpong (1060MW), which is 100 km north of its estuary. The lake itself has the average surface area about 8,500 km^2 and the full capacity is approximately 150 km^3 [110]. After this dam was completed, the newly stagnant waters not only affected the flow regime of the Volta River but also promoted malaria (from mosquitoes) and schistosomiasis outbreaks in lakeside villages [110]. The change to the natural system in turn requires more effective measures of water resources management to coordinate water use and environmental preservation [110].

Krishna Basin

The Krishna river originates in the Western Ghats of India at an elevation of about 1337 m, about 64 km east from the Arabian Sea and flows for about 1400 km and outfalls into the Bay of Bengal. The climate in the basin is mainly semiarid with some dry and subhumid areas in the Krishna Delta. More than 74% of the annual precipitation occurs during the monsoon (June-October) season. High altitude regions of the Western Ghats receive comparatively more rainfall and have evergreen broadleaf forest. The eastern part of the Western Ghats experience semiarid to arid climate, having mainly tropical dry deciduous vegetation. In addition to this natural vegetation, the Krishna Basin is one of the most intensely cultivated region, with sugarcane and cereals being the major crops. In recent decades, expansion in irrigation has led to a rapid decrease in discharge from the Krishna into the ocean. The cumulative reservoir capacity in the basin approximated the annual runoff volume and resulted in the basin closure in late 1990s [17].

About 93% of total water consumption in the basin is used for irrigation [56]. Water-related environmental problems in the area include: total demand exceeding sanctioned allocations, groundwater depletion from rapid irrigation development, and low runoff generation throughout the basin due to high evapotranspiration [17].

Ganges Basin

The Ganges River Basin is the most populous river basin in the world. Within its 750,000 square kilometers live more than 400 million people. The Ganges River begins in the central Himalayas and flows 2,500 kilometers to the Bay of Bengal. Over the course of millennia, this grand river and its tributaries have formed one of the largest flood plains in the world with the sediments from the erosion of mountainous areas. Flowing across the great alluvial Indo-Gangetic plains, the Ganges is bordered by the Himalayas to the north and the Vindhya-Satpura ranges to the south. The Ganges River basin system remains the main source of freshwater for half the population of India and Bangladesh and nearly the entire population of Nepal [111]. The basin comprises semi-arid valleys in the rain shadow north of the Himalaya, densely forested mountains south of the highest ranges, the scrubby Shiwalik foothills and the fertile Gangetic Plains. Central highlands south of the Gangetic Plain have plateaus, hills and mountains intersected by valleys and river plains. The Ganges and its tributaries provide a perennial source of irrigation to a large area. The important soil types found in the basin are sand, loam, clay and their combinations such as sandy loam, silty clay etc. The area has a typical monsoon climate with a warm and dry season from March to May. A rainy season from June to October follows as does a cool period from November to February. The mean annual rainfall is 2,000 millimeters (mm), of which approximately 70 percent occurs during the monsoon season. Potential evapotranspiration rates are of the order of 1,500 mm and exceed the rainfall rates from November to May. Massive deforestation of the mountain sides has significantly reduced the Himalaya's capacity to absorb the monsoon rains, and it has greatly increased the amount of eroded soil that is carried by the

flood waters.

The Ganges River and its tributaries are the main source of freshwater for Bangladesh, northern India and Nepal [112]. Major water management issues in the Ganges River Basin include increasing water demands, saltwater intrusion, the spread of waterborne diseases, water and soil pollution and threatened fisheries [112]. According to a report by World Wildlife Fund, water withdrawals pose a serious threat to the ecosystems in the basin. Dams regulate the flow from all of the major tributaries of the Ganges, 60% of which is diverted for irrigation.

Huai Basin

The Huai river in east-central China drains the plain between the Huang He (Yellow River) and the Yangtze River (Chang Jiang). The river has a length of 660 miles (1,100 km) and drains an area of approximately 174,000 square kms. The basin lies between the temperate and tropical climate zones in central China. The northern part of the basin is dry while the southern part is wet. The tropical rain belt causes additional rainfall during the monsoon season. The main rainfall season occurs from late June to mid-August.

Agriculture requires irrigation in the dry season and flood control in the wet season. The river has changed its course many times over the years and no longer flows into the Pacific Ocean, ending instead in Lake Hongze. The major summer crops grown in the Huai River basin include single crop rice, corn, and cotton. A growing population has aggravated long-standing flood control, wastewater discharge, water pollution and drought problems. Flooding is very common during the summer monsoon season. As a result, an elaborate and highly efficient water management system of canals, dikes, reservoirs, and water gates have been constructed to cope up with the problem. At present, water allocation conflicts between upstream and downstream users and wastewater reuse are the major concerns.

Chapter 3

Understanding Time Scales of Hydrologic Dynamics: Wavelet Analysis Approach

3.1 Introduction

The previous chapter described the hydrologic model and the general characteristics of the nine selected river basins from different hydro-climatic regions. The basins are so selected as to compare and contrast the impacts of climate and land use-land cover change on the hydrologic dynamics. In order to develop a predictive understanding of the seasonal hydrologic dynamics under climate and land use land cover change, it is important to first understand the time scales of hydrologic dynamics in the basins and to assess the ability of the hydrologic model to capture the variability of governing processes. We will explore and examine the dominant runoff processes in the selected basins using wavelet analysis approach.

The dominant runoff process for a basin is the process that contributes most to runoff for a given rainfall event. The identification of the dominant runoff processes allows detailed insights in the runoff generation of a basin. Four different dominant runoff processes are distinguished as Hortonian overland flow (HOF) due to infiltration excess, saturation overland flow (SOF) due to saturation excess, lateral subsurface flow (SSF) in the soil and deep percolation or groundwater recharge (DP). HOF reacts rapidly to precipitation, SOF producing areas first have to be saturated and show therefore a delayed reaction. More delayed but faster than usually assumed due to preferential flow is SSF. Areas with high infiltration rates and storage capacities or percolation into the bedrock contribute little to storm runoff. Based on geo-information of soils, geology, topography, and land use, as well

as rainfall and infiltration characteristics, different runoff processes dominate over different regions. The identification of dominant runoff processes requires a good understanding of the structure and variability of the hydrological processes [113].

Since different basins respond differently to the same change in climatic drivers, depending largely on basin's geographical and hydro-geological characteristics, the objective of this chapter is to identify if the dominant runoff-generating processes in the selected basins are being captured by the model. We would like to seek what inferences can we make about the hydrological behavior in the selected basins, on the basis of available precipitation and runoff time series. This study presents a unique approach in using wavelets as a tool to explore and explain the differences in hydrologic characteristics of the selected basins from humid, mediterranean and semi-arid regions.

Wavelet transforms expand time series into time frequency space and can therefore find localized intermittent periodicities [51]. The wavelet power spectrum of a given time series provides a highly compressed and integrative picture of the underlying processes. A theoretical description of wavelet analysis can be found in [114]. Wavelet analysis is used to facilitate the understanding of both global and local scale hydrologic processes [115, 51]. For example, the transformation of precipitation into runoff involves many physical processes which are highly non-linear and exhibit wide variability over a broad range of scales. Besides seasonal time scale, there are several factors which interplay at multiple time scales to affect the hydrologic response of a given region. It is important to characterize the time scales of interaction of hydrologic processes to better understand how the different factors of change will alter the hydrologic balance of a given region. For example, mediterranean and semi-arid regions are frequently affected by extreme weather events (flash floods, droughts) where the ability to predict such dramatic events remains weak because of the contribution of very fine scale processes and their non-linear interactions with the larger scale processes

[116]. Soil permeability, topography and land use-land cover are the important factors governing hydrologic response at a range of time scales. Knowledge of the underlying hydrologic processes at various scales is required to reduce the uncertainties in design and analysis and for effective water management.

Hydrologic processes have complex non-linear structure with multi-scale features and short lived transient components [51]. Most traditional methods that examine periodicities in the frequency domain, such as Fourier analysis, implicitly assume that the underlying processes are stationary in time. However, hydrologic processes (precipitation, runoff, evapotranspiration) are non stationary processes which can be better understood in a time frequency space [48]. Examining time series data in time frequency space leads to a much better understanding of the underlying processes because it leads to identification of different phenomena characterizing the hydrologic behavior at different scales.

There are several studies which have focused on hydrologic signal fluctuations and understanding of physical processes that operate under a large range of scales varying from one day to several decades both for rainfall rates [117, 46] and runoff rates [118]. However, there are very few studies for the scale variability of relationship between the rainfall and runoff rates. Scale dependence of the relationship reveals underlying dynamics of the processes involved. For example, the time lag between rainfall and runoff rates illustrate the response of underlying processes governed by the soil storage, basin slope and infiltration capacity. The knowledge of the dominant runoff generation processes allows one to identify the hydrologic variables that need to be monitored in order to derive important indications about the state of the basin from a hydrological point of view [119]. An improved understanding of when runoff is triggered, in what quantities and under what condition is useful to evaluate and help mitigate problems, such as soil erosion and non-point source pollution [120]. The cross wavelet analysis provides a time-scale distribution of the correlation between two signals [47],

which is used here for examining the relationship between two time series in time frequency space.

In this chapter, we derive the continuous wavelet transform and examine the phase relationship between precipitation and runoff using cross wavelet transform to understand the governing runoff generation processes. The dominant factors controlling the hydrologic response are investigated and compared among the basins selected from Mediterranean (California and Orange River Basin), Semi-arid (Western Gulf of Mexico and Krishna River Basin) and Humid (Congo and Ohio) regions. Each basin represents a unique climatic zone, topography, vegetation and soil cover. Results focus on identification of multiple time-varying frequencies and the details of local, non-periodic and multi-scaled processes. The phase relationship between precipitation and runoff reflects the dynamics of governing hydrologic processes in the basin.

3.2 Methodology

3.2.1 Continuous and Cross Wavelet Transform

Wavelet analysis is used to determine the frequency (or scale) content of a signal and to assess and determine the temporal variation of the frequency content [121]. Because of its localization properties in both time and scale, the wavelet transform allows tracking of the time evolution of processes at different scales in the signal. Basics of wavelet analysis is given in Appendix. The detailed introduction and comparison of fourier transform and wavelet analysis can be found in [51] and [47].

A wavelet is a function with zero mean that is localized in both frequency and time. There are two classes of wavelet transforms; the Continuous Wavelet Transform (CWT) and its discrete counterpart (DWT). The DWT is a compact representation of the data and is par-

ticularly useful for noise reduction and data compression whereas the CWT is better for feature extraction purposes. The Morlet wavelet is used for analysis because it provides a good balance between time and frequency localization and is most suitable for feature extraction purposes. The idea behind the CWT is to apply the wavelet as a bandpass filter to the time series [48]. The CWT of a time series (X_n, n=1,. . . ,N) with uniform time steps dt, is defined as the convolution of X_n with the scaled and normalized wavelet. The wavelet power is defined as $[W^X]^2$ and the complex argument of W^X is interpreted as the local phase. The CWT has edge artifacts because the wavelet is not completely localized in time. Therefore, a Cone of Influence (COI) is defined, where the wavelet power caused by a discontinuity at the edge has reduced to a certain value at the edge.

CWTs of two time series are used to construct the Cross Wavelet Transform (XWT) which determines if the two time series are linked in some way. The cross wavelet transform (XWT) of two time series X_n and Y_n is defined as $W^{XY}=W^X W^{Y*}$, where W represents the CWT of given time series and $*$ denotes complex conjugation. The cross wavelet power is defined as the absolute value of W^{XY}. The complex argument $\arg(W^{XY})$ can be interpreted as the local relative phase between X_n and Y_n in time frequency space. XWT exposes the common power of two time series and relative phase in time-frequency space. The software package developed by Grinsted et al.(2004) [48] is used to perform the wavelet transforms (http://www.pol.ac.uk/home/research/waveletcoherence/). The relative phase relationship between two time series is shown as arrows with in-phase pointing right, anti-phase pointing left and time series X_n leading Y_n by 90^o pointing straight down.

3.3 Results

3.3.1 Identification of Dominant Temporal Scales

Fig. 3.1 presents the twenty five year (1976-2000) time series data of precipitation, runoff and evapotranspiration (ET) over the Krishna River Basin alongwith the Continuous Wavelet Transform (CWT) of each time series. CWT plots wavelet power in units of normalized variance where the power, the frequency and the time are present in a representative space. The thick black contour designates the 5 % significance level against red noise and the cone of influence (COI) is shown as a lighter shade. Wavelet spectral power is maximum for the annual cycle (dominant red band) for all the three water balance components (precipitation, runoff and ET). Besides strong annual pattern in the broad range of 256 to 512 days, strong seasonal and inter-annual patterns are observed. As compared to precipitation, runoff response shows strong intermittent seasonal variability though a similar consistent annual temporal pattern is observed. The seasonal variability of ET is comparatively less dominant. High frequency response and inter-annual variability is similar for both precipitation and runoff. A number of shorter-term temporal patterns are noticed within 50 days, which are explained by high intensity precipitation events during the monsoon season.

3.3.2 A Comparative Overview of Precipitation-Runoff response over Semi-arid Basins: Krishna and WGM

Fig. 3.2 shows the continuous wavelet transform (CWT) for annual variation of precipitation and runoff over the Krishna and WGM basins. There are two peaks observed for the precipitation over Krishna basin, one characterizing the onset of southwest monsoon from the Arabian Sea in June and another peak in Aug. representing the northeast monsoon from the Bay of Bengal. In the time frequency space(CWT of precipitation), we can see the presence of two dominant high frequencies of 8-12 day for short time periods and a

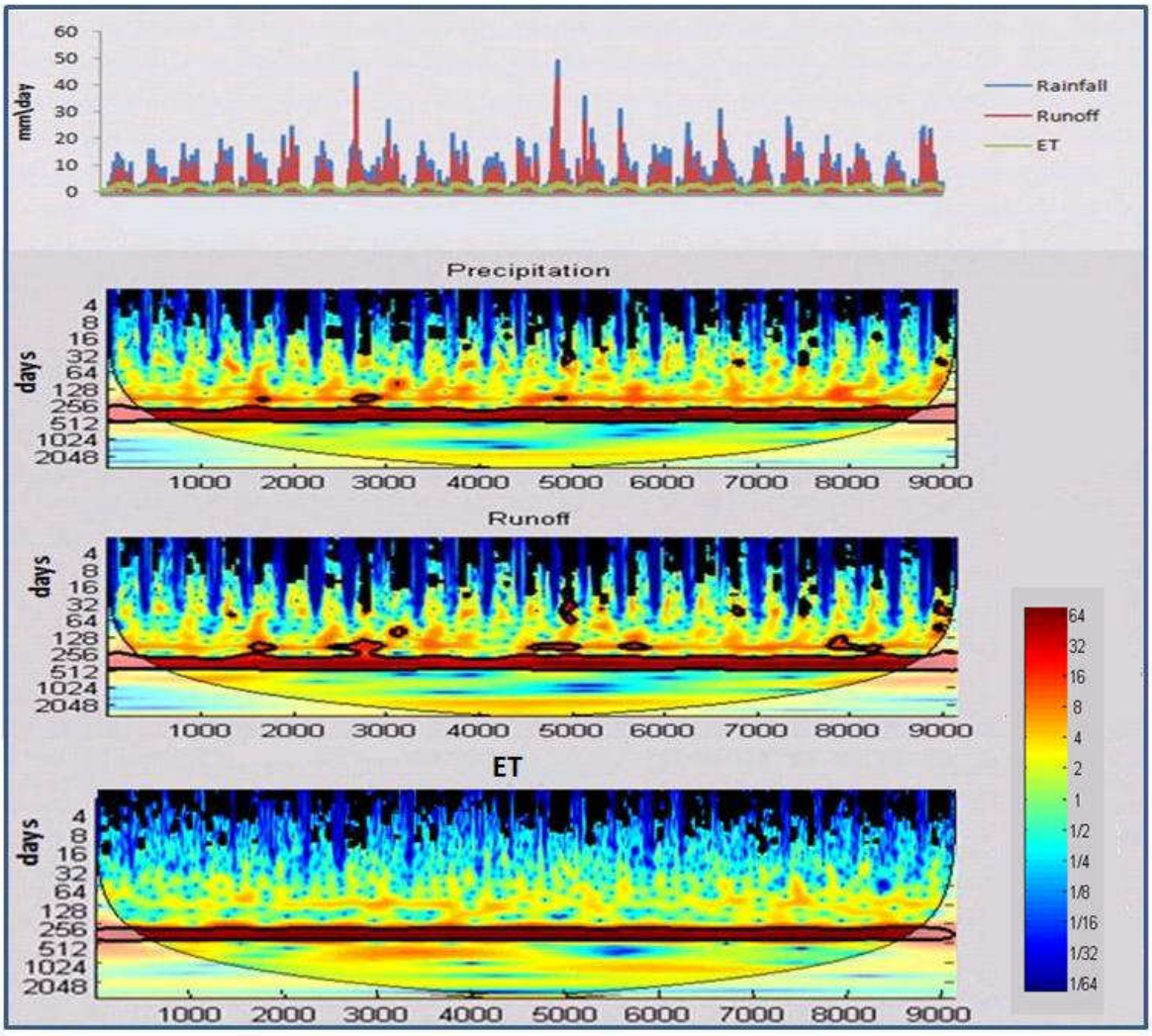

Figure 3.1: Twenty five year daily time series (1976-2000) and continuous wavelet transform (CWT) of Precipitation, Runoff and ET over the Krishna Basin.

dominant low frequency band of 30-60 day for the monsoon season from June to September. Over WGM, intense localized precipitation results from the southerly winds off the Gulf of Mexico. Similar to Krishna basin, two dominant high frequency signals between 8-16 day period and a low frequency signal of 32-64 day period is observed for both precipitation and runoff time series of the WGM basin.

Fig. 3.3 presents the Cross Wavelet Transform (XWT) of precipitation and runoff over the Krishna and WGM basins respectively. The in-phase linear relationship between precipitation and runoff reflects the dominance of fast surface runoff process. Due to low permeability of the topsoil (clay texture), the precipitation intensity exceeds the maximum infiltration rate of the soil during intense storm events, leading to Hortonian overland flow as the dominant runoff process. A significant portion of saturation excess flow also occurs after large storm events. Comparing the XWT plots for WGM and Krishna basins, in-phase linear relationship between precipitation and runoff upto the 30 day time scale is observed for both the basins as representative of Hortonion runoff mechanism. A phase lag is observed for the 30-60 day time period for the dominant low frequency response over the WGM basin. As compared to Krishna, WGM has a higher percentage of sand than clay cover which is one of the factor responsible for delayed runoff response in the basin since sandy loam has comparatively higher permeability and storage capacity than clay.

Modeling the hydrologic processes of semiarid basins is specially challenging due to the specific characteristics of this type of environment. The discontinuity of the processes both in space and in time produces a highly complicated rainfall-runoff relationship. Runoff production and reinfiltration areas produce a discontinuous spatial pattern of runoff. The hydrological connection of the different parts of the basin produces a nonlinear and complex hydrologic behaviour because different response mechanisms of the basin are triggered as the hydrological connectivity increases [120].

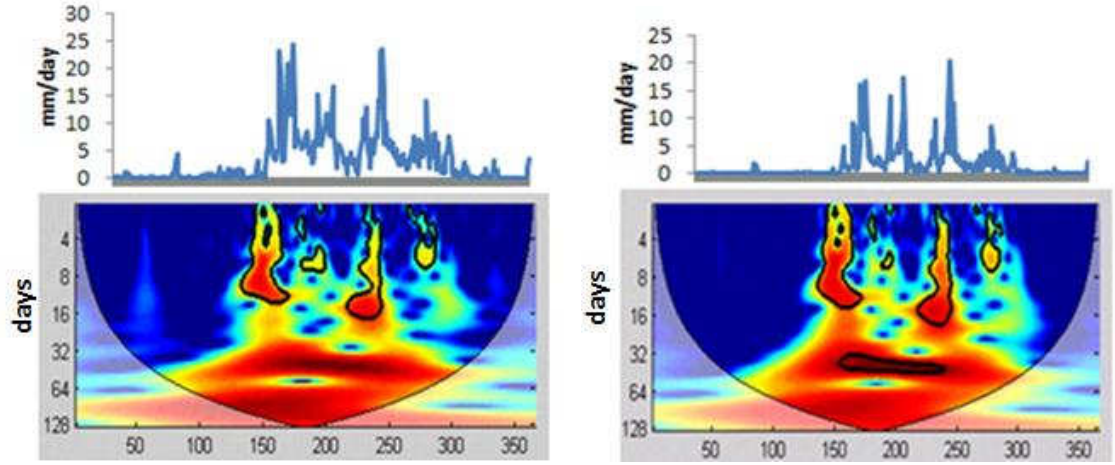

(a) CWT of Precipitation over Krishna

(b) CWT of Runoff over Krishna

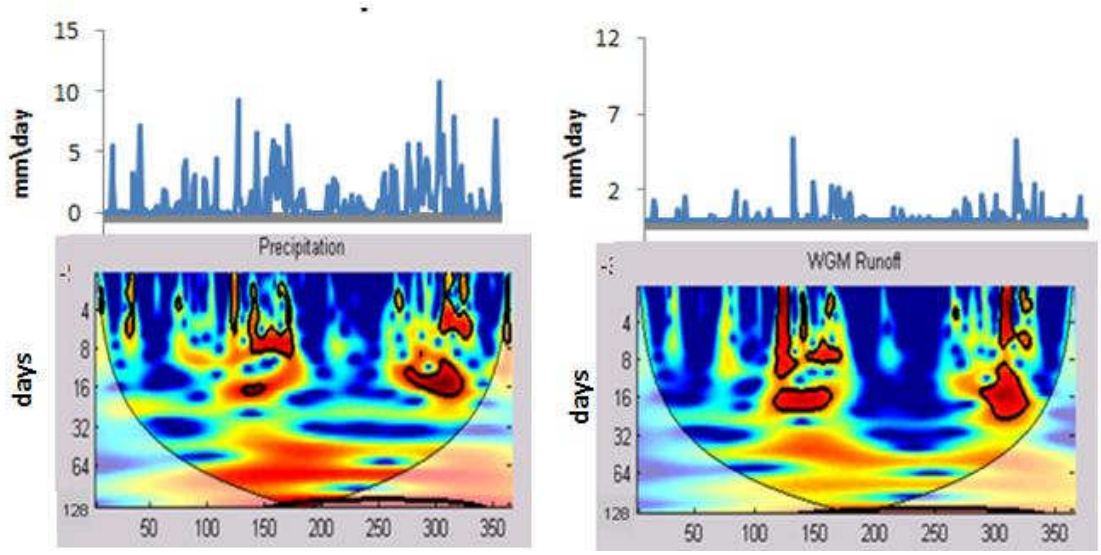

(c) CWT of Precipitation over WGM

(d) CWT of Runoff over WGM

Figure 3.2: A comparative overview of semi-arid basins: Krishna and WGM

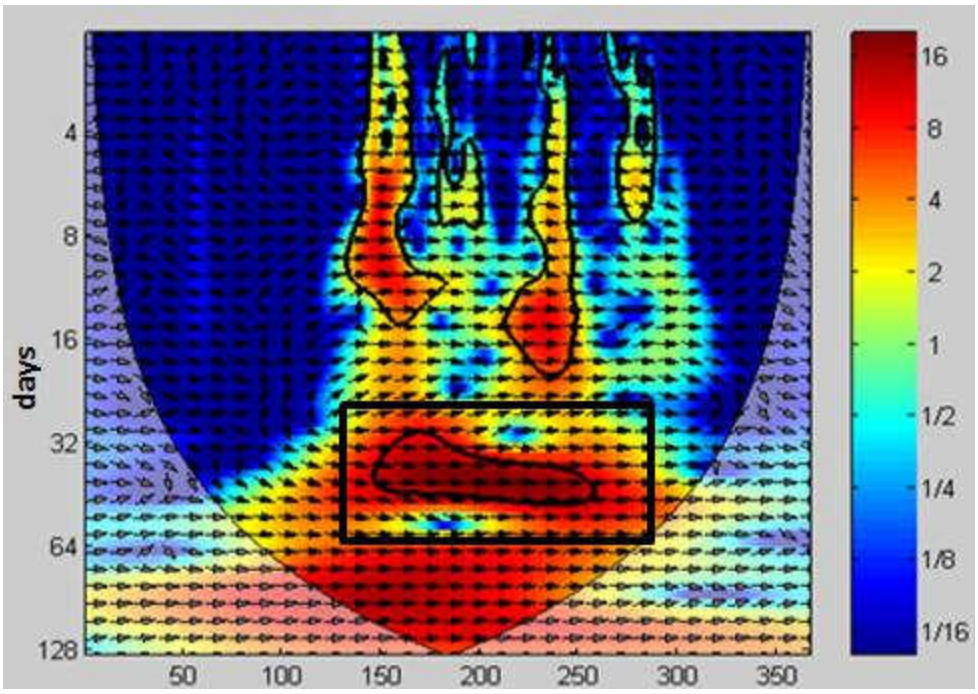

(a) Cross Wavelet Transform (XWT) of Precipitation and Runoff over Krishna River Basin

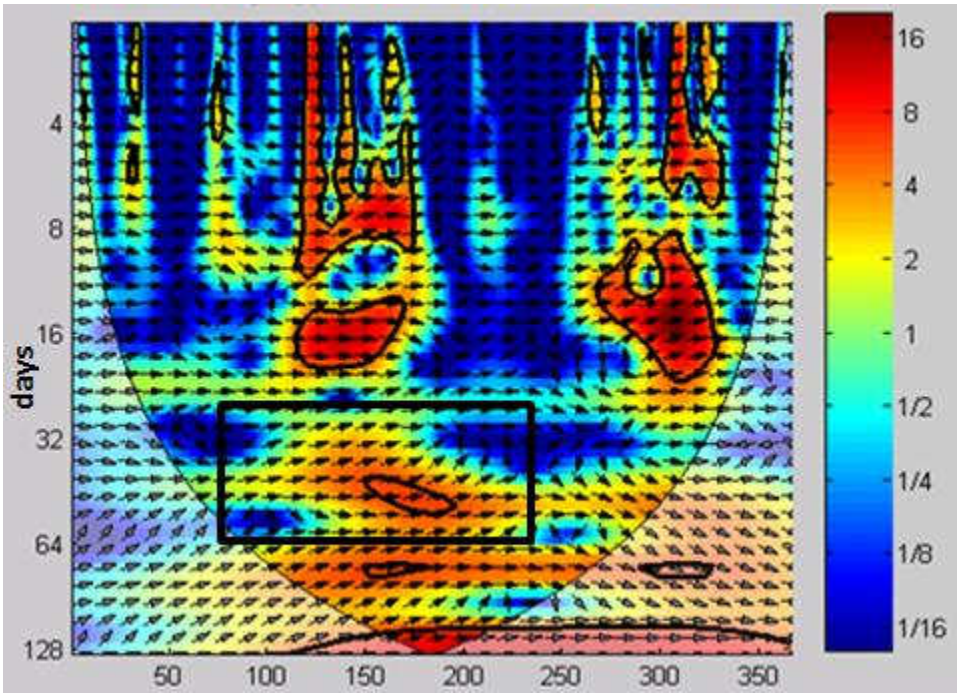

(b) Cross Wavelet Transform (XWT) of Precipitation and Runoff over WGM River Basin

Figure 3.3: A comparative overview of precipitation-runoff response over semi-arid basins: Krishna and WGM. The relative phase relationship between precipitation and runoff is shown as arrows (with in-phase pointing right, anti-phase pointing left and precipitation leading runoff by 90^o pointing straight down)

3.3.3 A Comparative Overview of Precipitation-Runoff response over Mediterranean Basins: California and Orange

California basins are characterized by Mediterranean climate, with cool rainy winters and dry summers. Wavelet spectrum plot shows high power during the winter time period for both precipitation and runoff (Fig.3.4). High frequency response of 4-12 day period is observed along with the low frequency response of 32-64 day period during the rainy winter season. As compared to California, Orange basin shows a delayed time-lag response at longer time scales (Fig.3.7). Runoff generation process is strongly affected by the heterogeneous distribution of the infiltration capacity of the basin.

Various characteristic features of Mediterranean basin hydrology have been pointed out by several studies [122, 123] where results emphasize the diversity of hydrologic processes governing the runoff formation, depending on basin characteristics, antecedent hydrologic conditions and characteristics of the rainfall events. Soil moisture appears to play a more important role than storm patterns for runoff generation during low and medium intensity storms, particularly in the wet season, due to its role in increasing the hydrological connectivity between hillslopes and the channel network [124]. It is shown for the Mediterranean forests that interception losses are greater when the precipitation patterns are more frequent and of low intensity rather than being abundant [122].

3.3.4 A Comparative Overview of Precipitation-Runoff response over Humid Basins: Congo and Ohio

In humid regions, permeability of the soil is high because the vegetation cover protects the soil from rain packing and creates an open soil structure. Under such conditions, rainfall intensities generally do not exceed infiltration capacities and consequently Hortonian overland flow does not occur. Fig. 3.6 shows the CWT for annual variation of precipitation

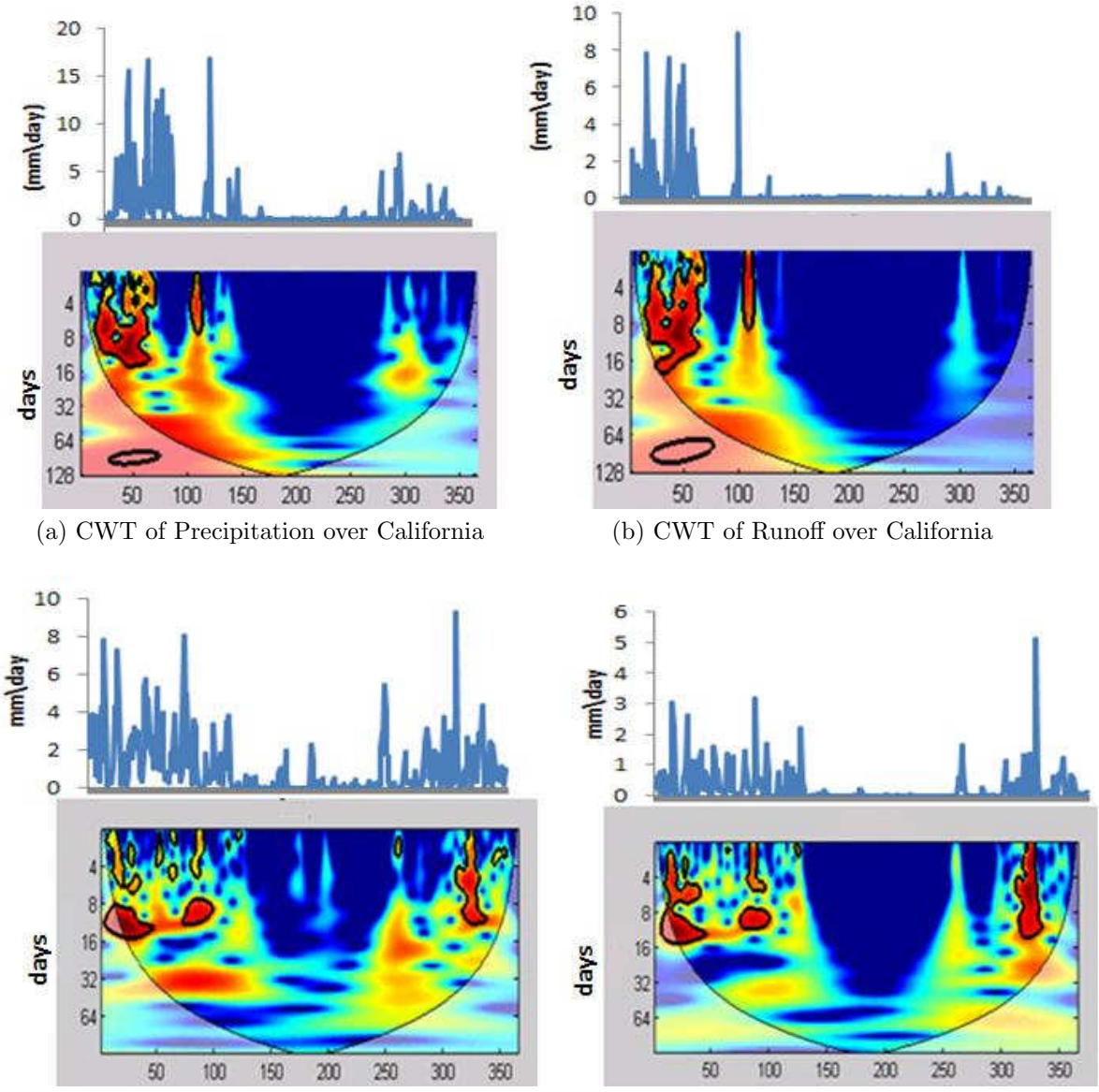

(a) CWT of Precipitation over California

(b) CWT of Runoff over California

(c) CWT of Precipitation over Orange

(d) CWT of Runoff over Orange

Figure 3.4: A comparative overview of mediterranean basins: California and Orange

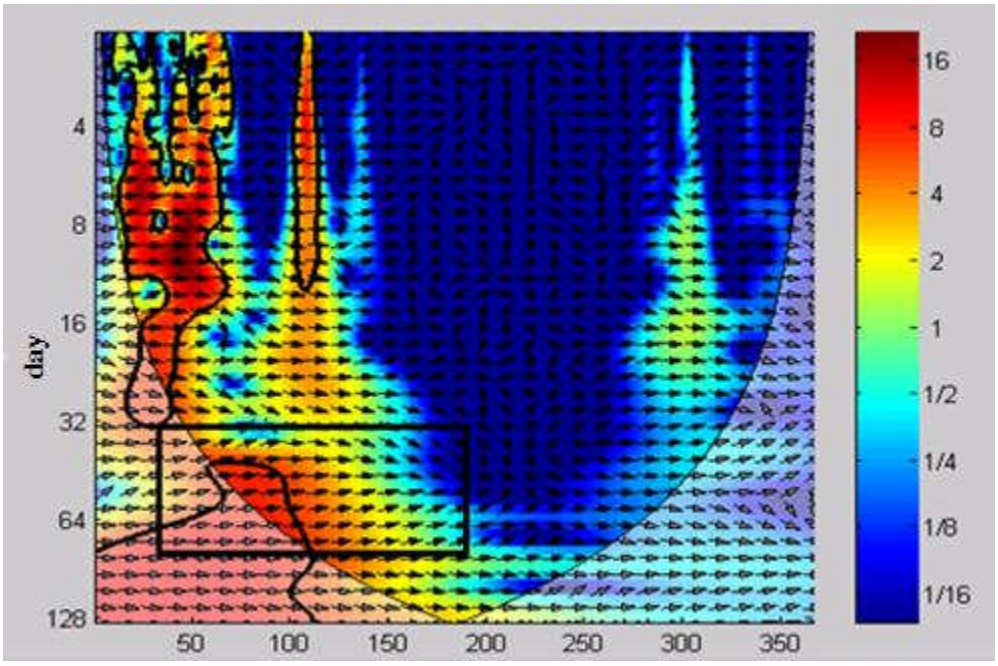

(a) Cross Wavelet Transform of Precipitation and Runoff over California Basins

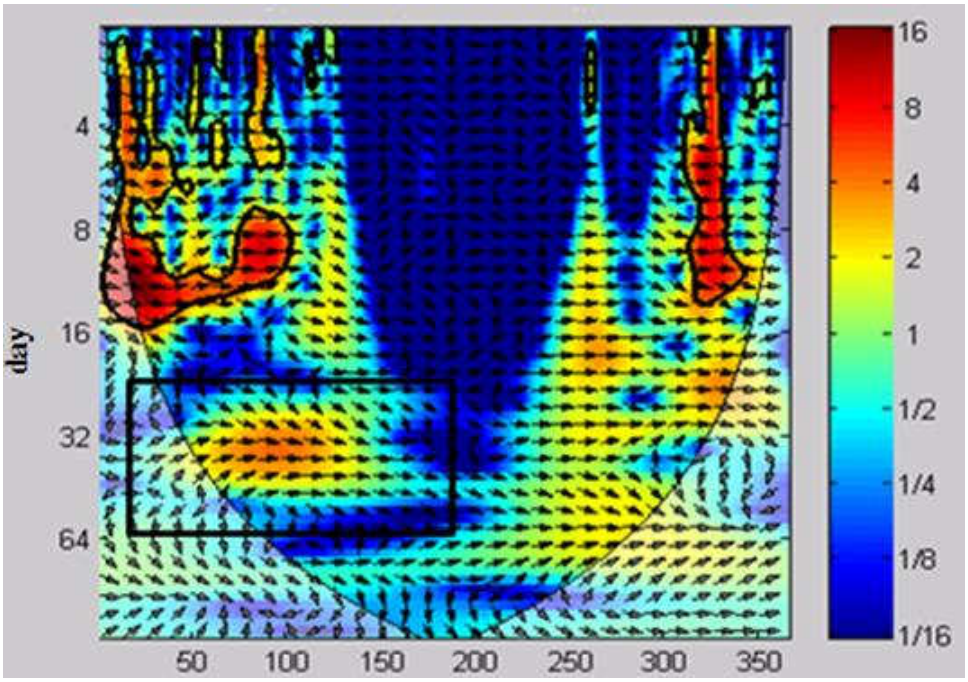

(b) Cross Wavelet Transform of Precipitation and Runoff over Orange River Basin

Figure 3.5: A comparative overview of precipitation-runoff response over mediterranean basins: California and Orange

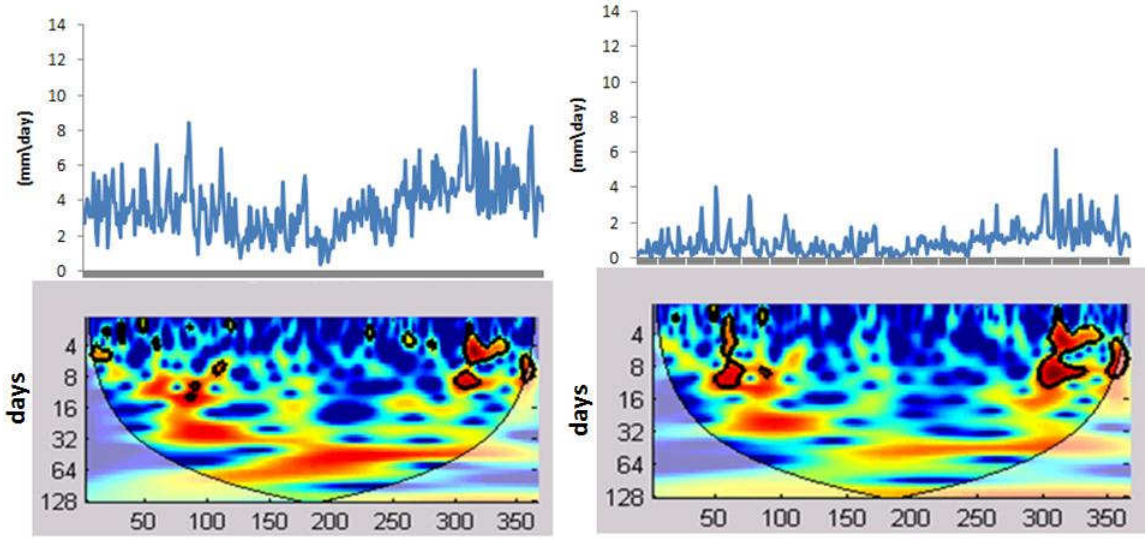

(a) CWT of Precipitation over Congo

(b) CWT of Runoff over Congo

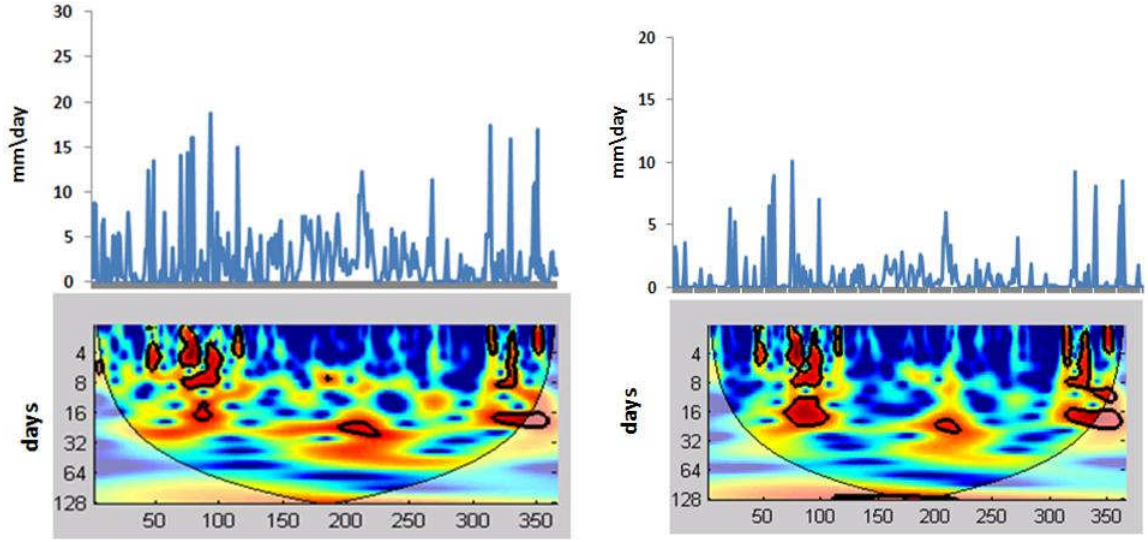

(c) CWT of Precipitation over Ohio

(d) CWT of Runoff over Ohio

Figure 3.6: A comparative overview of humid basins: Congo and Ohio

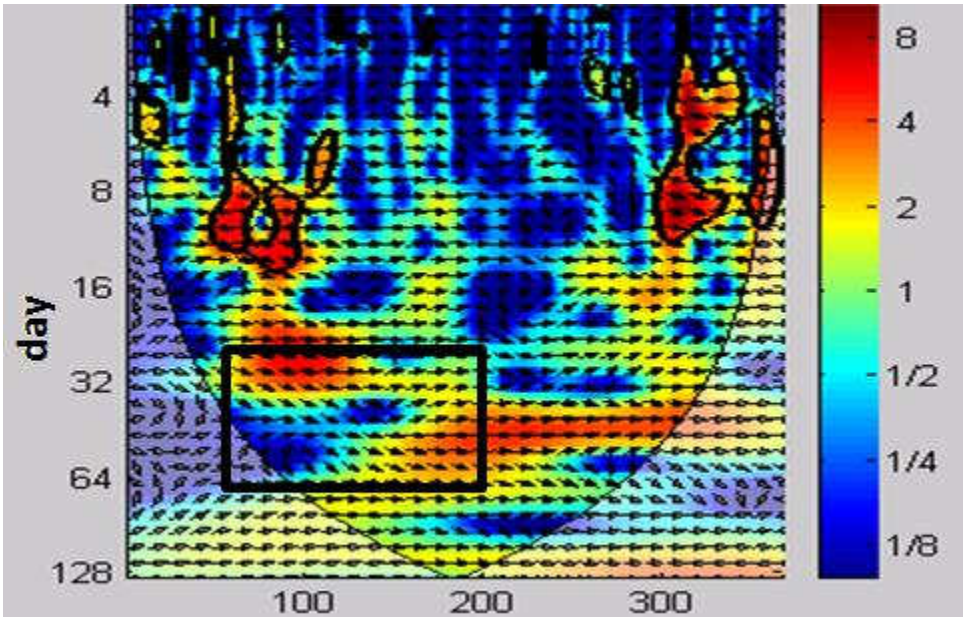

(a) Cross Wavelet Transform of Precipitation and Runoff over Congo Basin

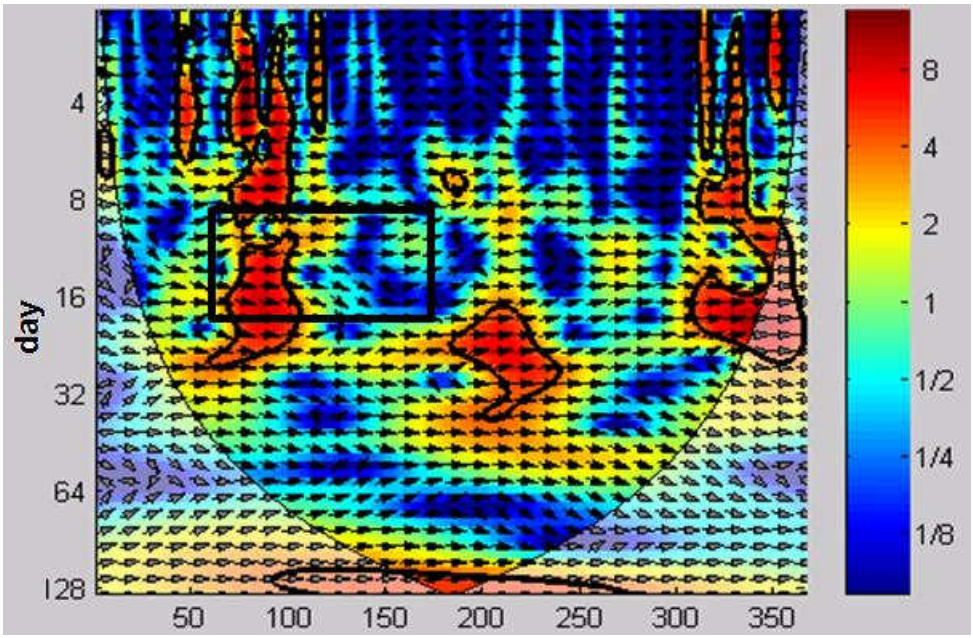

(b) Cross Wavelet Transform of Precipitation and Runoff over Ohio River Basin

Figure 3.7: A comparative overview of precipitation-runoff response over humid basins: Congo and Ohio

and runoff over the Congo and Ohio basins respectively. The basins are characterized by uniform precipitation distribution with no seasonal variability. Soil remains saturated most part of the year and leads to generation of subsurface runoff. Among others, the parameter that seems to play a major role in the dynamics of runoff production in these basins is the coefficient of soil water loss that depends on evapotranspiration [125]. Congo has the second largest rainforest area in the world where evapotranspiration governs the hydrologic dynamics. The soil has high permeability with high storage capacity as a result of deeper bedrock layer and a greater percentage of sand cover. However, the results do not show a delayed relation between precipitation and runoff as was expected. The model is not being able to capture the deep layer soil moisture dynamics in this basin.

The soil moisture spin up is very important in the land surface modeling and the spin-up time of soil moisture varies with the depth of soil layers. The deeper a soil level is, the longer the soil moisture takes to reach its equilibrium state. Du et al. (2009) [126] reports that the adjusting time of soil moisture in shallow layers (0.7 to 6.2 cm) is very short (less than one year) to reach equilibrium state because temperature and precipitation can quickly affect the soil moisture in these layers. In middle layers (11.8 to 36.6 cm), the adjustment time is much longer (about 10 years). The equilibration time is as many as 20 years in the layers below 1.5 m. Du et al. (2009) used Common Land Model (CLM) to show that the soil moisture is sensitive to its initial condition in the land-process model and that a long spin-up process is necessary in climate-modeling studies related with land hydrological processes. However, we used a two year spin up strategy for initialization of soil moisture in all the study basins. Therefore, there may exist errors between the actual and the simulated soil moisture in the deeper soil layers than in the shallow layers. Study by Song et al. (2009) [127] showed improvements in the result of sensible and latent heat fluxes by replacing the initial soil moisture to observed soil moisture conditions. Several studies conclude that better representation of the soil moisture can improve the model performance to a large degree.

3.4 Summary and Conclusions

There is a need for more complete understanding and characterization of the processes involved in the rainfall-runoff processes at different basin scales, under different climatic conditions and physiographic characteristics of the drainage basin [128, 113, 129].

The dominant factors controlling the hydrologic response are investigated and compared here among the basins selected from Mediterranean (California and Orange River Basin), Semi-arid (Western Gulf of Mexico and Krishna River Basin) and Humid (Congo and Ohio River Basin) regions. For Semi-arid regions, the precipitation is small and hence the amount of runoff is much more dependent on soil and vegetation characteristics of the region where different factors like soil permeability, topography and vegetation cover interplay at multiple time scales to affect the hydrologic response. Temporal frequencies and relationships among the governing hydrologic processes are identified using the time series of precipitation and runoff over the study basins. A time and scale resolved measure for the relationship between the two time series is evaluated using the continuous and cross wavelet transforms. The analysis of hydrologic time series over different periods of time show that the model can capture the dominant governing processes. However, the model requires a longer time period to capture the deep layer soil moisture dynamics as the deeper a soil level is, the longer it takes for the soil moisture to reach its equilibrium state.

The wavelet energy spectrum shows that the annual period is dominant for all the hydrologic components. Local processes blocked by the dominant global trends in the time series datasets are analyzed. High frequency runoff peaks are attributable to fast runoff processes resulting from the Hortonian overland flow during the wet season in semiarid basins. Since soils in the Krishna basin are shallow and clayey, more water gets stored as soil moisture and with flat topography of the basin, surface runoff gets promoted as the dominant

runoff generating process. Limited storage capacity of the soil results in saturated overland flow at longer time scales. Soils in the WGM basin have a higher % of sand than % of clay leading to higher permeability and storage capacity as compared to the Krishna basin. The obtained results show that the model is able to capture the interscale variability of hydrologic processes in the wavelet spectral domain quite realistically. The proposed wavelet analysis approach opens interesting insights into the relationships between basin properties, dominant hydrological processes and model concepts.

The complex associations between soil characteristics (depths and hydraulic properties), topography, and vegetation cover are more complicated to generalize for large basins. Additional processes associated with the spatial discontinuity of channel flow, permeable channel beds, high rates of evaporation and a lack of antecedent baseflow contribute to complex spatial variability at larger scales. As such it becomes extremely difficult to develop any generalisations about patterns of runoff generation over large river basins. Moreover, the controls on hydrologic response vary across the seasons and with respect to different time scales. More process-orientated research is needed to better identify runoff generation mechanisms.

Chapter 4

Assessing Water Use Effects on Hydrologic Discharges at the River Basin Scale[1]

4.1 Introduction

Human interferences significantly affect the hydrologic processes in different regions of the world. Therefore, quantification of the impact of human influence is essentially required for developing a predictive understanding of the hydrologic dynamics under climate and land use-land cover change scenario. Human activities interfere with hydrologic systems in both direct and indirect ways at various spatial scales. Direct impacts include dam and reservoir operation, surface and groundwater withdrawals for agricultural, municipal and industrial uses, return flows from these uses, and sustenance of baseflow during dry periods. Meanwhile, changes in land use land cover, from either immediate transformations in land use (e.g., urbanization) or gradual land degradation (e.g., soil erosion) indirectly interferes the hydrologic processes, in particular infiltration, surface runoff, and the rate of evapotranspiration into atmosphere.

In recent years, these human impacts have increasingly become a significant component of the hydrologic cycle. In the world, 54% of the rivers that are geographically and temporally accessible to human beings have been developed for different purposes [130]. It is insufficient to study only the natural hydrological cycle in river basins where human impacts on natural hydrologic processes are already very pronounced [131]. Therefore, human

[1]This chapter is under review in the Journal of Advances in Water Resources. This is a joint work with Ethan Yang as the first author.

impacts should be considered along with the impacts of climate, soil, vegetation and topography when applying the models for hydrologic simulation.

Studying and predicting the effects of indirect human interferences, such as the effects of land use-land cover change on the timing and magnitude of runoff has been a major focus of hydrologic research [28, 90, 132, 133]. However, assessing the indirect interferences is not the focus of this chapter. Recently, many efforts are being made to incorporate direct human interferences, such as reservoir operation [13], water withdrawals and return flows [15], groundwater pumping [14], and irrigation [57, 134, 38], into hydrologic simulation models. A number of studies have combined water supply and demand assessments based on datasets and models at a global scale [58, 59, 135, 16]. However, few of these modeling studies simulate hydrologic processes in a way that allows modifications from human water use on natural hydrologic processes to be detected.

This study assesses the interferences of human activities on hydrology of nine selected river basins through a coupled hydrologic-water management modeling framework. The Common Land Model (CLM) [96], a physically based distributed land surface model, is used to evaluate the hydrologic response in different hydroclimatic regions of the world. The model estimates basin discharge as governed by the basins topography, soil type, vegetation cover and climate, but does not take the aforementioned direct human interferences into account. The details of CLM model simulation are described in the second chapter. To account for the direct human interferences on observed discharge, the results of CLM are input into the Water Availability and Supply Model (WASM), a water resources management model developed by [16]. The WASM adjusts the naturally occurring discharge from the CLM by considering irrigation, industrial and municipal water withdrawals and return flows, and by considering the minimum required streamflow to preserve aquatic ecosystems. A number of indicators are computed from the results of this coupled model, including: 1) criticality ratio

[136], 2) water use regime [137], and 3) Budyko curve [138, 139], which relate water use levels to hydrologic and climatic parameters. These indicators can be used to derive implications for water management regarding both human and ecosystem water requirements.

4.2 Model Description

The hydrologic model was described in Chapter 2. Here, we describe the water management model and the human interference indicators used in the study.

4.2.1 Water Availability and Supply Model (WASM)

WASM represents each river basin by a node-link network and incorporates human interference through the interactions between water supply and demand nodes. It adjusts the naturally occurring discharge by considering irrigation, industrial and municipal water withdrawals and return flows, while meeting the ecological requirements. The WASM divides the world into 124 major basins featured with specific combinations of human and natural characteristics. These major basins are also named as "Hydro-Economical Zone" [16].

Each basin is represented by a node-link network (Fig.4.1).This network includes four source nodes: 1) surface water drainage units (SWDU), 2) river nodes (RD) representing reaches of the main river or tributaries; 3) groundwater sources (GWS), treated as single tanks, and 4) reservoirs (RSV) that represent the total combined storage available in all reservoirs within the basin under study. The network also includes three types of demand nodes: 1) food production units (FPU) for irrigation water demand; 2) non-agricultural water demand units (NAWU) for municipal and industrial water demand; and 3) riverine ecological units (REU) with minimum flow requirements. The links in the network include: 1) streamflow paths such as river channels; 2) water supply-demand paths such as diversion channels; 3) interactions between surface and ground water; and 4) return flow paths from both water

use and source nodes. A detailed description of the WASM is given in [16]. The WASM [16] was originally developed using data from 1995. The International Water Management Institute (IWMI) revised the model structure and changed the baseline year from 1995 to 2000.

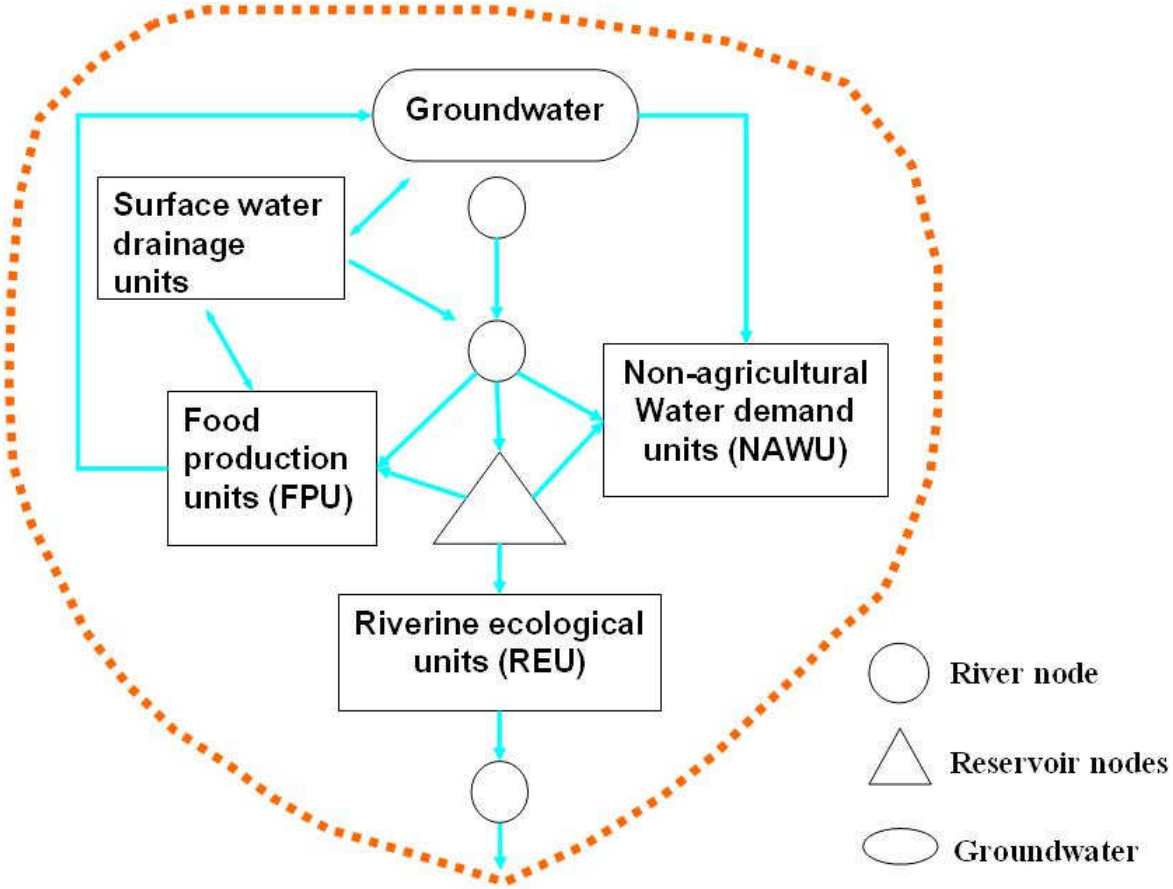

Figure 4.1: The node-link structure of WASM

The WASM has a number of parameters that must be estimated. These parameters are: basin efficiency, committed environmental flow, domestic water demand elasticity and twelve other parameters for industrial water demand [16]. Basin efficiency is the water use efficiency assessed at the river basin scale, considering the reuse of return flow [140], which is defined as the beneficial water consumption of the total consumption in the whole basin. Committed flow is the quantity of water that is reserved for environmental and instream

use and is unavailable for human use. Industrial water demand is calculated by multiplying the gross domestic product (GDP) of the industrial sector by a water use intensity (water use per unit of GDP), the latter of which is developed as a linear function of per capita GDP and water use technology [16]. Domestic water demand elasticity is estimated as a function of population, GDP, and income elasticity [16]. Since estimates for these parameters are unavailable from data, they are estimated through calibration. Tabu Search [141], a heuristic algorithm, is used to calibrate the model parameters. This algorithm is based on the notion that humans behave in certain ways when faced with similar circumstances. This algorithm starts with an initial value and searches for the best solution within a user-defined neighborhood of the initial solution. This solution then serves as the initial value in the subsequent iteration. The results from previous steps are treated as memory. Thus, with the tabu mechanism, the algorithm learns from the previous results stored in the memory, which helps to overcome the local optimum and proceed to the global optimum.

Tabu Search has been applied to model parameter estimation in prior water resources studies. For example, [142] applied it to find the least-cost design of looped water distribution networks while [143] used it to identify the spatial distribution of groundwater hydraulic conductivity in a confined aquifer. In this study, Tabu Search is combined with WASM to calibrate the model by searching for appropriate values of the model parameters described above.

Observed stream discharge data is required to calibrate WASM. In this study, discharge data for streams located in the United States were obtained from the United States Geological Survey (USGS) while the Global Runoff Data Centre (GRDC) data archive was used for the other basins. The observed discharge data from GRDC was extracted from the Global Terrestrial Network for River Discharge (GTN-R), which collects near real-time discharge data from national agencies with a discharge data monitoring mandate and redistributes the

data in a standardized format [144].

WASM uses year 2000 as the baseline, therefore, it utilizes the results from CLM for that year. The estimated surface discharge and groundwater recharge from CLM, are subsequently used as inputs in WASM. The WASM simulation incorporates human interference through the interactions between water supply and demand nodes. The outputs of WASM include water withdrawal, return flow and the basin discharge. The connections within the coupled model framework are shown in Fig.4.2.

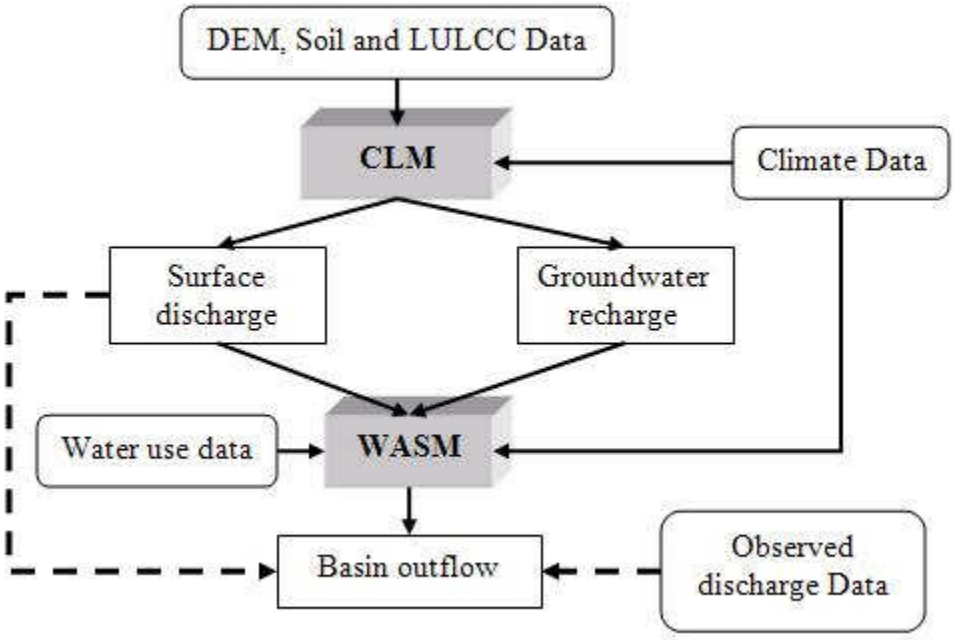

Figure 4.2: The framework of the coupled models: CLM and WASM.

4.3 Human Interference Indices

The outputs from both the CLM and WASM allow the computation of four indices that quantify the degree of human interferences with hydrologic processes in a particular river basin: the criticality ratio (CR) [136], depletion ratio (DR), human impact ratio (HR) and

outflow ratio (OR):

$$CR = WaterWithdrawal/TotalRenewableWater \tag{4.1}$$

$$DR = (WaterWithdrawal - ReturnFlow)/TotalRenewableWater \tag{4.2}$$

$$HR = (WaterWithdrawal + ReturnFlow)/TotalRenewableWater \tag{4.3}$$

$$OR = BasinOutflow(Discharge)/TotalRenewableWater \tag{4.4}$$

in which the total renewable water is the sum of surface discharge and groundwater recharge estimated from the CLM.

Two additional methods are further used to analyze the human interferences on the hydrologic processes, i.e., the water use regime [137] and Budyko curve [138, 139]. A study by Weiskel et al.(2007) [137] plots water withdrawals versus return flows by month, which shows how much water is diverted and how much is consumed during a given month. The original Budyko curve describes the patterns observed amongst the climate, evapotranspiration and runoff and has proven to be a useful model for predicting catchment energy and water balances [145]. We used the concept to integrate climate information to the analysis of human interferences. The curve shows the relationship between two ratios the ratio of mean annual potential evapotranspiration (Ep) over precipitation (P) in a basin and the ratio of actual evapotranspiration (Ea) to P. With human interferences, the relationship between Ep/P and Ea/P under the natural condition can be altered. Thus the human interferences can be assessed by comparing the relationships between Ep/P and Ea/P under the natural and human-influenced conditions.

4.4 Results and Analysis

In this section, the results from WASM, which includes the human interferences are first compared to those from the CLM, which only considers natural processes. Next, four water use indices are calculated to show different aspects of human interferences such as water withdrawal and return flow. Then, the concepts of water use regime [137] and Budyko curve [138, 139] are employed to provide further insights on the human interferences with hydrologic systems.

4.4.1 Comparison of Modeled and Observed Discharges

Fig.4.3 presents the modeled basin flow discharges from both CLM and WASM and compares them to the observed values. We first examine the gap between the estimated CLM discharges, which are taken to be the discharge that would occur under natural conditions, the WASM outflow, and the observed discharge values. As expected, the figure exhibits that the discharge from WASM is closer to the observed discharge since it also takes human interferences into account.

The gap between the results of the two models varies among basins, highlighting the differences in the magnitude and type of anthropogenic interferences to streamflow in each of them. The results demonstrate that there are three primary causes for these residuals. First, the CLM model over-predicts the discharge from basins in which there might be a higher rate of water consumption (Western Gulf of Mexico, Volta, Krishna, and Yellow basins, the annual gap between CLM and WASM simulated discharges were 17, 47, 52 and 114 km^3 respectively). Second, the peak monthly flows observed in the Ganges, Krishna, Huai and California basins, occur 1-2 months later than the month during which the model results suggest they occur due to seasonal storage regulation. Finally, the results from the CLM and WASM are almost identical in river basins, such as the Congo and the Ohio, in which

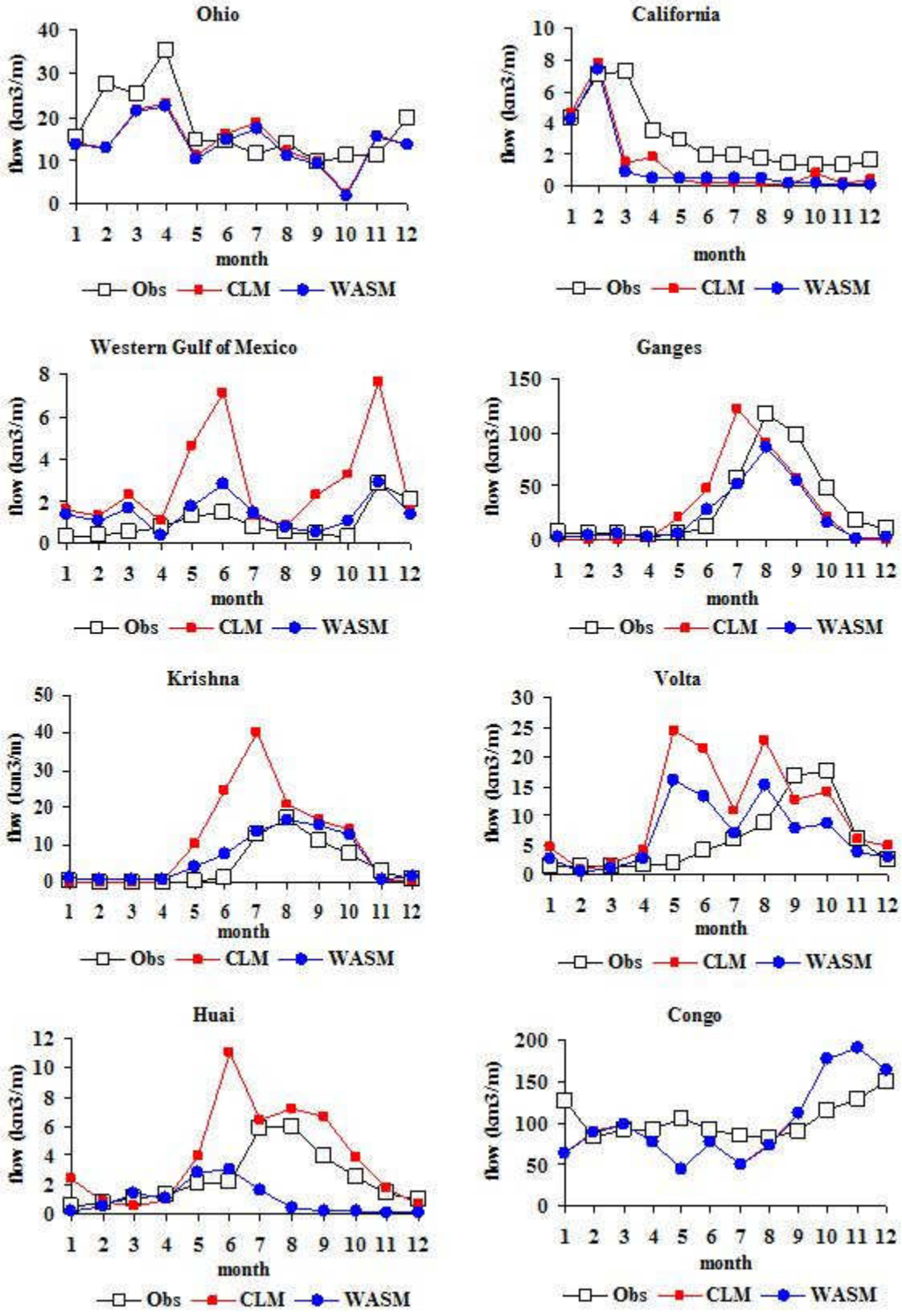

Figure 4.3: Comparison of simulated and observed discharge over the study basins

water withdrawals comprise a very small portion of the total runoff throughout the year.

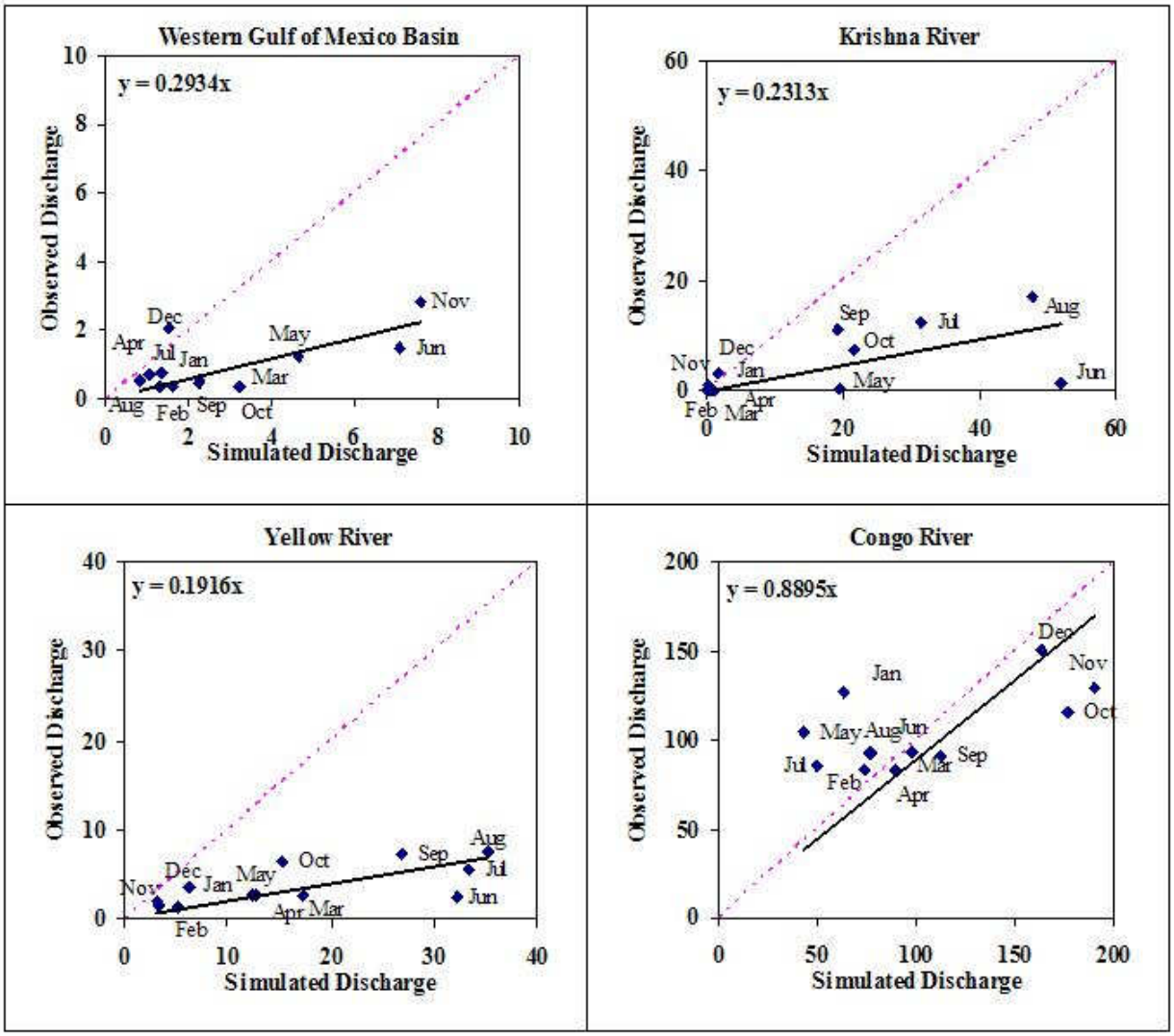

Figure 4.4: Comparison of simulated and observed discharge where each point represents the monthly discharge of the study basin. Dotted line represents 1:1 correlation between simulated and observed discharge.

The modeled and observed monthly discharge for four of the selected basins is shown in Fig. 4.4. Ideally, with minor human interferences the observed and simulated discharge for each month should be located on the line with a slope of 1:1. The withdrawal of discharge for human uses is one factor for the points to be located below the line The slope of the fitted line over the points of all months shows the degree of flow depletion in the basin, i.e.,

the greater the slope, the lower the depletion relative to the gross discharge. Among the four selected basins in Fig. 4.4, the Congo basin shows the lowest depletion level. Also, it is interesting to note that the distance between the points and the ideal line (with the slope of 1:1) varies for each month, showing the different degrees of human interferences with the natural flow in different months. Larger human interferences are found in summer months (June, July and August) due to more crop water consumption in the growing season.

It should be noted that the discharge estimates by WASM do not match the observed discharge records perfectly even after the calibration of the model. Limitations of the WASM model structure, the inaccuracy of the natural discharge modeled with CLM as well as possible errors in the observation data could all contribute to these errors.

4.4.2 Indices of Human Interferences and Water Use Regimes

The values of the four indices defined earlier are presented in Table 4.1, where the sample basins are ranked in terms of the degree to which human interferences modify the natural hydrology, as measured with the criticality ratio (CR). The higher the CR value, the more significant the human interferences are. The CR identifies the Huai and California basins as the ones subject to the greatest human influence in the sample, which is consistent with the findings presented above. By definition, DR and HR increase with CR, while OR tends to be lower if CR is higher. The OR value is low and the CR is high in the Huai, Western Gulf of Mexico, Yellow, and Krishna basins.

However, results from the California and Volta River Basin are not consistent with these postulated relationships among indices. California has a high value of CR, DR and HR but also a high value of OR, suggesting that withdrawals for human activities are large, but there is still a large amount of water flowing out of the basin One possible reason for this phenomenon might be the diversion of water across basin boundaries. According to

Table 4.1: Summary of different human interference indices for the selected basins.

Basin	CR	DR	HR	OR	Slope of Regression Analysis	Slope of Water Use Regime
Huai	0.94	0.70	1.17	0.23	0.52	0.25
California	0.89	0.60	1.18	0.86	1.10	0.30
Yellow	0.85	0.57	1.13	0.44	0.19	0.30
WGM	0.85	0.53	1.16	0.49	0.29	0.35
Krishna	0.80	0.49	1.10	0.59	0.23	0.38
Ganges	0.60	0.35	0.86	0.74	0.85	0.46
Ohio	0.11	0.04	0.18	0.96	1.18	0.60
Volta	0.0054	0.002	0.009	0.63	0.43	0.61
Congo	0.0002	0.0001	0.0004	1.00	0.89	0.63

CADWR, California imported about 1.5 km^3 of water that from the Colorado River Basin under the Colorado River Quantification Settlement Agreement (QSA) in year 2001. The low values of CR, DR and HR for the Volta River Basin signify that the percentage of total renewable water used by human (withdrawals or return flows) is small. However, the value of OR for the Volta is lower than that of the Congo, which has even higher values of CR, DR and HR, implying that runoff generated in the basin stays within it. This explanation is plausible since the Akosombo Dam retains a large amount of water in Volta Lake for hydropower generation, substantially reducing the discharge further downstream.

The results of water use regime analyses, normalized by maximum water withdrawals is shown in Fig.4.5. Note that both water withdrawal and return flow are the model results from WASM, rendering the normalized values subject to the same level of model error if it exists. In most of the study basins, the points representing May, June and July are located at the upper right part of those figures. The period including these months has been described as the human flow dominated period [137], during which the impact of human interferences is strongest during a year. The results are consistent with Fig.4.4, i.e., higher human interferences are caused by higher irrigation and municipal water use in summer

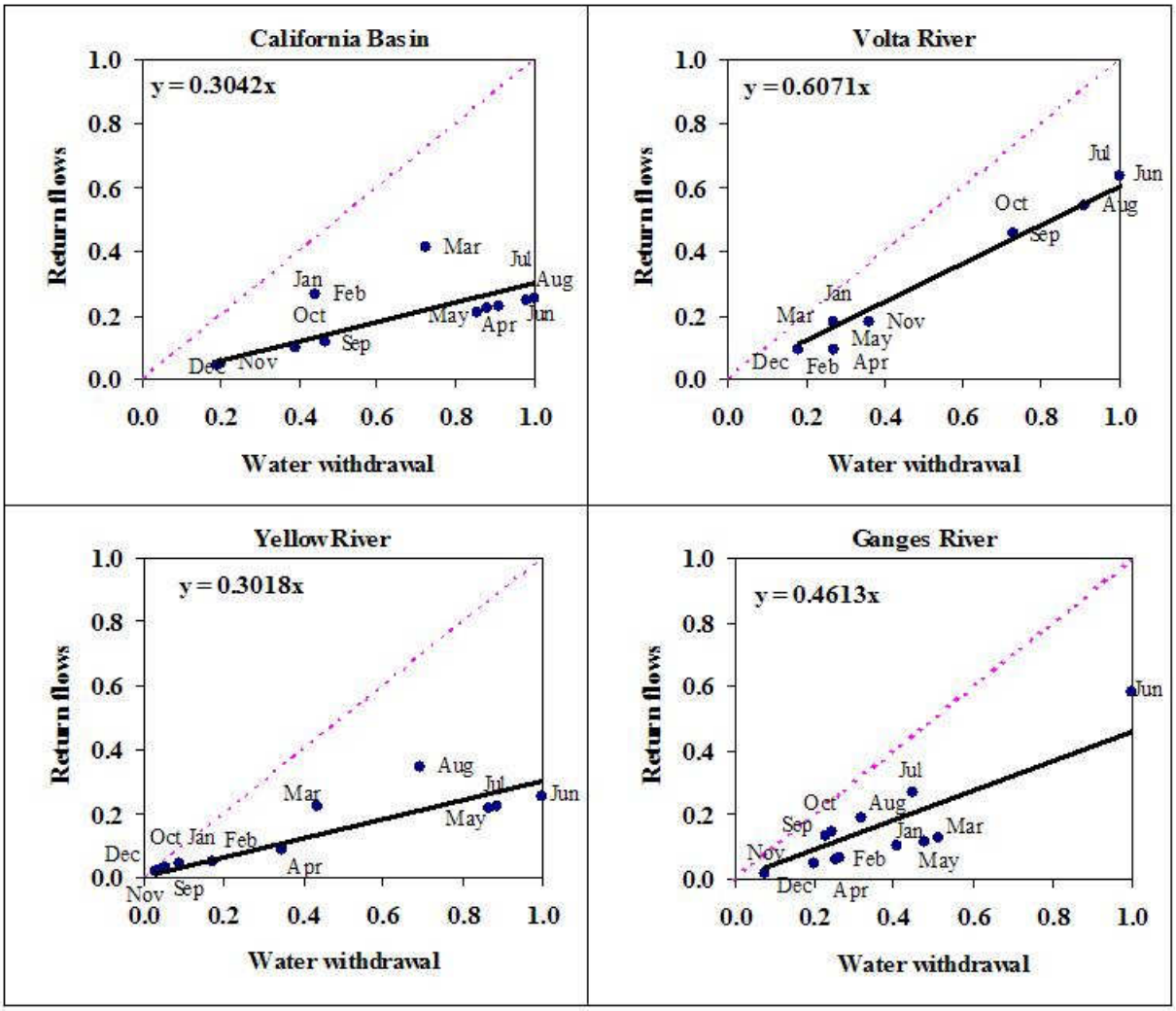

Figure 4.5: Monthly water use regime in different basins, normalized by maximum water withdrawals.

since most of the study basins are located in the Northern Hemisphere. The slope of the regression line is another index that reflects the degree of human interference, which has a meaning similar to the slope of the regression lines shown in the comparison of CLM results and observed discharges (Fig.4.4). In this case, if the slope is greater than one, the return flows exceed water withdrawals, which are unusual except under the following circumstances: 1) large amounts of deep groundwater pumping, 2) cross boundary water diversion, or 3) effluent discharge during low flow periods particularly from urban areas. A slope less than one corresponds to the typical case where water withdrawals exceed return flows. In general, the lower the slope is, the greater is the difference between water withdrawals and return flows. As can be seen in Fig.4.5, the California Basin and the Yellow River Basin both have a low slope, which can be explained by the high level of return flow reuse, or the water use recycling rate, in these two basins. In the California Basin the water reuse rate is greater for non-irrigation (municipal and industrial) water reuse while the level of return flow reuse is higher for irrigation in the Yellow River Basin [146].

In contrast, the Volta and the Ganges possess a relatively large slope, which implies that human impacts have a relatively smaller effect on streamflow in these basins. Currently, irrigation is the dominant use of water in the Volta and Ganges basins. Low water efficiency, including leakage in distribution lines and inefficient field water application may generate a large amount of return flow, although there is evaporation loss. In these basins, the reuse of the return flow by downstream users might not be as intensive as it is in the California and the Yellow basins. A particular case in which irrigation can boost flow is when groundwater is pumped for irrigation and return flow drains into nearby streams and rivers. Thus, this low irrigation water use efficiency may actually be beneficial for maintaining natural flow although it is responsible for water loss to the irrigation systems. This is reasonable when the amount of water withdrawn is large relative to the total renewable water, the annual basin discharge (i.e., high value of CR). The results obtained with the water use regime method are

consistent with those derived from the index of DR, the depletion ratio, as shown in Table 4.1. Moreover, the distribution of the data points show that human interference varies over the course of the year. When points are close to one another, human interferences are almost the same in all months. Otherwise, human interferences vary on a seasonal basis. In some of the selected basins, human interferences on discharge varied substantially between months. For example, the figure for the Ganges Basin shows that human interferences are far more significant in June than in other months. Under this circumstance, a water management plan has to account for the seasonal variability through water storage regulation.

Table 4.1 compares the different indices. Generally, high values of CR, DR and HR, small water use regime slopes, and small value of OR suggest high human interference. Results from the California and Volta basins suggest that OR reflects some human interferences that were not previously considered in WASM. For example, a high value of OR, combined with a high value of CR, DR and HR in California imply the effect of transboundary water transfers. On the other hand, the lower value of OR together with lower value of CR, DR and HR in the Volta are related to the large volume of water stored in the Volta Lake. The slope of the regression lines of modeled vs. observed flow allows for additional insights. The slope of this line is greater than one for the California Basin, which means that the observed discharges are generally greater than the one that the hydrologic model simulated. This result also indicates that cross-boundary water diversions boost discharges in the California Basin, which is consistent with the implication from the OR results. The slope is also greater than one for the Ohio Basin, suggesting that effluent discharges increase low flows. On the other hand, the smaller slope for the Volta is due to the aforementioned lake storage effect.

4.4.3 The Budyko curve analysis

A similar degree of human interference might modify discharges to different degrees under different climatic conditions. In this study, we applied the Budyko curve concept to

croplands within a basin during the agricultural growing season only (i.e. Ep, Ea, and P were calculated over croplands during the crop season). Therefore, Ep is calculated as the reference evapotranspiration using the software: CropWat developed by U.N. Food and Agriculture Organization (FAO) [147], while Ea is calculated in WASM using effective rainfall and irrigation water use data. Only five of the nine basins (Volta, Ganges, Krishna, Yellow and Huai) are analyzed since there is insufficient data for the remaining basins. The crop growth season runs through the entire year in the Volta and the Krishna basins while it is restricted to a period from March to August in the Yellow and Huai basins. While the Ganges basin has two growth seasons: from April to June and from October to December. Therefore, the data for the entire year are used.

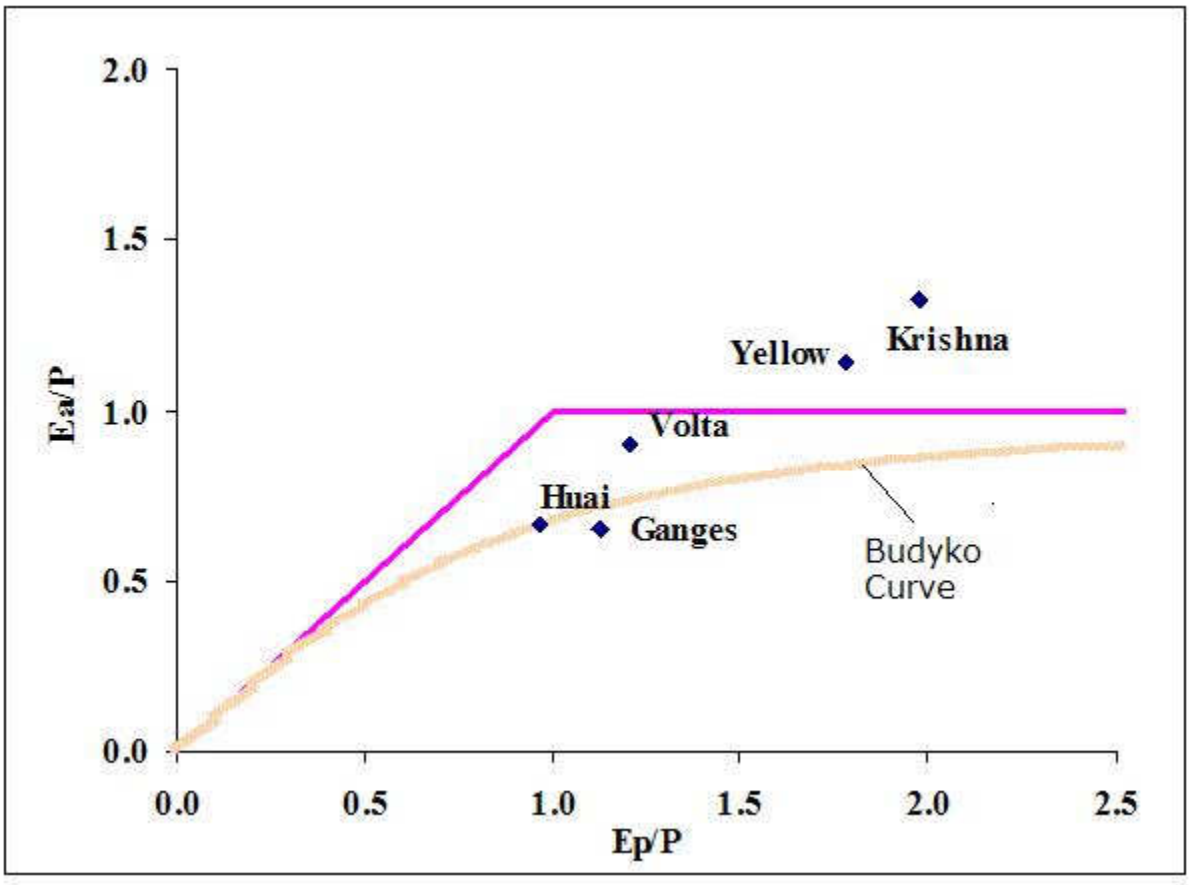

Figure 4.6: Representation of selected basins in comparison to the Budyko curve.

Fig.4.6 displays the results of these five basins. The Volta, Yellow, Ganges and Krishna are located in the water-limited zone (Ep/P $>$ 1). The Volta is located above the Budyko curve but below the horizontal line (Ea/P = 1), illustrating that human activities have substantially altered natural hydrologic conditions but that crop evapotranspiration is still lower than the rainfall within the basin. On the contrary, the Yellow and the Krishna are located above the line of (Ea/P=1), which shows that inter annual or seasonal water storage, deep groundwater pumping or trans-boundary water transfer has been developed, to sustain current agriculture use in those basins.

The Huai basin is located in the energy-limited zone (Ep/P $<$ 1) and within the 95% confidence interval of the Budyko curve, which implies human activities do not have much of a net effect on the natural hydrologic conditions in this basin. However, this contrasts the results based on other indices. For example, CR shows that human interference is intensive in the Huai basin. These contrasting results reflect a possible weakness in the Budyko curves ability to detect human interferences with hydrologic processes in basins with discharges that vary considerably over the course of the local growing season. The results presented in Fig. 4.6 are aggregated by the crop growth season and the intra-seasonal variability is not considered. During the period from April to July, which is the major crop growth season in the basin, both flooding and drought events are frequent in the Huai River Basin. When flooding occurs, water consumption is minor compared to runoff and it can even exceed runoff during droughts. Thus, the seasonal aggregation with the Budyko curve might conceal the intra-seasonal relationship between water use and runoff. The Ganges Basin is located slightly lower than the Budyko curve and in the water-limited zone. In the winter growing season, water is sufficient but the solar energy is relatively low. Thus an energy-limited condition can occur. In contrast, in the spring growth season, the temperature and solar energy are high but rainfall is not sufficient and a serious water-limited condition can occur. When the two crop growth seasons are aggregated for the entire year, the Ganges Basin ends up with

a location with a slightly water-limited condition as shown in Fig. 4.6. Interestingly, results extracted from the Budyko curve can also be related to the regression analysis of the modeled versus the observed streamflow (Fig. 4.4). The locations of the points representing the selected basins in Fig. 4.6 can be compared to the slope of the regression lines shown in Fig. 4.4. For example, the Yellow and the Krishna have smaller slope in Figure 6, corresponding to the points over the upper bound of precipitation use while other three basins have larger slopes (greater than 0.4), corresponding to the points below the precipitation bound.

4.5 Conclusions

The extent to which human interferences impact natural flow discharge can be quantified, using indices derived from basic mass balance equations as well as through water use regimes and Budyko curve. The human impact assessments presented in this chapter are based on a coupled hydrologic and water management modeling framework. The models are applied to nine case study basins from different continents and climates, subject to varying degrees of human interferences. Results for the selected basins show the various impacts, consequences and implications for further scientific study and implications for management policy reforms to control human interferences.

Although the various indices used in this study show consistent results when comparisons are made over the selected basins, each of the indices represent different aspects of the impacts of water use to the natural hydrology. Thus, when a basin is selected for the analysis, the diverse range of indices should be used to explore the different aspects of human interferences with natural hydrologic processes. Meanwhile, the Budyko curve analysis suggests that the evaluation of human interferences should also take climate into account since climatic differences can cause basins with the same degree of human interference on natural hydrologic processes to have different index values. In addition, we illustrate that the Budyko curve is

limited in its ability to assess the human impacts on discharges, especially in basins where irrigation is the predominant water use, since it does not consider the climatic variability within the growing season.

It should be noted that this study focuses on the human interferences with water quantity only and does not encapsulate water quality problems of anthropogenic origin that can further limit the quantity of water fit for municipal, agricultural and industrial consumption. Finally, while this study does not attempt to present a tool for the comprehensive assessment of human modifications to natural hydrologic systems, it encourages studies on more appropriate methods and more data for both the scientific understanding of coupled human and natural systems and sustainable basin management measures balancing both human and natural needs.

Chapter 5

Seasonal Hydrologic Dynamics under Climate and Land Use-Land Cover Change[1]

5.1 Introduction

Global warming is likely to alter future temperature and precipitation patterns, and will consequently affect both the amount and timing of water resource availability [148]. With higher temperatures, the water holding capacity of the atmosphere and evaporation into the atmosphere increase leading to the possibility of intensification of the hydrologic cycle [8] such as more intense precipitation and more droughts [149]. While temperatures are expected to increase everywhere over land and during all seasons of the year, precipitation is expected to increase in many regions and decrease in others. Moreover, precipitation may increase in one season and decrease in another [150]. These climatic changes will significantly modify the hydrologic flow regime of the river basins. Land use-land cover changes (LULCC) also play a significant role in further modifying the hydrologic processes within the river basins. With advances in modeling, satellite data and understanding of the interactions of society and physical processes of the climate system, more reliable regional LULCC and climate change projections are now available. However, resulting quantitative projection of changes on the hydrologic components at the river basin scale remain uncertain [9]. Quantification of the hydrologic response and understanding of the seasonal hydrologic dynamics for the next several decades are of paramount importance for the water resource managers and policy makers [148, 40, 41, 151, 42]. This study seeks to provide insights into the plausible changes in basin hydrology in the late 21st century due to LULCC and

[1]This chapter is under review in the Journal of Advances in Water Resources

climate change corresponding to the Intergovernmental Panel on Climate Change (IPCC) A1B emission scenario. Special Report on Emission Scenario of IPCC outlines six possible future states of the world of which A1B scenario describes a future world of very rapid economic growth, global population that peaks in mid-century and declines thereafter and a rapid introduction of new and more efficient technologies. It is a mild scenario in which major underlying themes are convergence among regions, capacity building, and increased cultural and social interactions, with a substantial reduction in regional differences in per capita income. An overview of IPCC scenarios is given in appendix A. This study uses A1B scenario for which consistent global LULCC and climate change projections are available.

Inter-comparison of hydrologic response of basins in different climatic regimes helps develop an improved understanding of the impact of LULCC and climate change on the hydrologic dynamics [90]. Comparative studies have been carried out in different climate-soil vegetation regions in small domains [82, 152], but few have presented a comparative analyses in the global context. In this study, nine river basins are selected from Asia, Africa and North America, where each basin represents a unique climatic zone, vegetation cover, soil type and land use-land cover. The Common Land Model [96] is used to provide hydrologic predictions. Detailed description of the model and the GIS based data prepared for the surface and sub-surface characteristics of the model are given in chapter 2. Forcing data are derived from the European Center for Medium Range Weather Forecasts (ECMWF) reanalysis data product, ERA-40 [153, 103]. Over other reanalysis products, ERA-40 benefits from recent developments of the ECMWF data assimilation system, higher horizontal and vertical resolution, and a more comprehensive use of observational and satellite data [153].

Though there are more than 20 coupled Atmosphere Ocean General Circulation Models (AOGCMs) for generating climate change projections; they show a large variation in magnitude of temperature and precipitation projections and even present contradictory directions

of change for precipitation when used for impact analysis at the regional scale [154]. Despite existing regional variability with AOGCMs, numerous impact assessment studies use projection from a single AOGCM [155, 156]. Several studies run their impact models using two or three different AOGCMs (e.g.,[75, 76]), leading to a wide range of outcomes and even opposing conclusions. Multi-model ensembles of projections for future climate change in the Fourth Assessment Report of IPCC [9] provide a higher quality and more consistent climate change information. This forms the basis of our study where climate change projections (i.e. mean surface air temperature response and percentage change in precipitation) are derived on a seasonal basis and at a regional scale from the Fourth Assessment Report of IPCC [9]. We first assess the impact of LULCC on the hydrological components. The same framework is further used to model the impact of climate change on hydrological components with the assumption that there is no LULCC. Finally, the combined effect of LULCC and climate change is evaluated for each selected basin. Among the different factors altering hydrologic response, we intend to determine the dominant driving factor, the knowledge of which will assist in adopting adaptive, planning and mitigative measures.

5.2 Land Use-Land Cover Change Projections

A multi disciplinary approach is used to predict the changed land use-land cover pattern since several factors like population growth, technological advances, economic, social, cultural and political factors play important roles in the generation of future land cover maps. Different types of models have been developed to predict the future state. Some models are based on gross amount of land use types and observed change while some models consider the spatial distribution, proximity of land use, changes in land use and socio-economic factors, national policy etc. Projections at global scale are preferred for impact analysis study since the results can then be compared over different regions of the world and assist in regional and national planning. The projection of land cover maps at global scale is more

complex than at national or basin scale since it has to account for varied national policies. Moreover, LULCC projection has to consider many factors because of the nature of the scale and diversity of land use over different regions.

The Integrated Model to Assess the Global Environment (IMAGE) uses IPCC scenarios to investigate the global issues, and their causes and links, in a comprehensive framework. IMAGE was initially developed in 1980s at the National Institute for Public Health and the Environment (RIVM), and further developed at the Netherlands Environmental Assessment Agency (MNP). IMAGE is an ecological-environmental framework that simulates the environmental consequences of human activities worldwide. It represents interactions between society, the biosphere and the climate system to assess sustainability issues like climate change, biodiversity and human well-being. A full description of the various components of IMAGE 2.4 is given in the MNP publication [3]. An overview of IMAGE framework is given in Appendix A. One of the most striking features of IMAGE is the geographically explicit land-use modeling, which considers both cropping and livestock systems on the basis of agricultural demand and demand for energy crops. Assuming land cover change, population and the macro-economy as key drivers, the model establishes physical indicators for both the energy/industry system and the agriculture/land-use system for assessment of changes in land cover, climate, and the carbon and nitrogen cycles.

For this study, projections of land use-land cover are derived from MNP using the IMAGE model (ref. http://www.mnp.nl/en/index.html). The projected maps as well as historical time series maps from IMAGE were compared to satellite derived land cover maps of USGS. The USGS land cover map was chosen as the base because Common Land Model (CLM) uses USGS classification of land cover category to define soil thermal and hydrualic parameters. IMAGE uses IGBP classification of land cover category. Each continent was clipped out from global coverage as some spatial inconsistency was determined for land cover classes

between USGS map and projected map at global level. While one class matched well in one part of the world, the other did not. To determine the degree of inconsistency and to decide which USGS class should be assigned to a particular class of projected map, the number of pixels of USGS class falling under each class of projected map was calculated. Afterwards the maximum number of pixels were counted to identify the dominant land cover of USGS map for each IGBP class of IMAGE map. Visual interpretation technique was then applied to check the spatial consistency of the dominant land cover class. Fig. 5.1 highlights the changes in land cover conditions of the selected basins for the years 2000 to 2100. Widespread deforestation and expansion of dryland, cropland and pasture is quite evident in most of the basins.

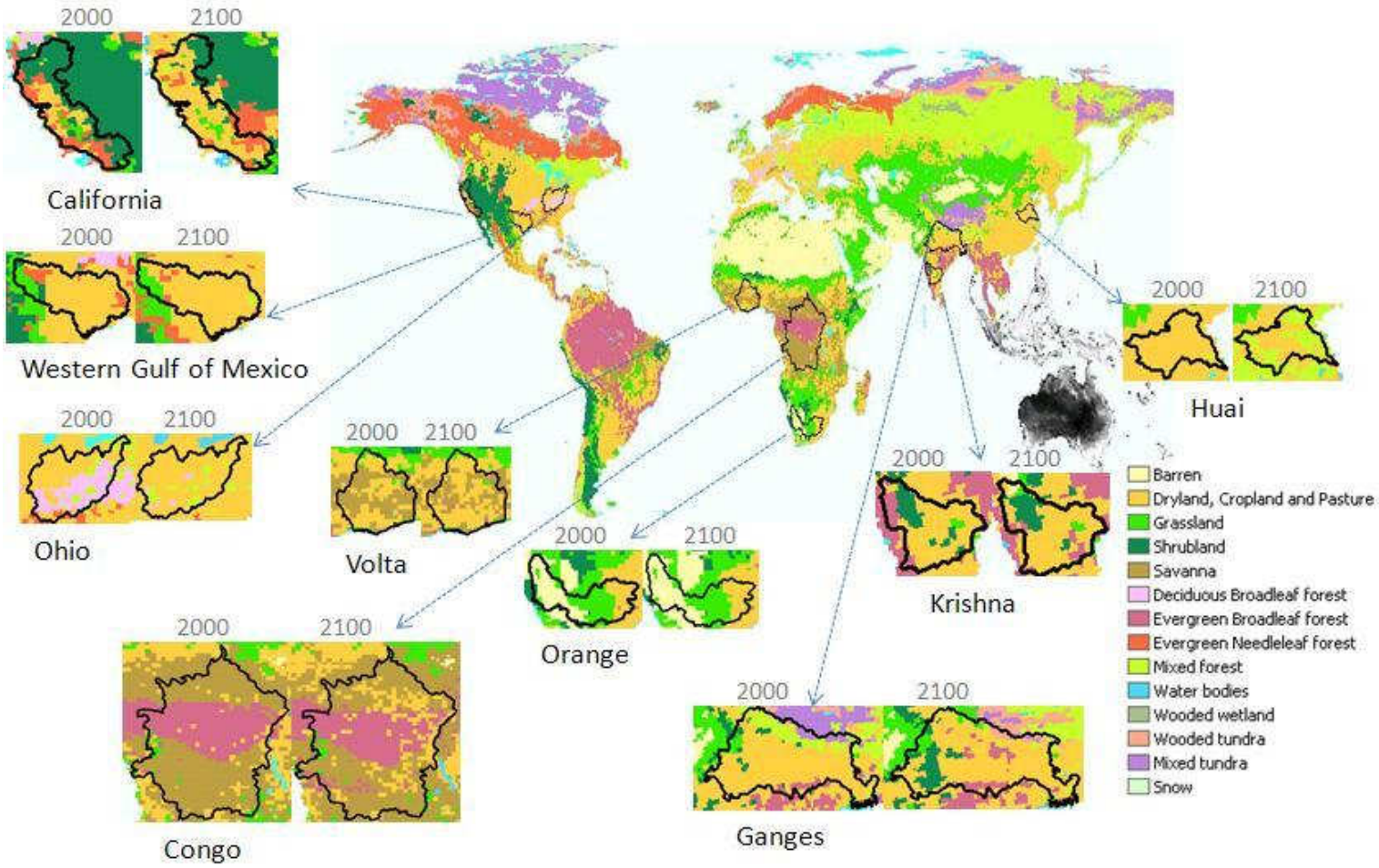

Figure 5.1: Land Use-Land Cover Change (LULCC) maps for the selected river basins under IPCC A1B scenario.

5.3 Climate Change Projections

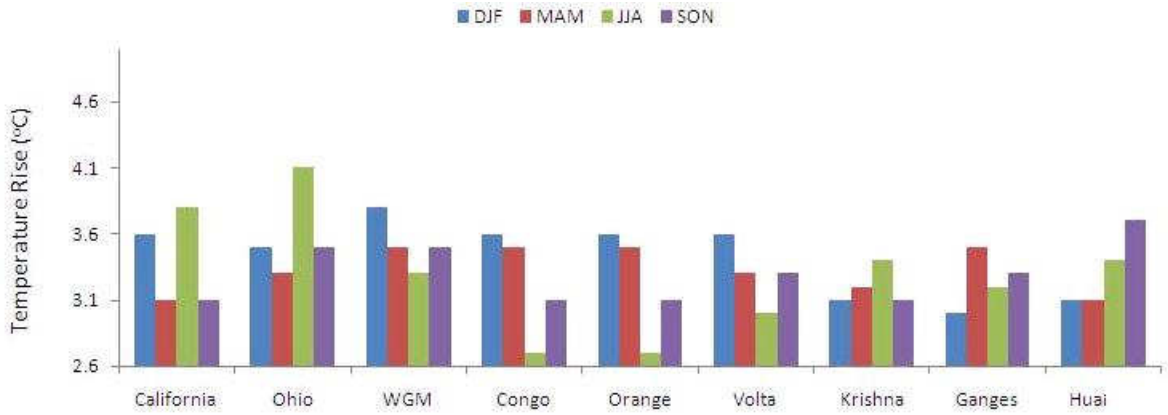

(a) Seasonal temperature change for the 2080-2099 period with respect to the 1980-1999 period.

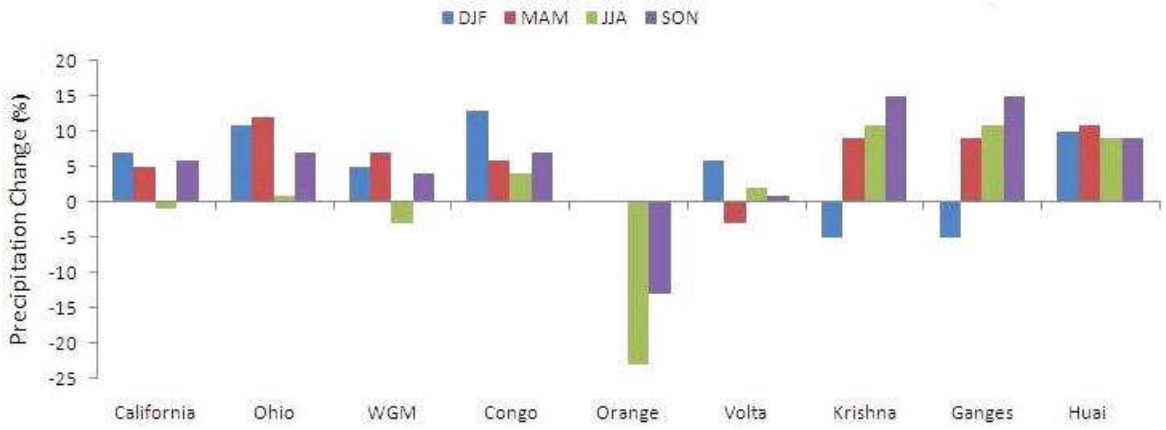

(b) Seasonal precipitation change for the 2080-2099 period with respect to the 1980-1999 period.

Figure 5.2: Climate change projections for the selected study basins under IPCC A1B scenario for different seasons: DJF (December, January, February), MAM (March, April, May), JJA (June, July, August) and SON (September, October, November), derived from AR4.

Climate projections in the Third Assessment Report of IPCC [157] were largely restricted to temperature projections using nine coarse-resolution Atmospheric Ocean General Circulation Models (AOGCMs) with limited statements about precipitation and no differences for sub-regions within a continent. Multi-model ensemble of projections of future climate change in the Fourth Assessment Report(AR4) of IPCC [9] provide more detailed climate change information on seasonal basis and at regional scale. In AR4, the mean temperature

and precipitation responses are first averaged for a set of 21 global models in the Multi Model Dataset (MMD) and then averaged over all available realizations of the 1980 to 1999 period from the 20th Century Climate in Coupled Model (20C3M) simulations and the 2080 to 2099 period of IPCC A1B scenario. The difference of temperature (C) and precipitation (%) change is then computed for the two periods.

Fig. 5.2 shows the median value of seasonal surface air temperature response and the percentage change in seasonal precipitation for the selected basins from AR4 [9]. The projections are characterized for four seasons comprising of three months each, for example, winter (December, January, February; DJF), spring (March, April, May; MAM), summer (June, July, August; JJA) and autumn (September, October, November; SON) for the northern hemisphere. It can be inferred that precipitation is projected to intensify in seasons when there is already more intense precipitation and reduce in seasons with low precipitation. This may lead to dramatic changes in water availability and hence necessitates the understanding of seasonal hydrologic dynamics.

5.3.1 Implementation Strategy of Simulating Climate Change

The hydrologic model is simulated under climate change conditions by incorporating the projected changes in climate into the meteorological forcing data. The difference of temperature (^{o}C) and precipitation change (%) as derived from the MMD-A1B models in the Fourth Assessment Report (AR4) of IPCC, is applied to the meteorological forcing of ECMWF with no change in other forcing variables. Precipitation is multiplied by the projected percentage change, while an absolute change is added to the temperature at each time step of model simulation as shown in equations 5.1 and 5.2.

$$P_{cc} = P_o(1 + \Delta P) \tag{5.1}$$

$$T_{cc} = T_o + \Delta T \tag{5.2}$$

Here, P_{cc} refers to precipitation under climate change conditions, P_o is the precipitation derived from reanalysis data product and ΔP is the projected precipitation change(%) for IPCC A1B scenario. Similarly, T_{cc} refers to temperature under climate change conditions, T_o is the temperature derived from reanalysis data product and ΔT is the projected temperature change (^{o}C).

It should be noted that the implementation strategy of shifting meteorological forcing to represent climate change is not able to capture certain aspects of predicted climate change. A climate change induced increase in precipitation may manifest itself through an increase in precipitation frequency rather than an increase in individual storm amounts, and depending on nonlinearities in the hydrologic model, a change in frequency rather than intensity could have a profound impact on predicted changes in the runoff generation. Chiew and McMohan, (2002) [158] addressed this limitation with a discussion on using the stochastic weather generator and stochastic downscaling approach. The stochastic downscaling approach relates large synoptic-scale atmospheric circulation variables to basin scale data [159]. This approach can take into account changes in the characteristics and relative frequency of synoptic patterns under climate change conditions. However, the calibration of a stochastic downscaling model and the choice of appropriate atmospheric variables to relate to basin scale variables has uncertainties.

Besides temperature and precipitation, changes in other forcing variables (pressure, humidity, wind and radiation components) also play a significant role in determining the climate change response. An increase in atmospheric moisture leads to increased relative humidity and increased clouds, which alter the solar radiation and the energy available at the surface

[160]. We accounted here only the variations in temperature and precipitation, the first order surface climate variables for hydrologic response to represent climate change conditions since there is less confidence in understanding of the forced changes in other variables, especially at regional and seasonal scales.

5.4 Results

5.4.1 Study Basins

A comprehensive description of the nine selected river basins is given in Chapter 2, where the climate, vegetation cover, hydrologic characteristics, expected changes and the role of human influence are described for each of the selected basin. Year 2000 is used as a representative basis for climate change assessment of all the basins. It is chosen as a baseline year for comparative analysis of different components of change. Figure 5.3 shows the annual precipitation of year 2000 over the boxplot of twenty five year (1976-2000) precipitation of the selected basins derived from ERA-40. The year 2000 lies within the range of first quartile for Congo, Orange, Volta and Ganges river basins representing a wetter year, while it lies in the range of third quartile for WGM, Huai and Ohio river basins representing dry conditions.

California Basins

The seasonal cycle of hydrologic components of the basin for baseline year is given in Fig. 5.4a, which shows high precipitation in the winter (DJF) season alongwith the simulated runoff and ET response. The range of variability of baseline year precipitation is shown over the boxplot of twenty five year (1976-2000) precipitation derived from ERA-40, in Fig. 5.4b. Winter (DJF) precipitation of the baseline year lies within the range of first quartile, while the other seasons represent median range values.

With rapidly expanding urbanization in the basin, large changes in land use-land cover

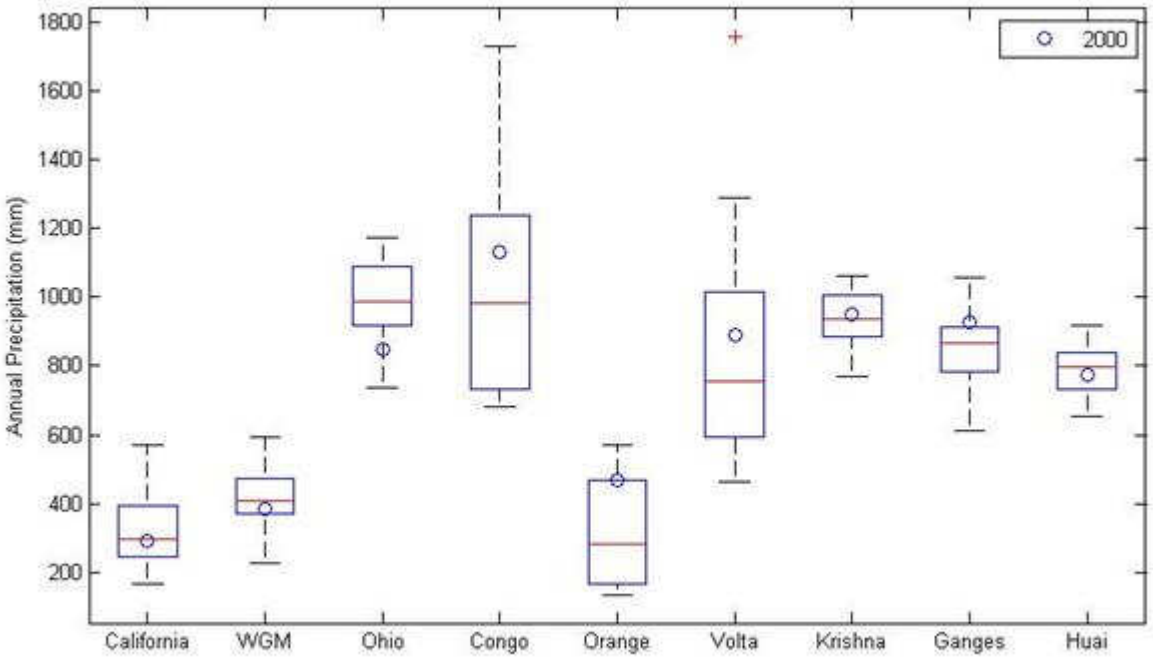

Figure 5.3: The range of variability of precipitation over the twenty five year period (1976-2000) derived from ERA-40 with circle representing the year 2000.

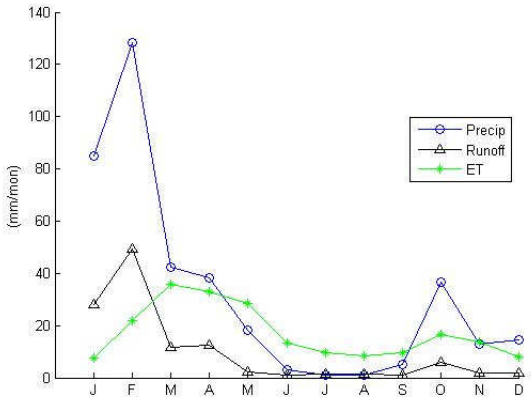

(a) Monthly Variation of Precipitation, Runoff and Evapotranspiration

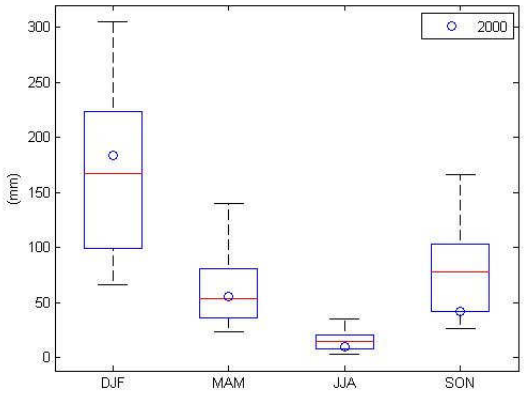

(b) Range of Variability for Precipitation during 1976-2000 with the year 2000 explicitly identified.

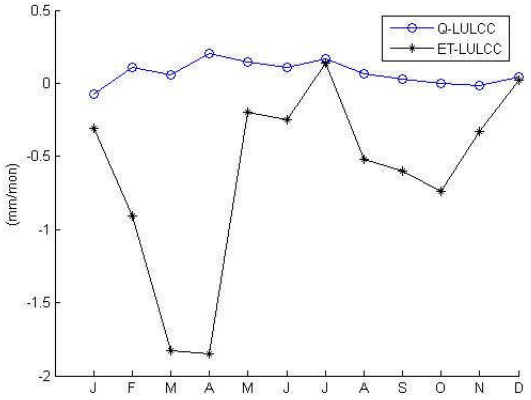

(c) Monthly change in Runoff(Q) and ET due to LULCC.

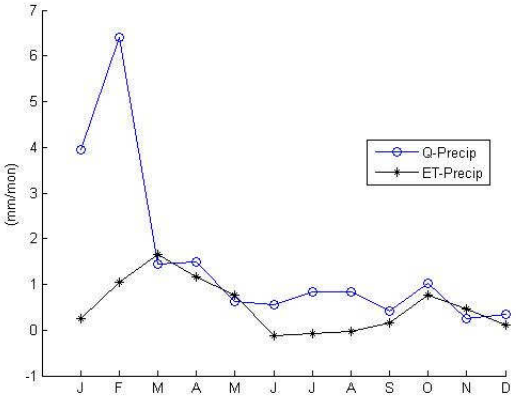

(d) Monthly change in Runoff(Q) and ET due to Precipitation change.

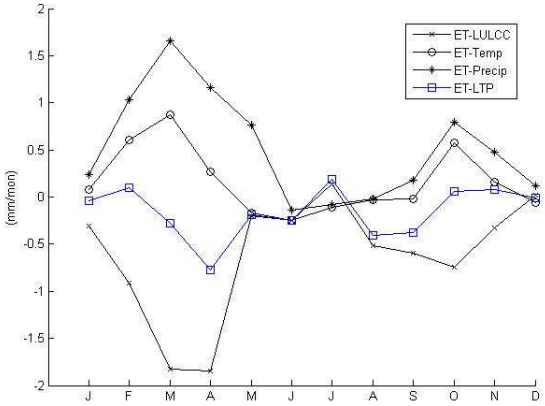

(e) Monthly change in ET response due to LULCC, Temperature and Precipitation change individually and the cumulative effect (ET-LTP).

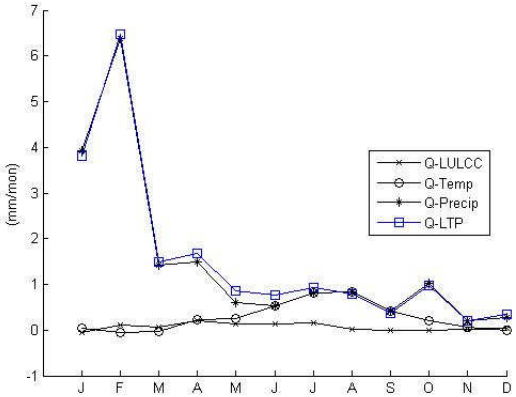

(f) Monthly change in runoff response due to LULCC, Temperature and Precipitation change individually and the cumulative effect (Q-LTP).

Figure 5.4: California Basins Analysis

are projected to occur in the 21st century. Fig. 5.1 presents the projected LULCC map of the basin. There is 11% reduction in the evergreen needleleaf forest and 32% reduction in shrubland in 2100 as compared to 2000 under IPCC A1B scenario. Consequently, 43% area of the basin is projected to convert to dryland, cropland and pasture. Subsequently, it will change the vegetation characterization leading to changes in the vegetation parameters: Leaf Area Index, Stem Area Index, rooting depth, roughness length and displacement height. This will lead to alterations in energy and water fluxes. Simulation of the model with LULCC alters the hydrologic response resulting in a decrease in ET with a corresponding gain in runoff (Fig. 5.4c). LULCC results in a 3.3% annual reduction of ET over the basin. Land with natural vegetation such as forest and shrubland has comparatively deeper roots than the land with row crops, and hence results in more transpiration loss.

Precipitation is projected to result in a 7% increase in winter (DJF) and 1% decreaase in summer (JJA) season, with an annual increase of 4% over the whole basin in the late 21st century (Fig. 5.2b). Corresponding to the precipitation change, there is an annual 15.4% increase in runoff of which the maximum relative change occurs in winter (DJF) season as depicted in Fig. 5.4d. Winter (DJF) being the rainy season for the basin, soil is wetter and a slight increase in precipitation leads to much higher increase in runoff. Model response shows a slight increase in summer (JJA) runoff despite negative change in precipitation. Maximum relative % increase in ET due to precipitation change is observed during the spring (MAM) season. End of 21st century temperature increase for the basin is approximately 3.4^{o}C under the IPCC A1B emission scenario. The combined effect of changes in precipitation, temperature and LULCC is then evaluated on the ET and runoff response of the basin. ET gets reduced as a result of deforestation but a rise in temperature and precipitation tends to overcome the ET loss, resulting in no significant change in the overall ET. Runoff increases as a result of deforestation though the change in runoff due to LULCC and rise in temperature is less than 2% of the change due to precipitation variability. Annual variation of the

impact of each component of change on ET and runoff response is depicted in Fig. 5.4e and Fig. 5.4f respectively.

Western Gulf of Mexico Basin

The Western Gulf of Mexico (WGM) basin is located in the south-central part of the United States. It has a highly variable weather - humid subtropical climate on the east and temperate semi-arid steppe climate on the northwest. The easternmost basin is covered by piney woods and as the climate gradually becomes more arid towards west, turns into prairie and desert. Soils are brown to reddish, mostly deep clay loams, sandy loams, and sands. The intense localized precipitation resulting from the southerly winds off the Gulf of Mexico often lead to flash floods.

Fig. 5.5a shows the monthly variation of precipitation, runoff and ET for baseline year 2000. Precipitation is relatively light and distributed throughout the year with an average rainfall being 350 mm/year. The baseline year precipitation lies in the lower quartile range for the period 1976-2000, except for MAM season (Fig. 5.5b). There is a projected 6% loss of evergreen needleleaf forest and 2% loss of shrubland to dryland, cropland and pasture in 2100 as compared to 2000 under IPCC A1B scenario. The response of LULCC on hydrologic components is negligible when aggregated over the whole basin (Fig. 5.5c).

Precipitation is projected to decrease by 3% in summer (JJA), reducing summer runoff while there is still an increase in summer ET (Fig. 5.5d). In summer, there is just enough water to satisfy the plant water needs and hence ET is not reduced with decreased precipitation. Temperature is projected to increase by more than 3.3^oC in each season and even higher than 4^oC in summer (JJA). Rise in temperature alters the water and energy fluxes, leading to higher ET loss. In arid ecosystem, radiation is high and leaf area is small, so high soil temperature drives more evaporation [161]. Total ET response due to LULCC,

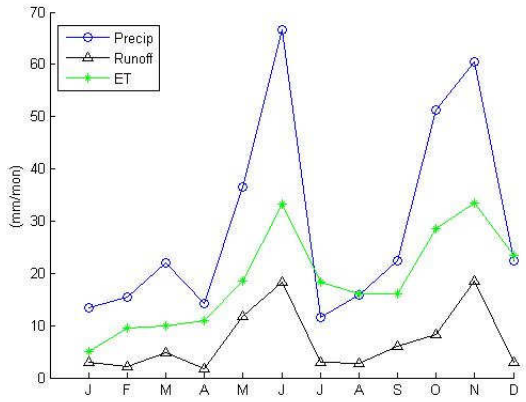

(a) Monthly Variation of Precipitation, Runoff and Evapotranspiration

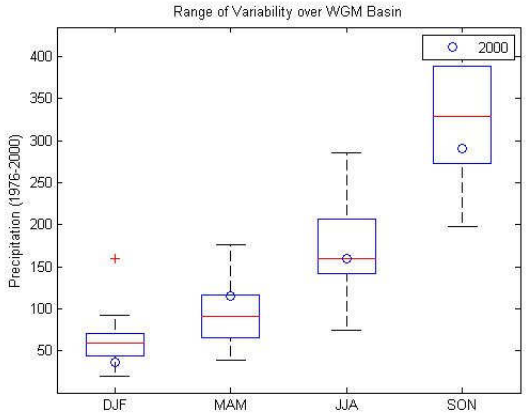

(b) Range of Variability for Precipitation during 1976-2000 with the year 2000 explicitly identified.

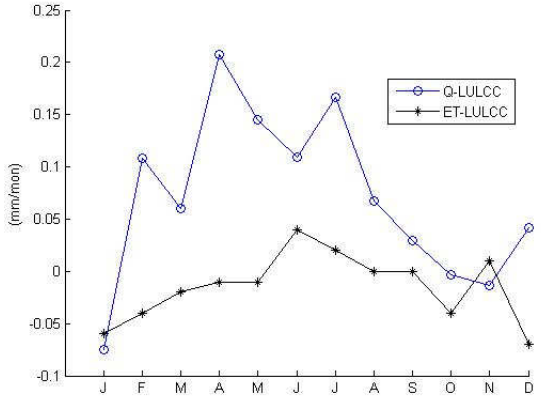

(c) Monthly change in Runoff(Q) and ET due to LULCC.

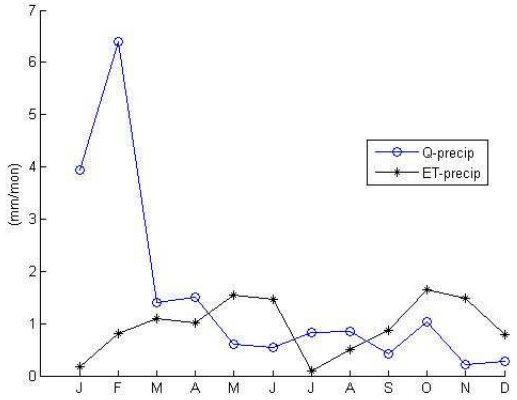

(d) Monthly change in Runoff(Q) and ET due to Precipitation change.

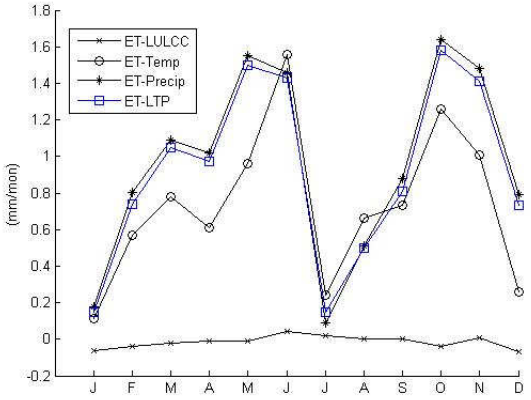

(e) Monthly change in ET response due to LULCC, Temperature and Precipitation change individually and the cumulative effect (ET-LTP).

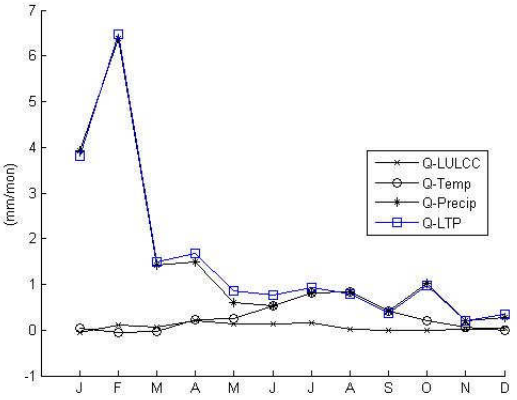

(f) Monthly change in runoff response due to LULCC, Temperature and Precipitation change individually and the cumulative effect (Q-LTP).

Figure 5.5: Western Gulf of Mexico (WGM) River Basin Analysis

temperature and precipitation change is not much influenced by the LULCC as illustrated in Fig. 5.5e. The combined effect of runoff response due to LULCC and climate change follows the precipitation change pattern (Fig. 5.5e). Several studies have shown that in arid and semiarid environments, changes in precipitation have greater impact than LULCC or temperature change because the spatio-temporal availability of water directly impacts the plant recruitment, growth and reproduction, nutrient cycling, and net ecosystem productivity [162, 163, 164].

Congo Basin

The Congo basin located in the western central Africa has the second largest rain forest area in the world, after the Amazon. The major part of Congo lies within the inner humid tropical climatic region extending five degrees north and ten degrees south of the equator, characterized by heavy rainfall, high temperatures and humidity. The basin is surrounded by plateaus merging into savannas in the south, mountainous terraces and grassland in the west and mountainous glaciers in the east. The changing demography and socio economic issues in the region is directly impacting land use-land cover of the basin.

Seasonal hydrologic cycle of the basin for baseline year is shown in Fig. 5.6a, which shows a bi-modal pattern of the equatorial region precipitation. The range of variability for baseline year precipitation lies in the upper quartile for all the seasons, except for winter(DJF) season (Fig. 5.6b). Fig. 5.1 presents the LULCC map of the basin, there is 10% decrease in savanna and 2% decrease in evergreen broadleaf forest in 2100 using 2000 as the baseline year. Fig. 5.6c plots the difference in hydrologic components as a result of LULCC, showing a decline in ET and a gain in runoff. Deforestation distorts the biogeophysical feedbacks by increasing surface albedo and reducing the amount of incoming absorbed solar radiation [165], which results in lowered ET and a subsequent gain in runoff.

With 8% annual increase in precipitation, there is 15% increase in projected runoff (Fig. 5.6d). Seasonal variation in runoff follows the precipitation change and shows the bi-modal pattern of precipitation. Alteration in the vegetation parameters due to increased precipitation and temperature results in lowering of ET. How climate change results in alteration of the water demand of vegetation is analyzed by Zhang et al.(2005). The contribution to ET and runoff response due to LULCC and climate change from the three contributing factors (LULCC, temperature and precipitation change) is assessed individually and all together in Fig. 5.6e and Fig. 5.6f respectively. The combined effect of LULCC and climate change on runoff results in a response governed dominantly by the change in precipitation.

Krishna Basin

The Krishna river originates in the Western Ghats of India at an elevation of about 1337 m, about 64 km from the Arabian Sea and flows for about 1400 km and outfalls into the Bay of Bengal. The climate in the basin is mainly semiarid with some dry and sub-humid areas in the Krishna Delta. More than 74% of the annual precipitation occurs during the monsoon (June-October) season. High altitude regions of the Western Ghats receive comparatively more rainfall and have evergreen broadleaf forest. The eastern part of the Western Ghats experience semiarid to arid climate, having mainly tropical dry deciduous vegetation. In addition to this natural vegetation, the Krishna Basin is one of the most intensely cultivated region, with sugarcane and cereals being the major crops. In recent decades, expansion in irrigation has led to a rapid decrease in discharge from the Krishna into the ocean. The cumulative reservoir capacity in the basin approximated the annual runoff volume and resulted in the basin closure in late 1990s [17].

Seasonal hydrologic cycle of the basin shown in Fig. 5.7a clearly depicts the monsoon season from late May to October. Baseline year precipitation lies in the upper quartile range representing wetter conditions over the long term record (Fig. 5.7b). LULCC projections show a

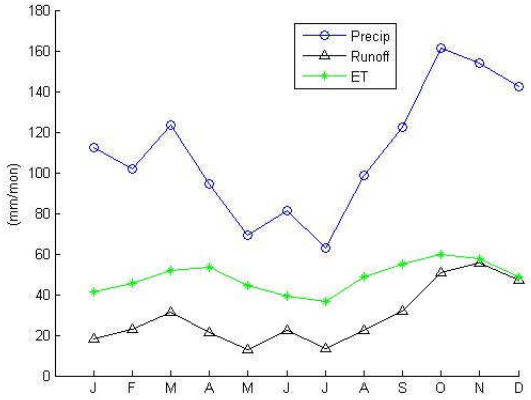

(a) Monthly Variation of Precipitation, Runoff and Evapotranspiration

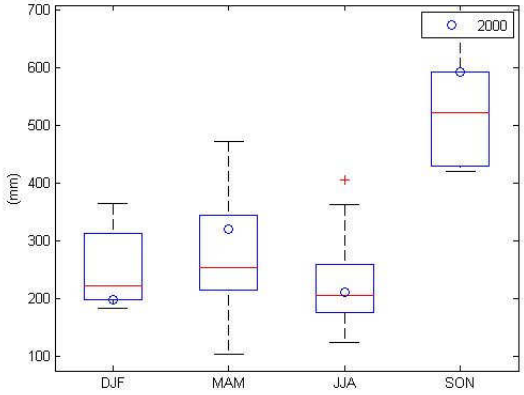

(b) Range of Variability for Precipitation during 1976-2000 with the year 2000 explicitly identified.

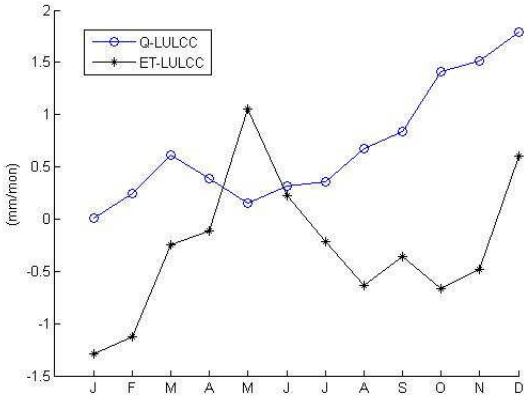

(c) Monthly change in Runoff(Q) and ET due to LULCC.

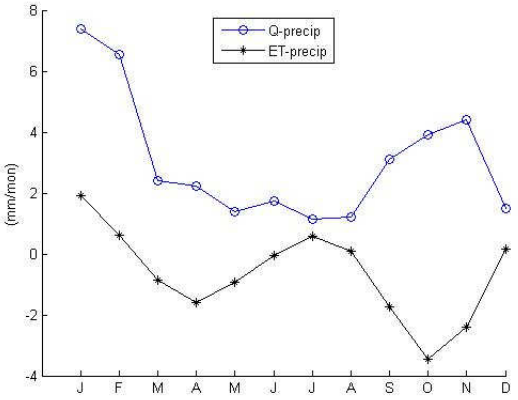

(d) Monthly change in Runoff(Q) and ET due to Precipitation change.

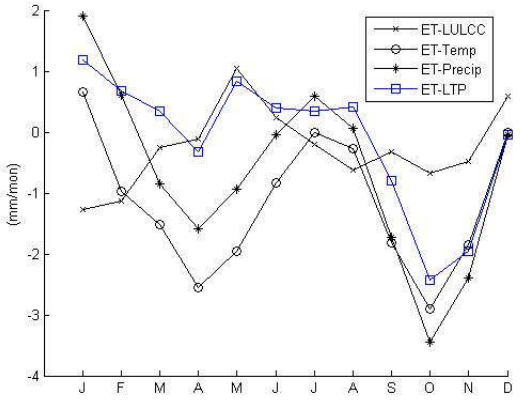

(e) Monthly change in ET response due to LULCC, Temperature and Precipitation change individually and the cumulative effect (ET-LTP).

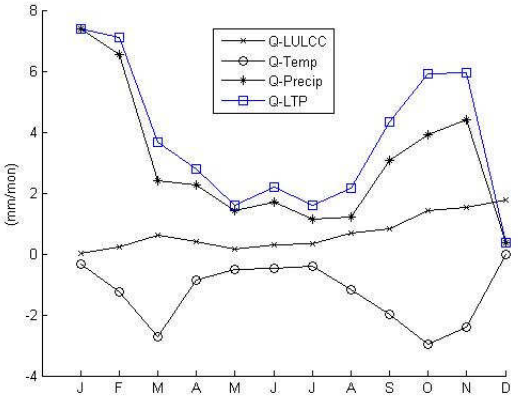

(f) Monthly change in runoff response due to LULCC, Temperature and Precipitation change individually and the cumulative effect (Q-LTP).

Figure 5.6: Congo River Basin Analysis

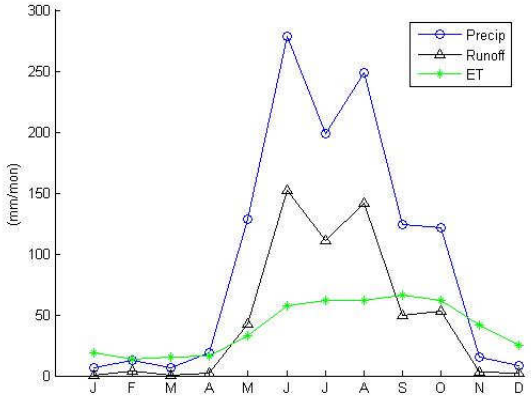

(a) Monthly Variation of Precipitation, Runoff and Evapotranspiration

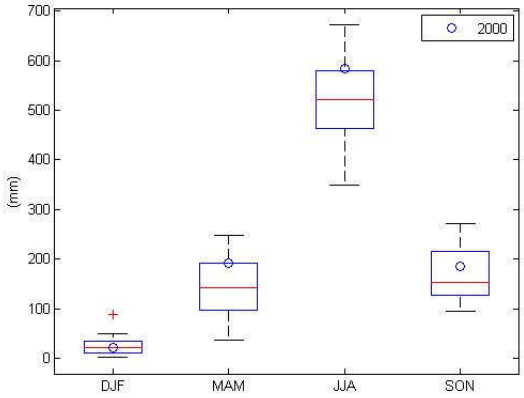

(b) Range of Variability for Precipitation during 1976-2000 with the year 2000 explicitly identified.

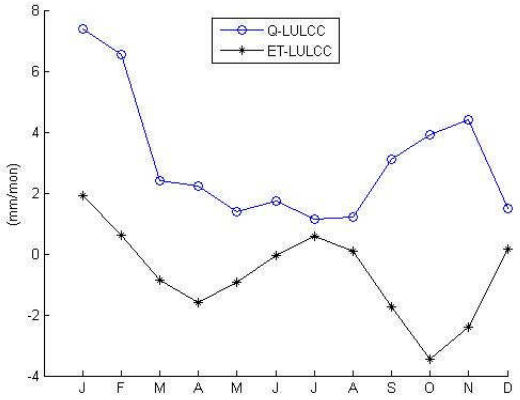

(c) Monthly change in Runoff(Q) and ET due to LULCC.

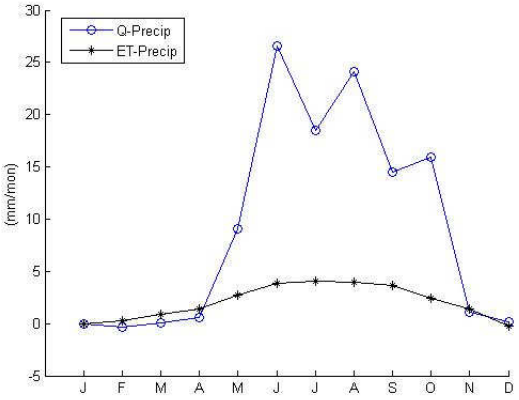

(d) Monthly change in Runoff(Q) and ET due to Precipitation change.

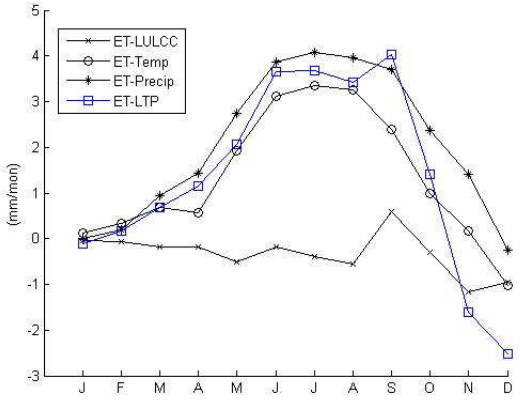

(e) Monthly change in ET Response due to LULCC, Temp. and Precip. change and the cumulative effect (ET-LTP).

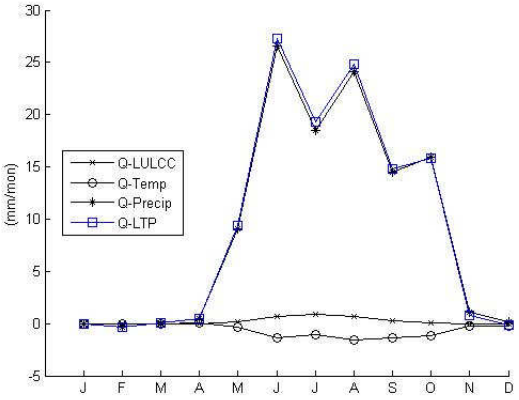

(f) Monthly change in runoff Response due to LULCC, Temp. and Precip. change and the cumulative effect (Q-LTP).

Figure 5.7: Krishna River Basin Analysis

5% loss of evergreen forests within the basin in 2100 as compared to year 2000. The annual variation of runoff and ET due to LULCC shows reduction in ET and a subsequent gain in runoff (Fig. 5.7c). There is an annual 8% increase in projected precipitation, which leads to considerable increase in runoff during the summer (JJA) monsoon season (Fig. 5.7d). As compared to the runoff response, a small increase is observed in ET due to precipitation change. Total ET response due to LULCC, temperature and precipitation change is influenced by each component of change as illustrated in Fig. 5.7e. Loss in ET due to LULCC is compensated by the gain in ET from rise in temperature and increase in precipitation. The combined effect of LULCC and climate change on runoff results in a response governed dominantly by the change in precipitation (Fig. 5.7f).

Ohio Basin

The climate of Ohio basin in the United States is classified as humid continental, warm summer type [109]. Most of Ohio's terrain is relatively flat, representative of the glaciated area. ET from plant and soil surfaces is relatively high in summer and early autumn and relatively low in winter and early spring. LULCC projections estimate that by 2100, a major fraction of the deciduous broadleaf forest in the basin would be converted to dryland, cropland and pasture (Fig. 5.1). Model simulation with LULCC results in a slight increase in ET and an annual decrease of 2.67% in runoff. Precipitation is projected to increase by 8% over the year, increasing runoff by 6.97% with a very similar pattern of seasonal change in runoff as projected for the precipitation (Fig. 5.8a). Relative seasonal % increase in ET is observed during the spring and summer season (Fig. 5.8b). The combined effect of LULCC and climate change on runoff response results in a higher % increase in the spring (MAM) season (Fig. 5.9) as a result of widespread deforestation in the late 21st century.

Orange Basin

The Orange river in South Africa flows across the central landscape of the basin from the highlands in the east through the Kalahari depression in the west to drain into the South Atlantic Ocean. The basin receives less than 500 mm rain on average and is characterized by extremely variable distribution of rainfall and dry conditions. The majority of the rainfall occurs during the wet season (Nov-Apr) with very little rainfall in the dry season (May-Oct). The region is covered by grassland and shrubland with sparse vegetation towards west. There is not much of a land cover change projected for the basin and the simulation with LULCC results in 0.5% loss in ET and no change in runoff.

Under IPCC A1B emission scenario, precipitation is projected to reduce by 23% in winter (JJA) followed by 13% reduction in the spring (SON) season (Fig. 3.7b). Lowered winter (JJA) precipitation results in a reduced runoff and further reduction in spring (SON) precipitation leads to a significant reduction in spring (SON) runoff. Since runoff is a non linear outcome of precipitation, reduction in precipitation drives runoff disproportionately lower, 4% annual deficit of precipitation lowers runoff by 15%. Evaluating runoff response due to the cumultaive effect of LULCC and climate change reveals that maximum relative % decrease in runoff occurs in the spring (SON) season. With temperature change, there is an increase in ET and a corresponding decline in runoff in all the seasons. Overall, both ET and runoff response is significantly governed by the precipitation change. A higher spatial and temporal variability in rainfall is highly likely to increase the frequency of droughts, thus severely impacting the agriculture and economy of the region.

Volta Basin

The Volta basin covers the subhumid to semiarid West African Savanna zone. Natural vegetation is characterized by a mosaic of small patches of grassland, woody grassland, forest, cropped fields, short and long fallow fields and wetlands. Comparing the land cover map of

2100 to 2000 (Fig. 5.1), there is no intensified land cover change but a gradual shift towards more cropped fields. Over the whole basin, there is 15% conversion of savanna to dryland, cropland and pasture. It alters the biogeophysical and biogeochemical feedbacks between the vegetation and atmosphere by increasing surface albedo and reducing near surface momentum and ET.

Though there is an annual 2% increase in projected precipitation, 3% decline in the spring (MAM) precipitation leads to much seasonal runoff variability. Simulation of the projected change in precipitation results in lowering of the runoff in spring (MAM) and autumn (SON) season (Fig. 5.8a). The effect of reduced spring (MAM) precipitation prolongs to other seasons through antecedent soil moisture conditions and the effect is much more evident in the autumn season (SON) for both runoff and ET.

Ganges Basin

Flowing across the great alluvial Indo-Gangetic plains, the Ganges is bordered by the Himalayas to the north and the Vindhya-Satpura ranges to the south. The Ganges River basin system remains the main source of freshwater for half the population of India and Bangladesh and nearly the entire population of Nepal [111]. The Ganges and its tributaries provide a perennial source of irrigation to a large area. Comparing the land cover map of 2100 to 2000 in Fig. 5.1, there is an increase in evergreen forest and shrubland with a loss of mixed forest in the basin. The effect of each component of change gets averaged when the response is evaluated over the whole basin. Precipitation projections show an 8% annual increase of which the maximum increase (15%) occurs in autumn (SON) and a 5% decrease in winter (DJF) season. Similar to the Krishna basin results, relative seasonal % runoff response is highest in summer (JJA) season since the basin response is influenced by the southwestern summer monsoon occurring from June through September. Relative seasonal % increase in ET is also highest in the summer (JJA) season, though the % increase is less

than the increase in runoff (Fig. 5.8b). The combined effect of LULCC, temperature and precipitation change on runoff response also results in the maximum relative seasonal % increase in the summer (JJA) season.

Huai Basin

The Huai basin in the southeast Asia lies between the temperate and tropical climate zones. The northern part of the basin is dry while the southern part is wet. The tropical rain belt causes additional rainfall during the monsoon season. LULCC shows 40% conversion of cropland to mixed forests under IPCC A1B scenario. Precipitation projections portray significant increase in all the seasons which result in a significant increase in both runoff and ET response. Though projected precipitation change is maximum in spring (MAM), relative seasonal % increase in runoff is highest in the summer (JJA) season, consistent with the response of Asian basins influenced much by the monsoon rainfall (Fig. 5.8a). The relative seasonal % increase in ET is greater than the runoff response in winter (DJF) and spring (MAM) seasons. The cumulative effect of LULCC and climate change on runoff response is similar to the response observed due to precipitation change alone.

5.4.2 Inter-comparison of Basin Results

The relative seasonal % change, signifying how the annual change under the climate change scenario is distributed over the seasons is used for the inter-comparison of basin hydrologic response. Fig. 5.8 provides an overview of the relative seasonal % change of runoff and ET in the nine selected basins due to precipitation change of IPCC A1B scenario in the late 21st century as compared to the late 20th century. It is clearly evident from Fig. 5.8a that maximum change in runoff is projected to occur over the summer (JJA) season for Krishna, Ganges and Huai basins though projected precipitation change is greater in other seasons. These results can be explained by the particular characteristics of the Asian monsoon region where conditions change dramatically between the rainy and dry seasons and the basins are

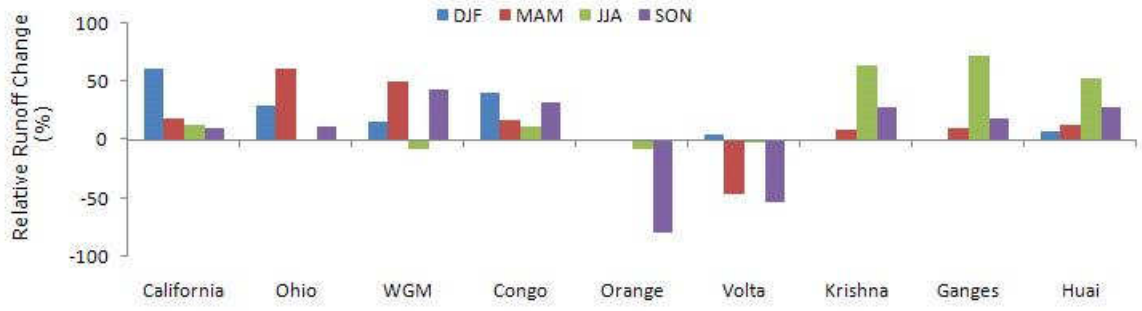

(a) Relative seasonal % runoff response due to precipitation change

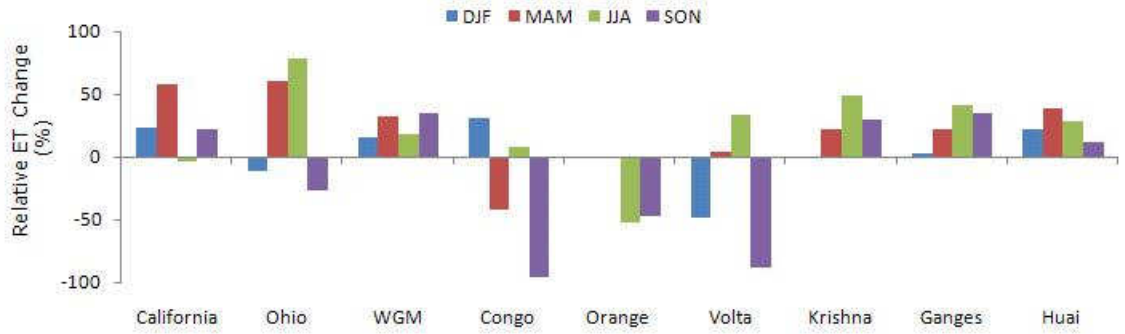

(b) Relative seasonal % ET response due to precipitation change

Figure 5.8: An overview of the relative seasonal % change in runoff and ET in the nine selected basins due to precipitation change in the late 21st century as compared to the late 20th century.

very vulnerable to any climatic shift. Looking into the semiarid basins (California, WGM and Orange) where precipitation is projected to decrease in June-August (JJA); a typically different response is projected to occur for each basin. For California basins, there is an increase in summer (JJA) runoff even though precipitation is reduced while the Western Gulf of Mexico (WGM) shows a decline in summer runoff corresponding to the projected precipitation. For Orange basin, there is a severe decline in runoff from September to November. The hydrologic response is governed by the soil and vegetation characteristics and climatic variability over each basin. Orange basin is characterized for very dry conditions and a precipitation decrease of 23% in its peak dry season (JJA) followed by another 16% decrease from September to November drains away all the soil water by transpiration loss, resulting in a significant decline of runoff.

Fig. 5.8b provides an overview of the relative seasonal % change in ET due to precipitation change in the nine selected basins. California, Ohio and WGM basins present a higher relative % change in the spring season (MAM) as compared to the winter season (DJF), reflecting higher ET demands of the growing season. Despite the negative change in summer (JJA) precipitation, WGM shows an increase in summer ET from the stored soil moisture of preceeding season. For Orange basin, relative seasonal % change in ET is highest in winter (JJA) though relative % change in runoff is highest in the spring (SON) which results from prolonged dry period. It leads to an understanding that in order to study the seasonal dynamics of hydrologic response, we should not limit ourselves exploring the variation of just one particular season. There are impending short and long term connections that translate the effect of one seasonal change to other through antecedent soil moisture conditions.

Analysis on relative seasonal % change of runoff and ET due to individual and cumulative effects of LULCC and climate change signify that precipitation variability is the dominant

factor in alteration of the runoff response while ET response is a mix of LULCC and climate change parameters which tend to offset each other. Fig. 5.9 presents the relative seasonal runoff response summary due to the cumulative effect of LULCC and climate change conditions of the late 21st century for the selected basins. The change in runoff is more sensitive in the summer (JJA) season for Krishna, Ganges and Huai basins which is explained by the particular characteristics of the Asian Monsoon region. California basins show maximum relative runoff increase in the winter (DJF) season owing to the wet conditions. Ohio baasin is more sensitive in the spring (MAM) season as a result of the variability in precipitation and deforestation of deciduous forests. Orange and Volta basins show a marked decline in runoff from September to November, following a long period of dry season. The relative seasonal % change differs for each basin according to basin's geographical and hydro-geological characteristics. Our results signify possible alterations in the seasonal distribution of water availability due to projected LULCC and climate change conditions in the late 21st century.

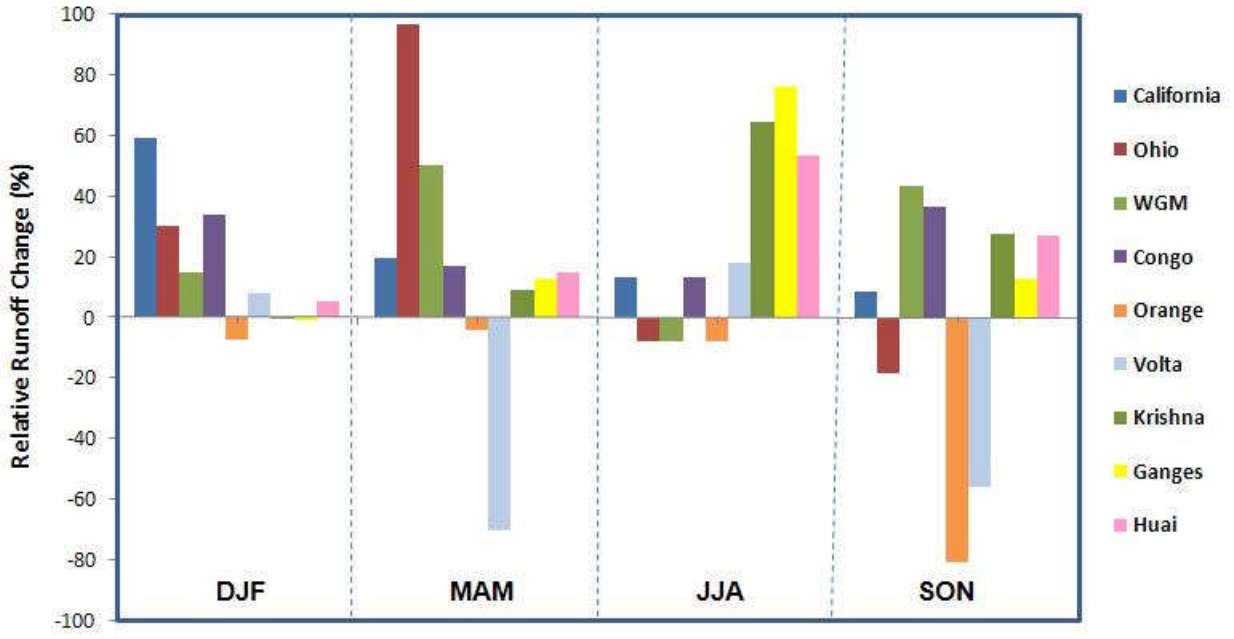

Figure 5.9: Relative seasonal runoff response summary of the nine selected basins due to the cumulative effect of LULCC and climate change.

5.4.3 Uncertainty Range of Hydrologic Response

There are uncertainties associated with future emissions of greenhouse gases and the response of the climate system to these changes at global and local scales. Climate change projections such as changes in temperature, precipitation and corresponding moisture and energy fluxes are characterized by major uncertainties regarding their magnitude, timing and spatial distribution.

The uncertainty range of hydrologic response is analyzed using the multi-model dataset projections of 21 GCMs from the fourth assessment IPCC report (AR4), where the distribution of the annual and seasonal mean surface air temperature response and percentage change in precipitation are described by the median, the 25 and 75% values (half of the models lie between these two values) and the maximum and minimum values in the model ensemble. Fig. 5.10 presents the GCM ensemble projections for annual temperature and precipitation change alongwith the simulated response in annual runoff for the nine selected river basins. Although basins respond differently depending on the magnitude of the precipitation change and climatic and hydrogeologic characteristics of the basin, the runoff response is found to be nonlinear in all the basins. For example, a projected reduction of 12% annual precipitation leads to a 43% reduction in annual runoff in the Orange basin owing to extremely dry conditions. The projected reduction in precipitation has a much higher influence in reducing the Orange basin runoff as compared to an increase in precipitation which does not lead to any significant increase in runoff. Unlike Orange basin, the Volta basin runoff response shows an equal variation with the projected increase or decrease in precipitation. The annual percentage change in precipitation ranges from -9 to 13%, leading to a change in runoff from -34 to 41%. For Congo basin, the annual % change in precipitation from -9 to 13% leads to a variation of -20 to 32% in runoff response. For Congo basin, the annual runoff response is towards the higher end with increase in rainfall. The Volta basin response

is equally distributed, while the Orange basin response is more predominant towards the lower end of reduced runoff.

Fig. 5.11 presents the ET and runoff variability under precipitation and temperature change on a monthly scale for the given range of uncertainty over Krishna Basin. Much variation in runoff response is observed during the monsoon season while ET response shows a consistent increase over the year. The magnitude of change in runoff is much higher to ET.

Fig. 5.12 presents an overview of the hydrologic dynamics of runoff in different hydro-climatic regions by plotting precipitation change adjacent to the resulting change in runoff on a seasonal basis (DJF, MAM, JJA and SON) for the nine selected study basins under IPCC A1B projections. Within the range of first and third quartile response, all the basins present an increase in runoff in DJF except for Krishna and Ganges as DJF is the dry winter season there. However in DJF; high and low extremes are observed over California and Krishna basins respectively. A 30 % increase in DJF precipitation over California may lead to 70 % increase in runoff owing to wet antecedent soil moisture conditions. While, a decline of DJF precipitation over Krishna by 30 % may lower the runoff as much as 70 % owing to dry antecedent soil moisture conditions. In MAM; Ohio and Huai basins show a significant nonlinear increase in runoff response corresponding to precipitation change. In JJA; Krishna, Ganges and Huai basins show a significant increase in runoff owing to wet soil moisture conditions of the monsoon season. The runoff response for Orange basin shows a non-linear decline in runoff corresponding to precipitation change. There is a large uncertainty in the projected change in JJA runoff for the basins in North America. In SON; Orange basin shows a higher range of uncertainty in the reduced runoff. An extreme outlier point for maximum change is observed for the WGM basin. Thus, each of the study basin presents a unique feature of the propagation of uncertainty in different seasons.

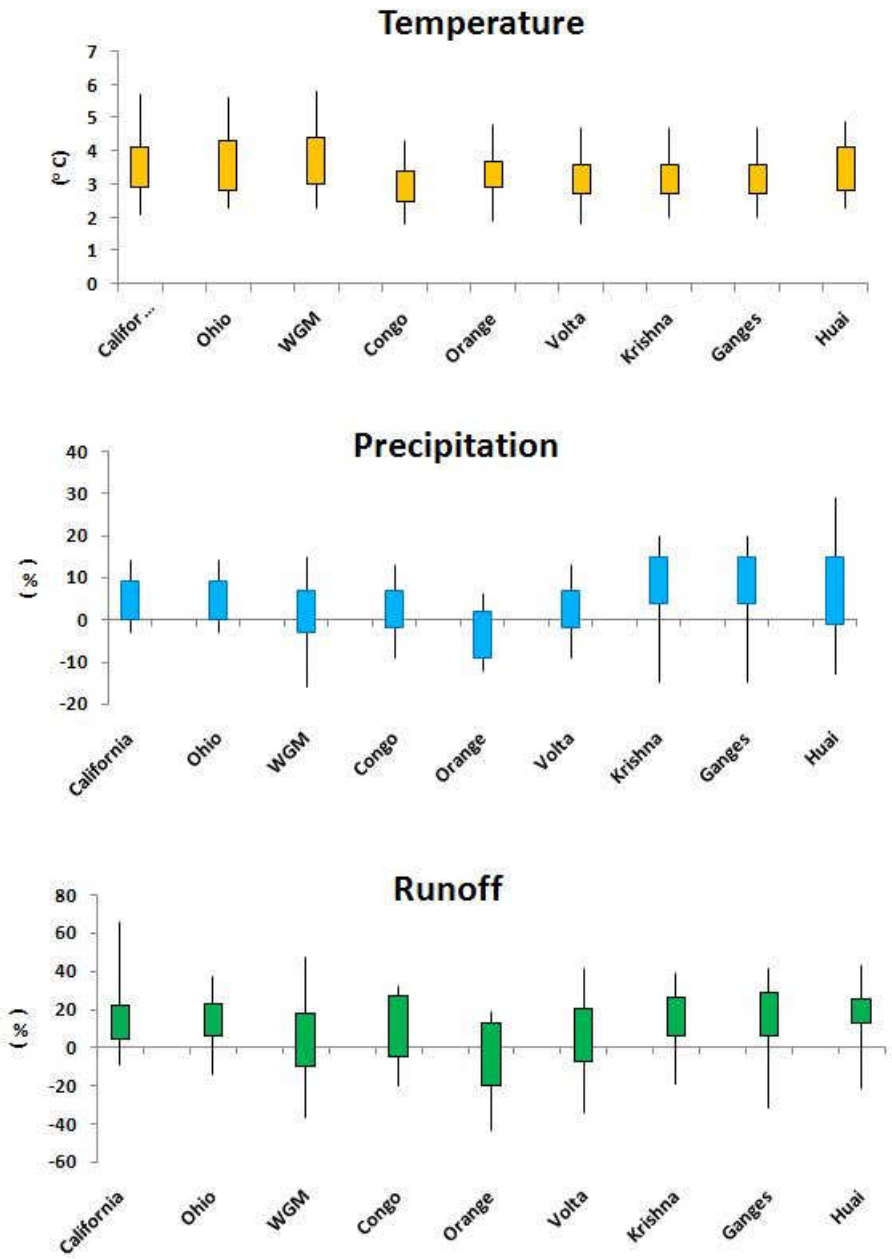

Figure 5.10: GCM ensemble predictions for annual temperature and precipitation anomalies alongwith the simulated results of runoff for the nine selected basins.

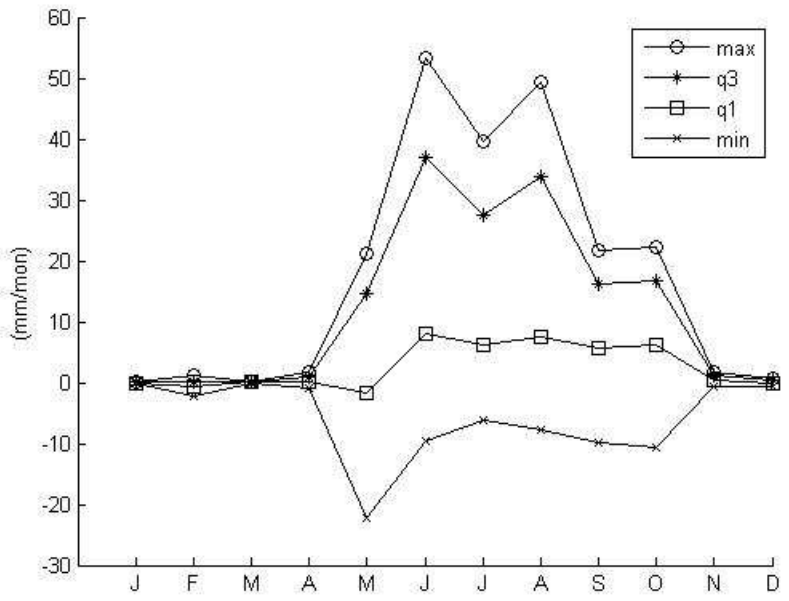

(a) Uncertainty Range of Runoff variability

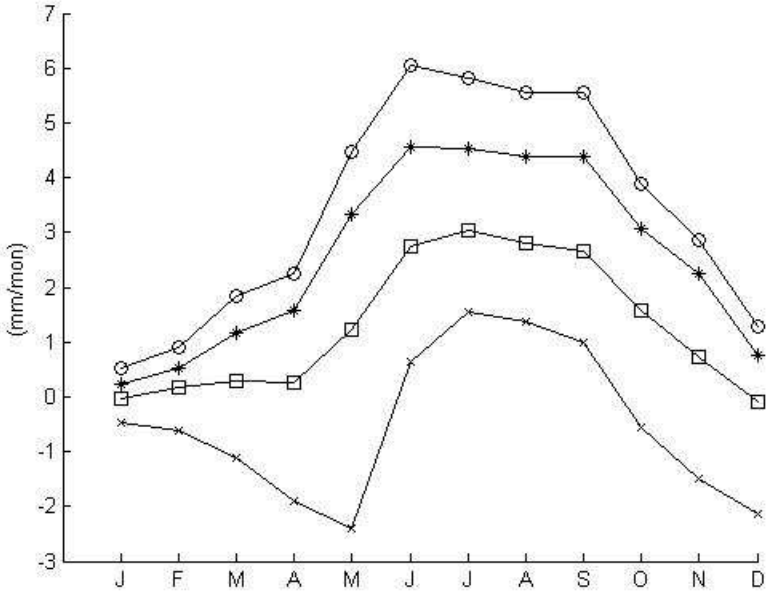

(b) Uncertainty Range of ET variability

Figure 5.11: Uncertainty range of runoff and ET as a result of projected changes in temperature and precipitation from MMD-A1B dataset over the Krishna River Basin.

The translation of precipitation to runoff response varies for each season depending upon antecedent moisture conditions and hydro-geologic characteristics of the basin. Nonlinear effects become very apparent during wet or dry seasons. For other seasons the runoff response is more linear or weakly nonlinear. Intercomparison of the seasonal anomalies for all nine study basins signify a much broader perspective on the propagation of climate change uncertainty. The results show that basins in humid zone have a higher uncertainty range resulting from an increase in precipitation while basins in semi-arid zone present a higher nonlinear response with a reduction in precipitation.

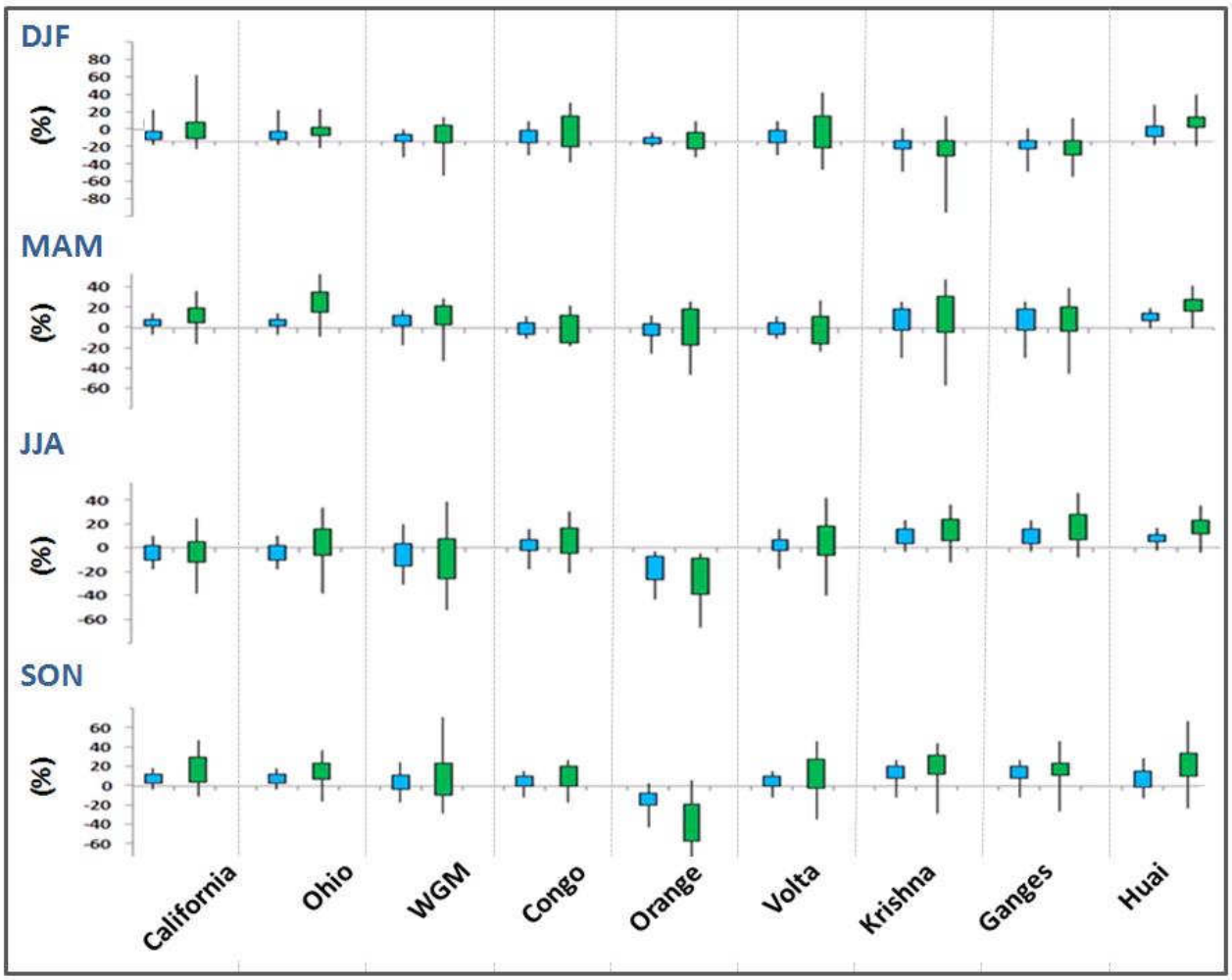

Figure 5.12: An overview of the seasonal uncertainty range of runoff (DJF, MAM, JJA and SON) for the nine selected basins under IPCC A1B scenario projections. (Precipitation change shown in blue color with the corresponding runoff response shown in green color).

5.5 Summary and Conclusions

In recent years, a clearer picture of the regional impacts of LULCC and climate change has emerged due to improvements in model resolution, simulation of processes of importance for regional change and ensembles of multi-model runs. However, resulting quantitative projection of changes on the regional scale hydrologic components at the seasonal time scale are sparse. Derived from the Fourth Assessment Report of IPCC (AR4), this study uses multi-model ensemble of projections for future climate change on a seasonal basis to study the seasonal hydrologic dynamics. The study is constrained by limited understanding of governing feedback loops in the complex earth system and inherent uncertainties in climate change projections, where changes in temperature and precipitation are characterized by major uncertainties regarding their magnitude, timing and spatial distribution.

The Common Land Model (CLM) is used to evaluate hydrologic response of late 21st century in terms of runoff and ET estimates. The model is applied to different hydroclimatic regions with the support of newly developed database constructed in this study. Despite using the best available resources, there remains uncertainty in the model structure, model parameters and forcing data, which result in translating large errors in the simulation results. Given the range of uncertainties involved, the focus of this study is to evaluate the relative seasonal % change in the hydrologic response of late 21st century to late 20th century. The study is performed over nine large river basins selected from Asia, Africa and North America to present the broad climatic and landscape controls on the seasonal hydrologic dynamics and to assess how the controls differ for basins lying in different hydroclimatic regions.

Precipitation change amongst the three contributors (LULCC, temperature and precipitation) was identified as the dominant driving factor in effecting the runoff response. While LULCC was found to be the dominant factor governing ET response in California, Ohio,

Volta, Ganges and Huai basins, precipitation change was found to be the dominant ET control in water limited (WGM, Orange and Krishna) basins. It is observed for all the study basins that small changes in precipitation lead to much larger changes in the runoff response. The non linearity in the runoff transformation is mainly caused by the interaction between soil, climate and vegetation and the transformation of total to effective rainfall. The translation of precipitation to runoff response varies for each season depending upon antecedent moisture conditions and hydro-geologic characteristics of the basin. Nonlinear effects become very apparent during wet or dry seasons. For other seasons, the runoff response is more linear or weakly nonlinear.

Inter-comparison of the seasonal anomalies for all nine study basins signify a much broader perspective on the propagation of climate change uncertainty. The analysis reveals that Orange basin in Africa is highly likely to experience significant reduction in future runoff in the months of September to November, while basins in Asia (Ganges, Krishna and Huai) are very likely to experience significant increase in runoff during the monsoon season. These seasonal differences may not be known through annual estimates of projections. Comparison and quantification of such differences are of particular importance for the water resource managers and policy makers.

Chapter 6

Conclusions

6.1 Summary

Hydrologic changes affect nearly every aspect of human well-being, from agricultural productivity and energy use to flood control, municipal and industrial water supply, fish and wildlife management. The tremendous importance of water in both society and nature underscores the necessity of understanding how a change in global climate could affect regional water supplies. Numerous studies have been conducted at scales ranging from small watersheds to the entire globe to assess the impacts of climate and land-use land cover change (LULCC) on hydrologic systems. However, very few studies have specifically quantified the human influence as well as assessed the combined effects of future climate and LULCC on basin hydrology at the seasonal time scale. This thesis quantifies the human influence and explores the seasonal hydrologic dynamics under both LULCC and climate change conditions of IPCC A1B emission scenario. Special Report on Emission Scenario of IPCC describes A1B emission scenario as a future world of very rapid economic growth, global population that peaks in mid-century and declines thereafter, and the rapid introduction of new and more efficient technologies.

Different regions respond differently to the same change in stress driver, depending largely on basin physio-geographical and hydro-geological characteristics. Since each region is representative of a unique characteristic of the hydrologic problem under climate change scenario, there is a need to develop a different set of water management plan and strategy. In this

thesis, nine river basins with drainage areas ranging from 174,000 to 3,680,000 square kilometers are selected from North America (Ohio, California and Western Gulf of Mexico), Africa (Congo, Volta and Orange) and Asia (Ganges, Krishna and Huai) to represent a wide range of conditions. For example, Ohio, Volta and Congo basins are selected from the humid zone while Western Gulf of Mexico (WGM), Orange and Krishna river basins are selected from the semiarid zone to compare and contrast the results from one basin to other. The human impact on natural hydrologic conditions of each of the selected basin is assessed by using a coupled hydrologic and water management modeling framework.

Direct impacts such as water withdrawal, consumption, and storage regulations are accounted for by taking the results of hydrologic model as input to a water resources management model, specifically the Water Availability and Supply Model (WASM). A number of indices derived from mass balance equations as well as through water use regimes and Budyko curve are used to quantify the extent to which human interferences impact natural flow discharge. Although the various indices show consistent results when comparisons are made over the selected basins, each of the indices represent different aspects of the impacts of water use to the natural hydrology.

The Common Land Model (CLM) is used as the hydrologic model to evaluate changes in future hydrologic response in terms of runoff and ET estimates. The model incorporates detailed physical process representation, uses physical parameterization without the need for calibration and can be run at high spatial and temporal resolutions. The model is applied to different hydro-climatic regions with the support of newly developed database constructed in this study. A consistent GIS-based database is constructed for the surface boundary conditions and meteorological forcing of the model from existing observational databases with various resolutions, map projections and data formats. Surface dataset is prepared at 30 km spatial resolution and meteorological forcing is derived from ECMWF reanalysis product

ERA-40 at 30 minute time step for the period 1976 through 2000. Though the uncertainties inherent in the hydrologic model are not accounted, the model is considered to be suitable for prediction study as it is based on physically interpreted parameters derived from the real world data. Derived time series data (in terms of precipitation and runoff) are analyzed in time frequency space for a better understanding of the underlying processes. For Semi-arid basins, the runoff response is determined to be more dependent on soil and vegetation characteristics where different factors like soil permeability, topography and vegetation cover interplay at multiple time scales to affect the hydrologic response.

6.2 Contributions

The most novel aspect of this thesis is the analysis of hydrologic components under LULCC and climate change conditions at the seasonal time scale. Though, there are a number of studies which have evaluated the impact of future LULCC and climate change on hydrologic responses in major river basins of the world, they have typically focused on averages of river discharge at the annual scale and very few studies show projections of seasonal differences. Our analysis reveals that there are regions (for example, Orange and Volta in Africa), where there are seasons which are highly likely to experience significant reduction in future runoff and there are other regions (Ganges, Krishna and Huai in Asia) with seasons very likely to experience significant increase in runoff under climate change scenario. These seasonal differences may not be known through annual estimates of projections.

Hirabayashi et al. (2008) [35] discussed the impact of climate change on river discharge of major river basins at shorter time scales i.e., flood and drought, using a high resolution coupled Atmospheric Ocean General Circulation Model (AOGCM). They showed summer flood frequency increase in Asian basins, and drought frequency increase in North America and South Africa and projected several regions to have increases in both flood and drought

frequency. Such regions show a decrease in the number of precipitation days, but an increase in days with heavy rain. Several regions show shifts in the flood season from spring snowmelt to the summer period of heavy precipitation. Since the results are specific to AOGCM, discrepancies result with the use of a different model. Despite existing regional variability with AOGCMs, numerous impact assessment studies use projection from a single AOGCM [155, 156], leading to a wide range of outcomes and even opposing conclusions. Multi-model ensembles of projections for future climate change in the Fourth Assessment Report of IPCC [9] provide a higher quality and more consistent climate change information. This forms the basis of our study where climate change projections (i.e. mean surface air temperature response and percentage change in precipitation) are derived on a seasonal basis and at a regional scale from the Fourth Assessment Report of IPCC [9].

Another unique contribution of this thesis is the inter-comparison of hydrologic response of basins in different climatic regimes. Comparative studies have been carried out in different climate-soil vegetation regions in small domains [82, 152], but few have presented a comparative analyses in the global context. In this study, nine river basins are selected from Asia, Africa and North America, where each basin represents a unique climatic zone, vegetation cover, soil type and land use-land cover. Moreover, projected changes and the role of human influence vary from basin to basin. Distinctive characteristics are determined for the semi-arid and humid basins under climate change conditions. Nohara et al. (2006) [26] investigated the projections of river discharge for 24 major rivers in the world and determined an increase in the annual mean precipitation, evaporation, and runoff in high latitudes of the Northern Hemisphere, southern to eastern Asia, and central Africa at the end of the twenty-first century. A decrease was reported in the Mediterranean region, Southern Africa, Southern North America, and Central America. For the nine river basins in our study, a similar regional characterization response in runoff is observed. Also, similar response is reported in semi-arid regions, where the decrease in runoff is larger than that for evaporation when

precipitation is reduced as precipitation in semi-arid regions is allocated more to evaporation.

There are a number of studies specific to either the LULCC or the climate change impact on hydrologic dynamics. This study is unique in its ability to assess the response of each component of change and also to integrate various components of change. Understanding the response of hydrologic components as a result of interconnected LULCC, temperature and precipitation change and the response due to each change separately assists in deciphering the vast complexity of projected variability in the seasonal hydrologic dynamics of different basins. Each change disrupts the hydrologic balance within the basin and the partitioning of precipitation into ET, runoff and soil storage flux differently. In general, results from different basin simulations agree with respect to the direction of change (i.e. increase in runoff with increase in precipitation), though the magnitude of change varies significantly. Precipitation change amongst the three contributors (LULCC, temperature and precipitation) was identified as the dominant driving factor in effecting the runoff response. While LULCC was found to be the dominant factor governing ET response in California, Ohio, Volta, Ganges and Huai basins, precipitation change was found to be the dominant ET control in water limited (WGM, Orange and Krishna) basins. Changes in precipitation patterns have a more dominant control on the runoff response, while changes in temperature have an effect on evapotranspiration. Several experiments and modeling studies demonstrate that river discharge has increased as a consequence of deforestation in recent years [166, 167, 168]. Rost et al. (2008) [70] showed that an expansion of agricultural land will result in a reduction of transpiration and interception loss as well as an increase in evaporation and river discharge, with the magnitudes of change comparable to those of the climate change effects. We obtained results showing a reduction in evapotranspiration and river discharge as a result of deforestation though the magnitude of change is smaller to those of the climate change effects.

It is observed for all the study basins that small changes in precipitation lead to much larger changes in runoff. The non linearity in runoff transformation is mainly caused by the interaction between soil, climate and vegetation and the transformation of total to effective rainfall. As a result of this complex interaction, soil saturation approaches different levels at different time steps, leading to a non-linear response of runoff to precipitation change. Inter-comparison of the seasonal anomalies for all nine study basins present a much broader perspective on the propagation of climate change uncertainty. The results show that basins in humid zone have a higher uncertainty range resulting from an increase in precipitation while basins in semi-arid zone present a higher range with a reduction in precipitation. Any changes in seasonality will severely impact the agricultural production. Thus, it is important to identify the key issues and challenges which an expected climate change will bring in the hydrology of a given region and provide a framework for adequate research and recommendations to enhance efficiency in the water sector to avoid future crises. This study leads one step forward to advance and integrate water and energy cycle observation, scientific understanding, and its prediction to enable society to cope with future water adversities.

6.3 Future Work

Climate change impact assessment studies are constrained by the limited understanding of feedback loops in the complex earth system and inherent uncertainties in climate change projections, where changes in temperature and precipitation are characterized by major uncertainties regarding their magnitude, timing and spatial distribution. Improvements in the characterization of climate change uncertainties will significantly improve the predictive understanding of hydrologic dynamics.

There are limitations with reanalysis data and how it is altered to represent climate change scenarios in the model. One is simply the limitations in shifting meteorological forcing

to represent climate change; it cannot capture certain aspects of predicted climate change (e.g., greater intermittency in precipitation, or the intensification of the hydrologic cycle). Uncoupled modeling of the land surface and climate is another compromise that can affect response as certain forcing may not be appropriate for the new land use-land cover conditions. Precipitation is the most important factor for hydrologic dynamics, and much work is required to be done for a better representation of precipitation for hydrologic studies.

Though, there are a number of land surface models (LSMs) which are used to assess climate change dynamics on the hydrologic response of different hydro-climatic regions, there are differences in the model structure, complexity, economy of physics and usage and tuning of model parameters among different LSMs. A single LSM does not represent the variations in hydrologic response that may result from using alternate LSMs in the changing world. The structure and parameterizations of LSMs differ considerably, as do, in turn, their representations of soil moisture and runoff. The differences in soil moisture from different LSMs are generally much larger in the dry season and in arid regions. Use of multiple LSMs is proposed as future work to derive an optimal solution for the simulation of water and energy partitioning under the climate change scenario.

Given the range of downscaling techniques and the fact that each approach has its own advantages and shortcomings, there exists no universal method which works for all situations. A statistical downscaling approach using multiple scenarios is adopted by several studies for climate change assessment. It would be interesting to study how the differences in GCMs and IPCC emission scenarios (A1, A2, B1, B2), lead to differences in the hydrologic response. Moreover, detailed analysis on evaluation of underlying hydrologic components would reveal the changes in underlying processes, thus enhancing the predictive understanding.

Appendix A

A.1 IPCC Scenarios

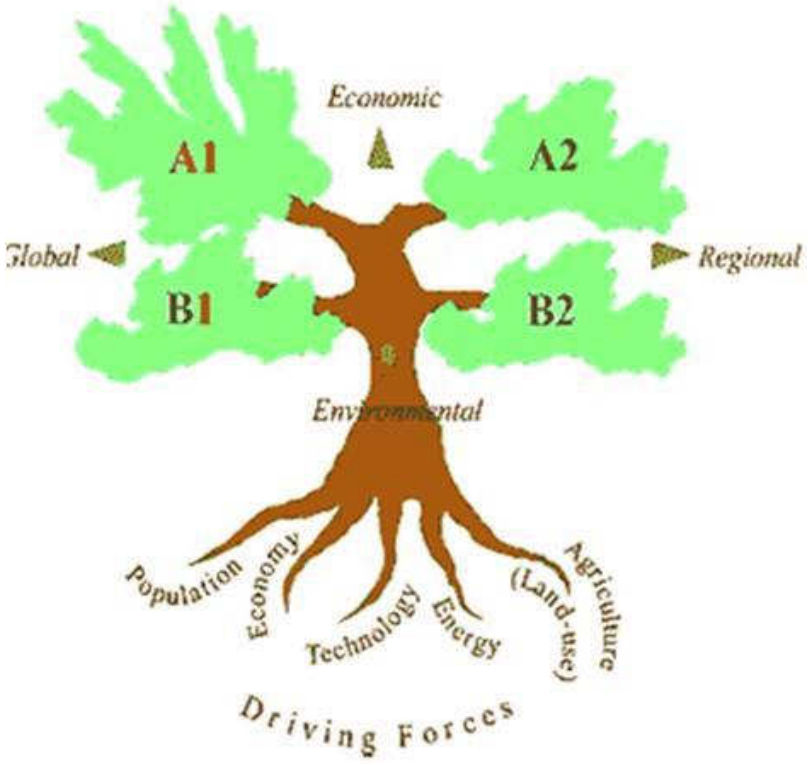

Figure A.1: Schematic illustration of the four SRES storylines from IPCC SRES Scenarios [2]

Scenarios are the images of how the future might unfold, and thus an appropriate tool for analysing how driving forces may influence future emissions and in assessing the associated uncertainties. The Intergovernmental Panel on Climate Change (IPCC) has developed long-term emissions scenarios which have been widely used in the analysis of possible climate and

land use-land cover change, its impacts, and mitigation efforts. IPCC published a new set of scenarios in the Special Report on Emissions Scenarios (SRES) in 2001 [2]. These scenarios are based on a thorough review of the literature, the development of narrative 'storylines' and the quantification of these storylines using six different integrated models from different countries.

IPCC has laid out four storylines where each storyline assumes a distinctly different direction for future development. Together they describe divergent futures that encompass a significant portion of the underlying uncertainties in the main driving forces. They cover a wide range of key future characteristics such as demographic change, economic development, and technological change. Figure A.1 gives a schematic illustration of the four SRES storylines. The four storylines combine two sets of divergent tendencies: one set varying between strong economic values and strong environmental values, the other set between increasing globalization and increasing regionalization.

The storylines are summarized as follows [169]:

The A1 storyline and scenario family describes a future world of very rapid economic growth, global population that peaks in mid-century and declines thereafter, and the rapid introduction of new and more efficient technologies. Major underlying themes are convergence among regions, capacity building, and increased cultural and social interactions, with a substantial reduction in regional differences in per capita income. The A1 scenario family develops into three groups that describe alternative directions of technological change in the energy system. The three A1 groups are distinguished by their technological emphasis: fossil intensive (A1FI), non-fossil energy sources (A1T), or a balance across all sources (A1B).

The A2 storyline and scenario family describes a very heterogeneous world. The underlying theme is self-reliance and preservation of local identities. Fertility patterns across regions

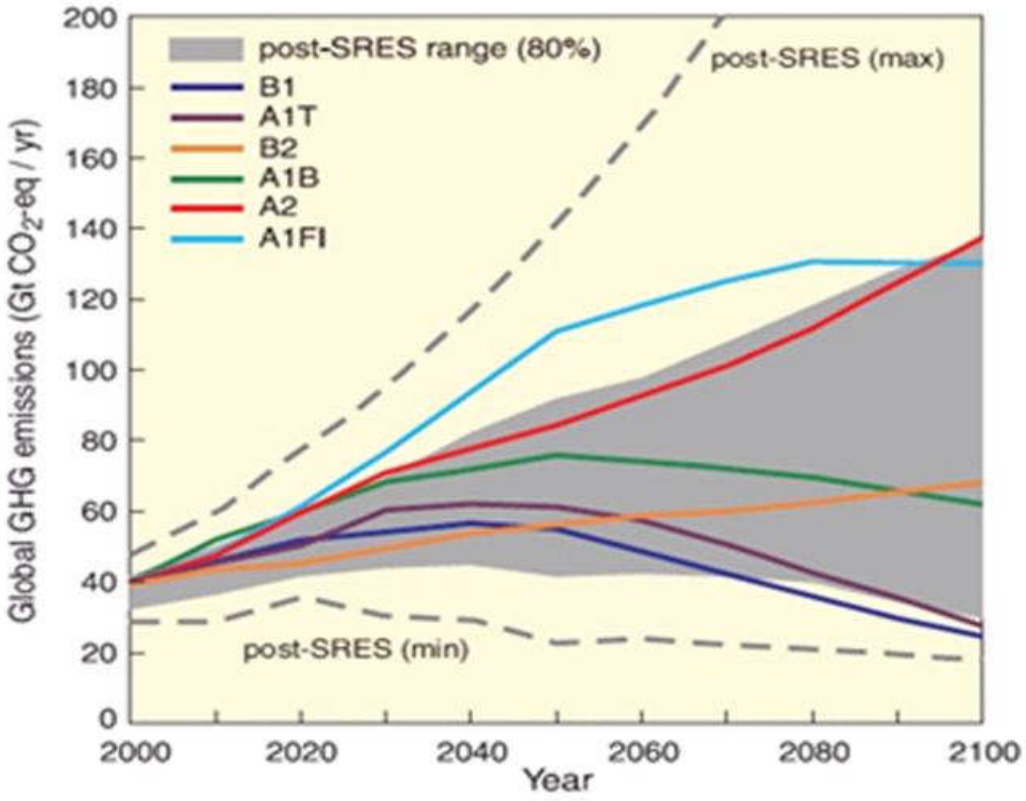

(a)

Figure A.2: An overview of IPCC Scenarios [2]

converge very slowly, which results in continuously increasing global population. Economic development is primarily regionally oriented and per capita economic growth and technological change are more fragmented and slower than in other storylines.

The B1 storyline and scenario family describes a convergent world with the same global population that peaks in mid-century and declines thereafter, as in the A1 storyline, but with rapid changes in economic structures toward a service and information economy, with reductions in material intensity, and the introduction of clean and resource-efficient technologies. The emphasis is on global solutions to economic, social, and environmental sustainability, including improved equity, but without additional climate initiatives.

The B2 storyline and scenario family describes a world in which the emphasis is on local solutions to economic, social, and environmental sustainability. It is a world with continuously increasing global population at a rate lower than A2, intermediate levels of economic development, and less rapid and more diverse technological change than in the B1 and A1 storylines. While the scenario is also oriented toward environmental protection and social equity, it focuses on local and regional levels.

A.2 An Overview of IMAGE

The Integrated Model to Assess the Global Environment (IMAGE) uses IPCC scenarios to investigate the global issues, and their causes and links, in a comprehensive framework. IMAGE is an ecological-environmental framework that simulates the environmental consequences of human activities worldwide. It represents interactions between society, the biosphere and the climate system to assess sustainability issues like climate change, biodiversity and human well-being. IMAGE was initially developed in 1980s at the National Institute for Public Health and the Environment (RIVM), and further developed at the Netherlands Environmental Assessment Agency (MNP). IMAGE version 2.4 released in 2006, explores the long-term dynamics of global change as a result of interacting demographic, technological, economic, social, cultural and political factors. A full description of the various components of IMAGE 2.4 is given in the MNP publication, Integrated modelling of global environmental change: An overview of IMAGE 2.4 [3].

The IMAGE 2.4 framework consists of a number of sub models, structured in a framework as shown in Figure A.3. Energy, supply and demand is assessed by using the IMAGE energy regional model which analyses the long-term trends in energy demand and efficiency and the possible transition towards renewable energy sources. Demography model considers future changes in the population size and structure in relation to the socio-economic conditions and state of the environment. The agricultural economy model computes the regional demand for food, feed crops and timber. The required production is determined by the sum of domestic regional demand and net trade. It includes models for describing the global carbon cycle and the global nitrogen and phosphate cycle. The natural vegetation model simulates the potential distribution of natural vegetation and crops on the basis of climate conditions and soil characteristics on a spatial resolution of 0.5 degree latitude by 0.5 degree longitude.

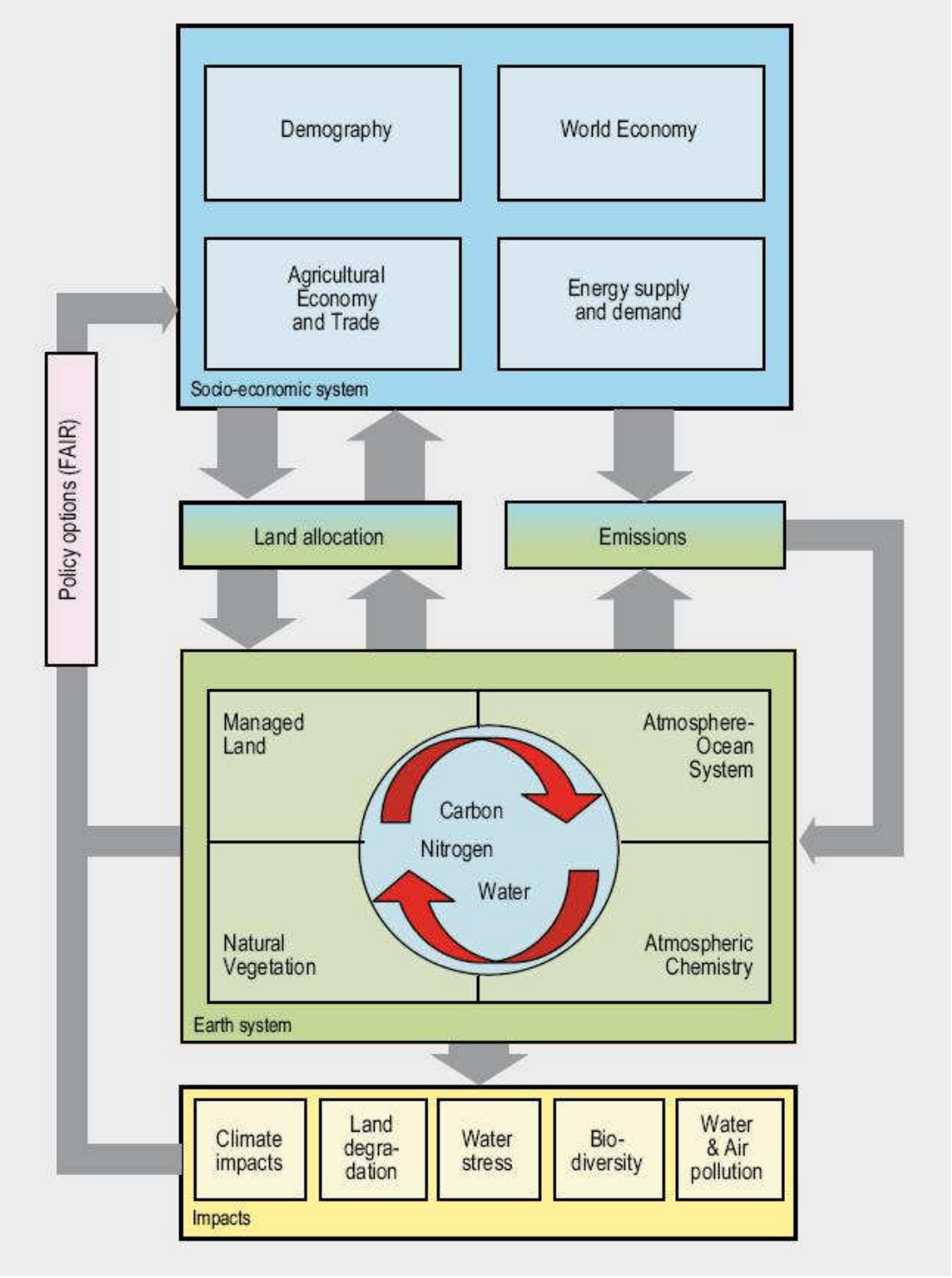

Figure A.3: Schematic diagram of IMAGE 2.4 [3]

Appendix B

B.1 Comparison of ERA-40 to Observation Datasets

The European Centre for Medium Range Weather Forecasts (ECMWF) prepared a 40 year reanalysis dataset (ERA-40) from 1958 to 2001. Based on the observational data that were used, the whole ERA-40 time period of 1958 to 2001 is divided into three parts: the satellite period (1989-2001) when a large amount of satellite data were assimilated into the ERA-40 system, the pre-satellite period (1958-1972) when no satellite data were available, and the transition period (1973-1988) when the amount of satellite data that were assimilated increased with time. The quality of the hydrological cycle differs between the periods as the biases in the hydrological cycle are strongly influenced by the different observing systems available in the three periods.

Figure B.1 shows the comparison of trends and variability in CRU (Climate Research Unit; [104], ERA-40 and NCEP/NCAR analyses for surface air temperature over the period 1958 to 2001 on left and over the period 1979 to 2001 on right. CRU data uses all available monthly station averages of mean temperature from land regions of the world. It is observed that the overall warming trends are smaller for ERA-40 than for CRU. Over the northern hemisphere, and for Europe and North America separately, the ERA-40 trend is about 30% smaller than the CRU trend for the full period, but within 10% of the CRU trend for 1979 to 2001. The trends for 1979-2001 from ERA-40 are in closer agreement with CRU than are the corresponding trends from NCEP/NCAR. Part of the reason ERA-40 performs better

than NCEP/NCAR is in its use of observation datasets of surface air temperature [106].

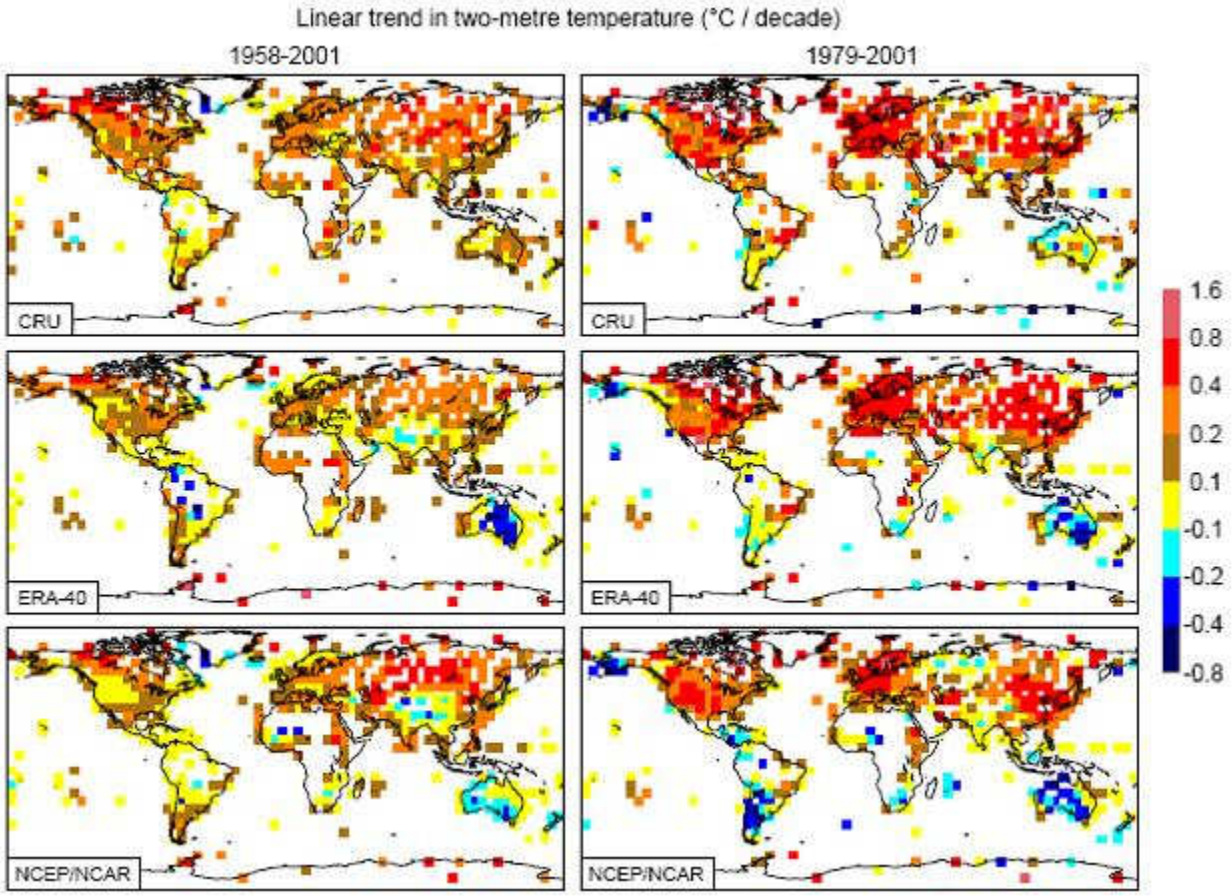

Figure B.1: Comparison of trends and variability in CRU, ERA-40 and NCEP/NCAR analyses for surface temperature over the periods 1958-2001(left) and 1979-2001 (right), derived from ECMWF ERA-40 Project Report Series [4].

Figure B.2 shows the plot of monthly mean precipitation over land from 1987 to 2001 derived from CMAP (CPC Merged Analysis of Precipitation; [170], GPCP (Global Precipitation Climatology Project; [171], ERA-15 (ECMWF 15 Year Reanalysis Dataset) and ERA-40. For CMAP and GPCP, precipitation values are derived from satellite measurements of infrared and microwave emissions with empirically based algorithms. Though the monthly ERA-40 precipitation is observed to be overestimated when compared to the observations of CMAP and GPCP, the precipitation values are much closer to observations over land, than over the ocean. The overestimation of precipitation over land and ocean is largely over the tropics. It is analyzed that the problem of excessive rainfall results in part from

the way the humidity analysis spread increments in the horizontal, which moistens regions that the data indicates are too dry and also adds moisture in neighbouring regions that are already saturated. Rainfall thus gets increased where it occurs naturally [103].

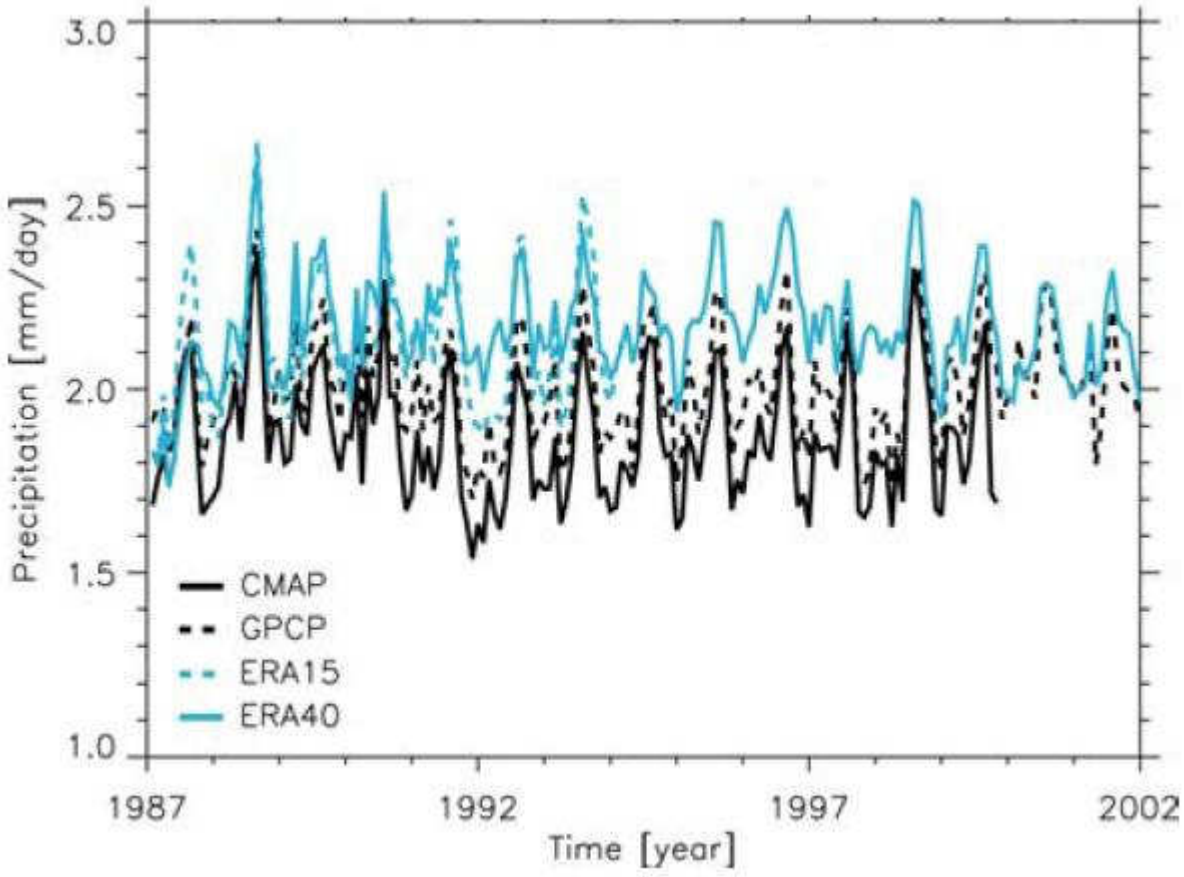

Figure B.2: Monthly mean precipitation over land from 1987-2001, derived from ECMWF ERA-40 Project Report Series [5].

Various large regions from different climates and continents were used to validate ERA-40 hydrological cycle. The selected regions include: Amazon, Amur, Arctic Ocean catchment represented by its 6 largest rivers (Yenisey, Kolyma, Lena, Mackenzie, Northern Dvina, Ob), Baltic Sea catchment (land only), Congo, Danube, Ganges/Brahmaputra, Mississippi, Murray, Nile, Parana, Yangtze Kiang. Figure B.3 shows the precipitation ratio of ERA-40 data against observations for three different periods. GPCC data are used as observations for the 1989-2001 period, and CRU data are used for the two other periods. The precipitation ratio

is an indicator of the precipitation bias which varies for the three periods. For the earliest period, the precipitation ratio is lower than in the two later periods for most of the regions. For the Nile river, the ERA-40 precipitation is close to the observations only in the latest period while it is largely overestimated in the two earlier periods. For Ganges/Brahmaputra, precipitation is largely overestimated only in the latest period (1989-2001). The fact that the precipitation bias is not the same in all three periods leads to the conclusion that the different observing systems and assimilation data in the three periods influence the quality of the ERA-40 precipitation over land.

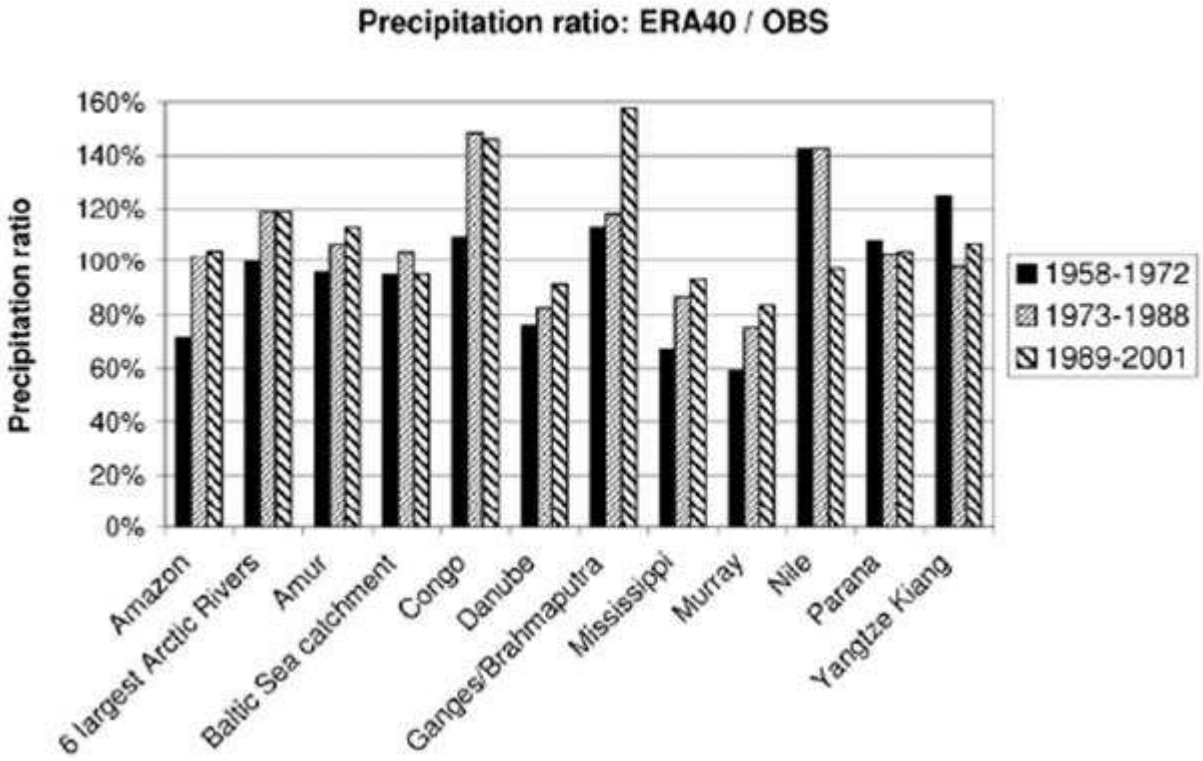

Figure B.3: Precipitation ratio of ERA-40 to observations for large river basins. Observations comprise GPCC data for 1989-2001 and CRU data for 1958-1972 and 1973-1988, derived from ECMWF ERA-40 Project Report Series [5].

References

[1] G.B. Bonan. *Ecological Climatology: Concepts and Applications.* New York, NY: Cambridge University Press, 2002.

[2] *IPCC Special Report on Emissions Scenarios*. Cambridge, UK, 2001.

[3] A.F. Bouwman, T. Kram, and G.K. Klein. *Integrated modeling of global environmental change. An overview of IMAGE 2.4*. Netherlands Environmental Assessment Agency (MNP), 2006.

[4] A.J. Simmons, P.D. Jones, V. da Costa Bechtold, A.C.M. Beljaars, P.W. Kållberg, S. Saarinen, S.M. Uppala, P. Viterbo, and N. Wedi. Comparison of trends and low-frequency variability in CRU, ERA-40 and NCEP/NCAR analyses of surface air temperature. *Journal of Geophysical Research*, 109, 2004.

[5] S. Hagemann, K. Arpe, and L. Bengtsson. *Validation of the hydrological cycle of ERA-40*. Reports on Earth System Science, 2005.

[6] R. Srikanthan and T.A. McMahon. Stochastic generation of annual, monthly and daily climate data: A review. *Hydrology and Earth System Sciences*, 5:653–670, 2001.

[7] C.Y. Xu and V.P. Singh. Review on regional water resources assessment models under stationary and changing climate. *Water Resources Management*, 18:591–612, 2004.

[8] T.G. Huntington. Evidence for intensification of the global water cycle: Review and synthesis. *Journal of Hydrology*, 319:83–95, 2006.

[9] *Climate Change 2007: The Physical Science Basis, Fourth Assessment Report (AR4) of the Intergovernmental Panel on Climate Change.* Cambridge, UK, 2007.

[10] P.H. Whitfield and A.J. Cannon. Recent variations in climate and hydrology in Canada. *Canadian Water Resources Journal*, 25:19–66, 2000.

[11] I. Muzik. Sensitivity of hydrologic systems to climate change. *Canadian Water Resources Journal*, 26:233–252, 2001.

[12] J.S. Risbey and D. Entekhabi. Sensitivity of hydrologic systems to climate change. *Journal of Hydrology*, 184:209–223, 1996.

[13] M.I. Hejazi, X. Cai, and D.K. Borah. Calibrating a watershed simulation model involving human interference: an application of multi-objective genetic algorithms. *Journal of Hydroinformatics*, 10:97–111, 2008.

[14] L. Claessens, C. Hopkinson, E. Rastetter, and J. Vallino. Effect of historical changes in land use and climate on the water budget of an urbanizing watershed. *Water Resources Research*, 42, 2006.

[15] Y. Jia, H. Wang, Z. Zhou, Y. Qiu, X. Luo, J. Wang, D. Yan, and D. Qin. Development of the WEP-L distributed hydrological model and dynamic assessment of water resources in the Yellow River Basin. *Journal of Hydrology*, 331:606–629, 2006.

[16] X. Cai and M.W. Rosegrant. Global Water Demand and Supply Projections Part 1: A modeling approach. *Water International*, 27:159–169, 2002.

[17] T.W. Biggs, A. Gaur, C.A. Scott, P. Thenkabail, G.R. Parthasaradhi, M.K. Gumma, S. Acharya, and H. Turral. *Closing of the Krishna Basin: Irrigation, streamflow depletion and macroscale hydrology (IWMI Research Report III)*. International Water Management Institute: Colombo, 2007.

[18] P.H. Gleick and E.L. Chaleki. The impacts of climatic changes for water resources of the Colorado and Sacramento-San Joaquin River Basins. *Journal of American Water Resources Association*, 35:1429–1441, 1999.

[19] J. Alcamo and T. Henrichs. Critical regions: a model-based estimation of world water resources sensitive to global changes. *Aquatic Science*, 64:352–362, 2002.

[20] N.W. Arnell, M.J.L. Livermore, S. Kovats, P.E. Levy, R. Nichollas, M.L. Parry, and S.R. Gaffin. Climate and socio-economic scenarios for global-scale climate change impacts assessments: characterising the SRES storylines. *Global Environmental Change*, 14:3–20, 2004.

[21] A.M. Thomson, A.B. Robert, N.J. Rosenberg, R.C. Izaurralde, and V. Benson. Climate Change Impacts for the Conterminous USA: An Integrated Assessment. *Climate Change*, 69:43–65, 2005.

[22] T. Barnett, D.W. Pierce, H.G. Hidalgo, C. Bonfils, B.D. Santer, T. Das, G. Bala, A.W. Wood, T. Nazawa, A. Mirin, D.R. Cayan, and M. Dettinger. Human-induced changes in the hydrology of the western United States. *Science*, 319:1080–1083, 2008.

[23] J.E. Herring, J. Hunt, J.M. Crutcher, and J.K. Ward. *Water for Texas*. Texas Water Development Board, 2007.

[24] K.J. Hennessy, J.M. Gregory, and J.F.B. Mitchell. Changes in daily precipitation under enhanced greenhouse conditions. *Climate Dynamics*, 13:667–680, 1997.

[25] D.A. Miller and R.A. White. A Conterminous United States multilayer soil characteristics dataset for regional climate and hydrology modeling. *Earth Interactions*, 2:1–26, 1998.

[26] D. Nohara, A. Kitoh, M. Hosaka, and T. Oki. Impact of climate change on river discharge projected by multimodel ensemble. *Journal of Hydrometeorology*, 7:1076–1089, 2006.

[27] S. Manabe, P.D. Milly, and R.T. Wetherald. Simulated long-term changes in river discharge and soil moisture due to global warming. *Journal of Hydrological Sciences*, 49:625–642, 2004.

[28] C.J. Vörösmarty, P. Green, J. Salisbury, and R.B. Lammers. Water Resources: Vulnerability from Climate Change and Population Growth. *Science*, 289:284–288, 2000.

[29] V.K. Arora and G.J. Boer. Effects of simulated climate change on the hydrology of major river basins. *Journal of Geophysical Research*, 106:3335–3348, 2001.

[30] H.J. Fowler, S. Blenkinsopa, and C. Tebaldi. Linking climate change modeling to impacts studies: Recent advances in downscaling techniques for hydrological modeling. *International Journal of Climatology*, 27:1547–1578, 2007.

[31] C. Prudhomme, N. Reynard, and S. Crooks. Downscaling of global climate models for flood frequency analysis: Where are we now? *Hydrological Processes*, 16:1137–1150, 2002.

[32] F.H.S. Chiew, P.H. Whetton, T.A. McMahon, and A.B. Pittock. Simulation of the impacts of climate change on runoff and soil moisture in Australian catchments. *Journal of Hydrology*, 167:121–147, 1995.

[33] A. Avila, C. Neal, and J. Terradas. Climate change implications for streamflow and streamwater chemistry in a Mediterranean catchment. *Journal of Hydrology*, 177:96–116, 1996.

[34] P. Singh and N. Kumar. Impact assessment of climate change on the hydrological response of a snow and glacier melt runoff dominated Himalayan river. *Journal of Hydrology*, 193:316–350, 1997.

[35] Y. Hirabayashi, S. Kanae, S. Emori, T. Oki, and M. Kimoto. Global projections of changing risks of floods and droughts in a changing climate. *Journal of Hydrological Sciences*, 53:754–772, 2008.

[36] N.W. Arnell. Effect of IPCC SRES emission scenarios on river runoff: a global perspective. *Hydrological Earth System Science*, 7:619–641, 2003.

[37] P. Horton, B. Schaefli, A. Mezghani, B. Hingray, and A. Musy. Assessment of climate-change impacts on alpine discharge regimes with climate model uncertainty. *Hydrological Processes*, 20:2091–2109, 2006.

[38] D. Wang and X. Cai. Robust data assimilation in hydrological modeling A comparison of Kalman and H-infinity filters. *Advances in Water Resources*, 31:455–472, 2008.

[39] W. Buytaert, R. Celleri, and L. Timbe. Predicting climate change impacts on water resources in the tropical Andes: Effects of GCM uncertainty. *Geophysical Research Letters*, 36, 2009.

[40] M.H. Costa, A. Botta, and J.A. Cardille. Effects of large scale changes in land cover on the discharge of the Tocantins River. *Journal of Hydrology*, 283:206–215, 2003.

[41] B.F.W. Croke, W.S. Merritt, and A.J. Jakeman. A dynamic model for predicting hydrologic response to land cover changes in gauged and ungauged catchments. *Journal of Hydrology*, 291:115–131, 2004.

[42] K.Y. Li and M.T. Coe. Modeling the hydrological impact of land use change in West Africa. *Journal of Hydrology*, 337:258–268, 2007.

[43] B. Fakete, C. Vörösmarty, and W. Grabs. *Global, composite runoff fields of observed river discharge and simulated water balances*. Technical Report 22, Global Runoff Data Centre, Koblenz, Germany, 1999.

[44] P. Döll, F. Kaspar, and B. Lehner. Global hydrological model for deriving water availability indicators: model tuning and validation. *Journal of Hydrology*, 270:105–134, 2003.

[45] M.T. Coe. Modeling terrestrial hydrological systems at the continental scale: Testing the accuracy of an atmospheric GCM. *Journal of Climate*, 13:704, 2000.

[46] Y. Tessier, S. Lovejoy, P. Hubert, D. Schertzer, and S. Pecknold. Multifractal analysis and modeling of rainfall and river flows and scaling, causal transfer functions. *Journal of Geophysical Research*, 26:427–440, 1996.

[47] D. Labat. Recent advances in wavelet analyses: Part 1. A review of concepts. *Journal of Hydrology*, 314:275–288, 2005.

[48] A. Grinsted, J. C. Moore, and S. Jevrejeva. Application of the cross wavelet transform and wavelet coherence to geophysical time series. *Nonlinear Processes in Geophysics*, 11:561–566, 2004.

[49] R. Bracewell. *The fourier transform and its applications*. McGraw-Hill Inc., New York, 1978.

[50] M.B. Priestley. *Spectral Analysis and Time Series*. Academic Press, London, 1981.

[51] P. Kumar and E. Fouroula-Georgiou. Wavelet analysis for geophysical application. *Reviews of Geophysics*, 35:385–412, 1997.

[52] S. Kang and L. Henry. Wavelet analysis of hydrological and water quality signals in an agricultural watershed. *Journal of Hydrology*, 338:1–14, 2007.

[53] M. Nakken. Wavelet analysis of rainfall runoff variability isolating climatic from anthropogenic patterns. *Environmental Modeling and Software*, 14:283–295, 1999.

[54] P. Kabat, M. Claussen, P.A. Dirmeyer, J.H.C. Gash, L. Bravo de Guenni, M. Meybeck, R.A. Pielke Sr., C.J. Vörösmarty, R.W.A. Hutjes, and S. Lütkemeier. *Vegetation, Water, Humans and the Climate: A new perspective on an interactive system.* Springer, Berlin, Global Change: The IGBP Series, 2004.

[55] J.O. Adegoke, R.A. Pielke, J. Eastman, R. Mahmood, and K.G. Hubbard. Impact of irrigation on midsummer surface fluxes and temperature under dry synoptic conditions: A regional atmospheric model study of the U.S. high plains. *Monthly Weather Review, AMS*, 131:556–564, 2003.

[56] M.W. Rosegrant and X. Cai. Global Water Demand and Supply Projections Part 2: Results and Prospects to 2025. *Water International*, 27:170–181, 2002.

[57] E.M. Douglas, D. Niyogi, S. Frolking, J.B. Yeluripati, R.A. Pielke, N. Niyogi, C.J. Vörösmarty, and U.C. Mohanty. Changes in moisture and energy fluxes due to agricultural land use and irrigation in the Indian Monsoon Belt. *Geophysical Research Letters*, 33, 2006.

[58] P.H. Gleick. *Water in Crisis: A Guide to the Worlds Fresh Water Resources.* Oxford University Press, 1993.

[59] P. Raskin, E. Hansen, and R. Margolis. *Water and Sustainability. Polestar Series Report No. 4.* Boston, MA, 1995.

[60] H. Matthews, A. Weaver, K. Meissner, N. Gillet, and M. Eby. Natural and anthropogenic climate change : incorporating historical land cover change, vegetation dynamics and the global carbon cycle. *Climate Dynamics*, 22:461–479, 2004.

[61] F.H. Sklar and R. Costanza. The development of dynamic spatial models for landscape ecology: a review and prognosis. *Ecological Studies*, 82:239–288, 1991.

[62] W.E. Riebsame, W.B. Meyer, and B.L. Turner II. Modeling land use land cover as part of global environmental change. *Climatic Change*, 28:45–64, 2000.

[63] A. Angelsen and D. Kaimowitz. Rethinking the causes of deforestation: Lessons from economic models. *The World Bank Research Observer*, 14:73–98, 1999.

[64] E.F. Lambin, M. Rounsevell, and H. Geist. Are current agricultural land use models able to predict changes in land use intensity? *Agricultural Ecosystem Environment*, 1653:1–11, 2000.

[65] F. Gerhardt and D. Foster. Physiographical and historical effects on forest vegetation in central New England, USA. *Journal of Biogeography*, 29:1421–1437, 2002.

[66] B. Hall, G. Motzkin, D.R. Foster, M. Syfert, and J. Burk. Three hundred years of forest and land-use change in Massachusetts, USA. *Journal of Biogeography*, 29:1319–1335, 2002.

[67] A. Veldkamp and E.F. Lambin. Predicting land-use change. *Agriculture Ecosystems and Environment*, 85:1–6, 2001.

[68] S. Rost, D. Gerten, and U. Heyder. Human alterations of the terrestrial water cycle through land management. *Advances in Geosciences*, 18:43–50, 2008.

[69] L.J. Gordon, W. Steffen, B.F. Jonsson, C. Folke, M. Falkenmark, and A. Johannessen. Human modification of global water vapor flows from the land surface. *Proceedings of National Academic Science*, 102:7612–6717, 2005.

[70] S. Rost, D. Gerten, A. Bondeau, W. Lucht, J. Rohwer, and S. Schaphoff. Agricultural green and blue water consumption and its influence on the global water system. *Water Resources Research*, 44, 2008.

[71] H.E. Andersen, B. Kronvang, S.E. Larsen, C.C. Hoffmann, T.S. Jensen, and E.K. Rasmussen. Climate-change impacts on hydrology and nutrients in a Danish lowland river basin. *Science of the Total Environment*, 365:223–237, 2006.

[72] Y.B. Dibike and P. Coulibaly. Validation of hydrological models for climate scenario simulation: the case of Saguenay watershed in Quebec. *Hydrological Processes*, 21:3123–3135, 2007.

[73] K. Stahl, R.D. Moore, J.M. Shea, D. Hutchinson, and A.J. Cannon. Coupled modeling of glacier and streamflow response to future climate scenarios. *Water Resources Research*, 44:451–469, 2008.

[74] M.S. Markoff and A.C. Cullen. Impact of climate change on Pacific Northwest hydropower. *Climate Change*, 87:451–469, 2008.

[75] N. Miller, K.E. Bashford, and E. Strem. Potential impacts of climate change on California hydrology. *Journal of American Water Resources Association*, 39:771–784, 2003.

[76] L. Brekke, N. Miller, K. Bashford, N. Quinn, and J. Dracup. Climate change impacts uncertainty for water resources in the San Joaquin river basin, California. *Journal of American Water Resources Association*, 40:149–164, 2004.

[77] M.R. Allen and W.J. Ingram. Constraints on future changes in climate and the hydrologic cycle. *Nature*, 419:224–232, 2002.

[78] D.A. Stainforth, M.R. Allen, E.R. Tredger, and L.A. Smith. Confidence, uncertainty and decision-support relevance in climate predictions. *Philosophical Transactions of the Royal Society*, 365:2145–2161, 2007.

[79] N.W. Arnell. Climate change and global water resources. *Global Environmental Change*, 9:531–539, 1999.

[80] C. Tebaldi, R.L. Smith, D. Nychka, and L.O. Mearns. Quantifying Uncertainty in Projections of Regional Climate Change: A Bayesian Approach to the Analysis of Multi-model Ensembles. *Journal of Climate*, 5, 2005.

[81] K.H. Cook and E.K. Vizy. Coupled Model Simulations of the West African Monsoon System: Twentieth and Twenty-first Century Simulations. *Journal of Climate*, 19:3681–3703, 2006.

[82] D.L. Framer, M. Sivapalan, and C. Jothityangkoon. Climate, soil and vegetation controls upon the variability in temperate and semiarid landscapes: Downward approach to hydrological analysis. *Water Resources Research*, 39:1035, 2003.

[83] L.L. Nash and P.H. Gleick. Sensitivity of streamflow in the Colorado Basin to climatic changes. *Journal of Hydrology*, 125:221–241, 1991.

[84] N.S. Christensen, A.W. Wood, N. Voisin, D.P. Lettenmaier, and R.N. Palmer. The effects of climate change on the hydrology and water resources of the Colorado River Basin. *Climatic Change*, 62:337–363, 2004.

[85] G.J. McCabe and D.M. Wolock. General-Circulation-Model simulations of future snowpack in the western United States. *Journal of American Water Resources Association*, 35:1473–1484, 1999.

[86] A.F. Hamlet and D.P. Lettenmaier. Effects of climate change on hydrology and water resources in the Columbia River Basin. *Journal of American Water Resources Association*, 35:1597–1623, 1999.

[87] D.P. Lettenmaier, A.W. Wood, R.N. Palmer, E.F. Wood, and E.Z. Stakhiv. Water Resources Implications of Global Warming: A U.S. regional perspective. *Climate Change*, 43:537–579, 1999.

[88] E.L. Miles, A.K. Snover, A.F. Hamlet, B. Callahan, and D. Fluharty. The impacts of climate variability and climate change on the water resources of the Columbia River Basin. *Journal of American Water Resources Association*, 36:399–420, 2000.

[89] K.D. Frederick and D.C. Major. Climate Change and Water Resources. *Climate Change*, 37:7–23, 1997.

[90] M. Sivapalan, K. Takeuchi, S.W. Franks, V.K. Gupta, H. Karambiri, V. Lakshmi, X. Liang, J.J. McDonnell, E.M. Mendiondo, P.E. O'Connell, T. Oki, J.W. Pomeroy, D. Schertzer, S. Uhlenbrook, and E. Zehe. IAHS decade on Prediction in Ungauged Basins (PUB), 2003-2012: Shaping an exciting future for the hydrological sciences. *Journal of Hydrological Sciences*, 48:857–880, 2003.

[91] G.B. Bonan. *A land surface model (LSM version 1.0) for ecological, hydrologicaland atmospheric studies: Technical description and user's guide.* NCAR Technical Note. National Center for Atmospheric Research, Boulder, Colorado, 1996.

[92] R.E. Dickinson, A. Henderson-Sellers, and P.J. Kennedy. Biosphere Atmosphere Transfer Scheme (BATS) version 1e as coupled to the NCAR Community Climate Model. *NCAR Tech*, 1993.

[93] Y. Dai and Q.C. Zeng. A land surface model (IAP94) for climate studies, Part I: Formulation and validation in off-line experiments. *Advances in Atmospheric Science*, 14:433–460, 1997.

[94] R.B. Clapp and G.M. Hornberger. Empirical equations for some soil hydraulic properties. *Water Resources Research*, 14:601–604, 1978.

[95] B.J. Cosby, G.M. Hornberger, R.B. Clapp, and T.R. Ginn. A statistical exploration of the relationships of soil moisture characteristics to the physical properties of soils. *Water Resources Research*, 20:682–690, 1984.

[96] Y. Dai, X. Zeng, R.E. Dickinson, I. Baker, G.B. Bonan, M.G. Bosilovich, A.S. Denning, P.A. Dirmeyer, P.R. Houser, G. Niu, K.W. Oleson, C.A. Schlosser, and Z.L. Yang. The Common Land Model. *Bulletin of American Meterological Society*, 84:1013–1023, 2003.

[97] H.I. Choi, P. Kumar, and X.Z. Liang. 3-D Volume Averaged Soil Moisture Transport Model with a Scalable Parameterization of Subgrid Topographic Variability. *Water Resources Research*, 43:4414, 2007.

[98] X. Zeng, M. Shaikh, Y. Dai, R.E. Dickinson, and R. Myneni. Coupling of the Common Land Model to the NCAR Community Climate Model. *Journal of Climate*, 15:1832–1854, 2002.

[99] X.Z. Liang, H. Choi, K.E. Kunkel, Y. Dai, E. Joseph, J.X.L. Wang, and P. Kumar. Surface boundary conditions for mesoscale regional climate models. *Earth Interactions*, 9:1–28, 2005.

[100] J.K. Gibson, P. Kållberg, S. Uppala, A. Hernandez, A. Nomura, and E. Serrano. *ECMWF Re-analysis Project Report 1. ERA descriptions*, 1997.

[101] E. Kalnay, M. Kanamitsu, R. Kistler, W. Collins, D. Deaven, L. Gandin, M. Iredell, S. Saha, G. White, J. Woollen, Y. Zhu, A. Leetmaa, R. Reynolds, M. Chelliah, W. Ebisuzaki, W. Higgins, J. Janowiak, K.C. Mo, C. Ropelewski, J. Wang, R. Jenne, and D. Joseph. The NCEP/NCAR 40-Year Reanalysis Project. *Bulletin of American Meteorological Society*, 77:437–471, 1996.

[102] S.D. Schubert and R.B. Rood. Proceedings of the Workshop of the GEOS-1 Five Year Assimilation. *NASA Technical Memorandum*, 7:201, 1995.

[103] S. Uppala, P. Kållberg, A. Hernandez, S. Saarinen, M. Fiorino, X. Li, K. Onogi, N. Sokka, and U. Andraeand V. DaCosta Bechtold. ERA-40: ECMWF 45-year Reanalysis of the global atmosphere and surface conditions 1957-2002. *ECMWF Newsletter*, 101:2–21, 2004.

[104] M. New, M. Hulme, and P. Jones. Representing twentieth-century space-time climate variability. Part II: Development of 1901-96 monthly grids of terrestrial surface climate. *Journal of Climate*, 13:2217–2238, 2000.

[105] B. Rudolf, H. Hauschild, W. Ruth, and U. Schneider. Comparison of raingauge analyses, satellite-based precipitation estimates and forecast model results. *Advances in Space Research*, 18:53–62, 1996.

[106] E. Andersson, P. Bauer, A. Beljaars, F. Chevallier, E. Hólm, J. Marta, P. Kållberg, G. Kelly, P. Lopez, A. Mcnally, E. Moreau, A.J. Simmons, J.N. Thépaut, and A.M. Tompkins. Assimilation and modeling of the hydrological cycle in the ECMWF forecasting system. *American Meteorological Society*, 86:387–402, 2005.

[107] P.D. Jones and A. Moberg. Hemispheric and large-scale surface air temperature variations: An extensive revision and update to 2001. *Journal of Climate*, 16:206–223, 2003.

[108] W.L. Kahrl. *The California Water Atlas.* Sacramento: The Governor's Office of Planning and Research. William Kaufman Inc., Los Altos, 1978.

[109] A.G. Noble and A.J. Korsok. Ohio-An American heartland. *Ohio Division of Geological Survey Bulletin*, 65:35–42, 1975.

[110] B. Barry, E. Obuobie, M. Andreini, W. Andah, and M. Pluquet. *Volta River Basin Synthesis, (IWMI/CA).* International Water Management Institute: Colombo, 2005.

[111] R.H. Sharma and N.M. Shakya. Hydrological changes and its impact on water resources of Bhagmati watershed: Nepal. *Journal of Hydrology*, 327:315–322, 2006.

[112] H.E. Rashid and B. Kabir. Case Study: Water resources and population pressures in the Ganges River Basin. *Water and Population Dynamics: Case Studies and Policy Implications Workshop Report*, 1996.

[113] S. Scherrer, F. Naef, A.O. Faeh, and I. Cordery. Formation of runoff at the hillslope scale during intense precipitation. *Hydrology and Earth System Sciences*, 3:2523–2558, 2006.

[114] I. Daubechies. Review of Wavelets and Operators by Y. Meyer (Cambridge Univ. Press, New York, 1993) and Wavelets:Algorithms and Applications by Y. Meyer, (Soc. for Ind. and Appl. Math., Philadelphia, 1993). *Science*, 262:1589–1591, 1993.

[115] S.G. Mallat and Z. Zhang. Matching pursuits with time-frequency dictionaries. *IEEE Transactions on Signal Processing*, 41:3397–3415, 1993.

[116] J. Latron, M. Soler, P. Llorens, and F. Gallart. Spatial and temporal variability of the hydrological response in a small Mediterranean research catchment (Vallcebre, Eastern Pyrenees). *Hydrological Processes*, 22:775–787, 2008.

[117] B.B. Mandelbrot and J.R. Wallis. Computer Experiments with Fractional Gaussian Noises Part 2, Rescaled Ranges and Spectra. *Water Resources Research*, 5:242–259, 1969.

[118] D. Labat, R. Ababou, and A. Mangin. Rainfall runoff relations for karstic springs. Part I: convolution and spectral analyses. *Journal of Hydrology*, 238:123–148, 2000.

[119] L. Montanari, M. Sivapalan, and A. Montanari. Investigation of dominant hydrological processes in a tropical catchment in a monsoonal climate via the downward approach. *Hydrological Earth System Sciences,*, 10:769–782, 2006.

[120] M. Maneta, S. Schnabel, and V. Jetten. Continuous spatially distributed simulation of surface and subsurface hydrological processes in a small semiarid catchment. *Hydrological Processes*, 22:2196–2214, 2008.

[121] C.E. Heil and D.F. Walnut. Continuous and Discrete Wavelet Transforms. *Siam Review*, 31:628–666, 1989.

[122] C. Cosandey, V. Andreassian, C. Martinc, J.F. Didon-Lescotc, J. Lavabred, N. Foltond, N. Mathyse, and D. Richarde. The hydrological impact of the Mediterranean forest: A review of French research. *Journal of Hydrology*, 301:235–249, 2005.

[123] F. Gallart, P. Llorens, J. Latron, and D. Regues. Hydrological processes and their seasonal controls in a small Mediterranean mountain catchment in the Pyrenees. *Hydrology and Earth System Sciences*, 6:527–537, 2002.

[124] M. Kirkby, L. Bracken, and S. Reaney. The influence of land-use, soils and topography on the delivery of hillslope runoff to channels in Spain. *Earth Surface Processes Landforms*, 27:1459–1473, 2002.

[125] N.W. Arnell and C. Liu. *Hydrology and Water Resources*. Cambridge University Press, 2001.

[126] C.L. Du, X.L. Liu, and W.D. Wu. CLM3-simulated soil moisture in east Asia and its possible response to global warming during 1979 through 2003. *Sciences in Cold and Arid Regions*, 1:51–58, 2009.

[127] Y. Song, W. Guo, and Y. Zhang. Numerical study of impacts of soil moisture on the diurnal and seasonal cycles of sensible/latent heat fluxes over semi-arid region. *Advances in Atmospheric Sciences*, 26:319–326, 2009.

[128] J.K. Lorup, J.C. Refsgaard, and D. Mazvimavi. Assessing the effect of land use change on catchment runoff by combined use of statistical tests and hydrological modelling: case studies from Zimbabwe. *Journal of Hydrology*, 205:147–163, 1998.

[129] J.F. Chen and X.B. Li. Simulation of hydrological response to land-cover changes. *Chinese Journal of Applied Ecology*, 15:833–836, 2004.

[130] S.L. Postel, G.C. Daily, and P.R. Rhrlich. Human appropriation of renewable fresh water. *Science*, 271:785–788, 1996.

[131] T. Oki and S. Kanae. Global Hydrological Cycles and World Water Resources. *Science*, 313:1068–1072, 2006.

[132] J.A. Foley, R. DeFries, G.P. Asner, C. Barford, G. Bonan, S.R. Carpenter, F.S. Chapin, M.T. Coe, G.C. Daily, H.K. Gibbs, J.H. Helkowski, T. Holloway, E.A. Howard, C.J. Kucharik, C. Monfreda, J.A. Patz, I.C. Prentice, N. Ramankutty, and P.K. Snyder. Global Consequences of Land Use. *Science*, 309:570–574, 2005.

[133] K.N. Adams and A.M. Fowler. Improving empirical relationships for predicting the effect of vegetation change on annual water yield. *Journal of Hydrology*, 321:90–115, 2006.

[134] D. Wang and X. Cai. Optimal estimation of irrigation schedule - An example of quantifying human interferences to hydrologic processes. *Advances in Water Resources*, 30:1844–1857, 2007.

[135] T. Oki, Y. Agata, S. Kanae, T. Sarhashi, D. Yang, and K. Msiake. Global assessment of current water resources using total runoff integrating pathways. *Journal of Hydrological Sciences*, 46:983–995, 2001.

[136] J. Alcamo, P. Döll, T. Henrichs, F. Kaspar, B. Lehner, T. Rosch, and S. Siebert. Development and testing of the WaterGAP 2 global model of water use and availability. *Journal of Hydrological Sciences*, 48:317–337, 2003.

[137] P.K. Weiskel, R.M. Vogel, P.A. Steeves, P.J. Zarriello, L.A. DeSimone, and K.G. Ries. Water use regime: Characterizing direct human interaction with hydrologic systems. *Water Resources Research*, 43, 2007.

[138] M.I. Budyko. *Evaporation under Natural Conditions.* Gidrometeoizdat: St. Petersburg, Russia, 1948.

[139] M.I. Budyko. *Climate and Life, translated from Russian by D.H. Miller.* Elsevier: New York, 1974.

[140] X. Cai, M. Rosegrant, and C. Ringler. Physical and economic efficiency of water use in the River Basin: Implications for efficient water management. *Water Resources Research*, 39, 2003.

[141] F. Glover. Future paths for integer programming and links to artificial intelligence. *Computers and Operations Research*, 5:533–549, 1986.

[142] M.D. Cunha and L. Ribeiro. Tabu search algorithms for water network optimization. *European Journal of Operations Research*, 157:746–758, 2004.

[143] C.P. Tung and C.C. Tan. An optimal procedure for identifying parameter structure and application to a confined aquifer. *Environmental Geology*, 47:1062–1071, 2005.

[144] T. Maurer. The Global Terrestrial Network for River Discharge (GTN-R) - Near real time data acquisition and dissemination tool for online river discharge and water level information. In *Proceedings of First International Symposium on Geo-information for Disaster Management*, 2005.

[145] R.J. Donohue, M.L. Roderick, and T.R. McVicar. On the importance of including vegetation dynamics in Budykos hydrological model. *Hydrological Earth System Sciences*, 11:983–995, 2007.

[146] X. Cai and M.W. Rosegrant. Irrigation technology choices under hydrologic uncertainty: A case study from Maipo River Basin, Chile. *Water Resources Research*, 40, 2004.

[147] R. Allen, L.S. Pereira, D. Raes, and M. Smith. Crop Evapotranspiration Guidelines for computing crop water requirements. *FAO: Irrigation and Drainage*, 1998.

[148] N. Hanasaki, S. Kanae, T. Oki, K. Masuda, K. Motoya, Y. Shen, and K. Tanaka. An integrated model for the assessment of global water resources Part 1: Input meteorological forcing and natural hydrological cycle modules. *Hydrology and Earth System Sciences Discussions*, 4:535–582, 2007.

[149] K.E. Trenberth, A.G. Dai, R.M. Rasmussen, and D.B. Parsons. The changing character of precipitation. *Bulletin of American Meteorological Society*, 84:1205–1217, 2003.

[150] G.A. Meehl, T.F. Stocker, W.D. Collins, P. Friedlingstein, A.T. Gaye, J.M. Gregory, A. Kitoh, R. Knutti, J.M. Murphy, A. Noda, S.C.B. Raper, I.G. Watterson, A.J. Weaver, and Z.C. Zhao. *Climate Change 2007: The Physical Science Basis. Contribution of Working Group I to the Fourth Assessment Report of the Intergovernmental Panel on Climate Change.* Cambridge University Press, Cambridge, UK, 2007.

[151] A.K. Gosain, S. Rao, and D. Basuray. Climate change impact assessment on hydrology of Indian river basins. *Current Science*, 90:346–353, 2006.

[152] K. van Werkhoven, T. Wagener, P. Reed, and Y. Tang. Characterization of watershed model behavior across a hydroclimatic gradient. *Water Resources Research*, 44:289–310, 2008.

[153] A.J. Simmons and J.K. Gibson. *The ERA-40 Project Plan, ERA-40 Project Report Series No. 1.* The ERA-40 Project Plan, 2000.

[154] R. Laurent and X. Cai. A maximum entropy method for combining AOGCMs for regional intra-year climate change assessment. *Climate Change*, 82:411–435, 2007.

[155] G. Tan and R. Shibasaki. Global estimation of crop productivity and the impacts of global warming by GIS and EPIC integration. *Ecological Model*, 168:357–370, 2003.

[156] N. Rosenberg, R. Brown, R. Izaurralde, and A. Thomson. Integrated assessment of Hadley centre (HadCM2) climate change projections on agricultural productivity and irrigation water supply in the conterminous United States: I. Climate change scenarios and impacts on irrigation water supply simulated with the HUMUS model. *Agriculture and Forest Meteorology*, 117:73–96, 2003.

[157] *Climate Change 2001: The Scientific Basis. Contribution of working group I to the Third Assessment Report (TAR) of the Intergovernmental Panel on Climate Change.* Cambridge, UK, 2001.

[158] H.S. Chiew and T.A. McMahon. Modelling the impacts of climate change on Australian streamflow. *Hydrological Processes*, 16:1235–1245, 2002.

[159] S.P. Charles, B.C. Bates, P.H. Whetton, and J.P. Hughes. Validation of downscaling models for changed climate conditions: case study of southwestern Australia. *Climate Research*, 12:1235–1245, 1999.

[160] K.E. Trenberth. Conceptual framework for changes of extremes of the hydrologic cycle with climate change. *Climatic Change*, 42:327–339, 1999.

[161] R.L. Scott, W.J. Shuttleworth, D.C. Goodrich, and T. Maddock. The water use of two dominant vegetation communities in a semiarid riparian ecosystem. *Agriculture and Forest Meteorology*, 105:241–256, 2000.

[162] E. Noy-Meir. Structure and function of desert ecosystems. *Israel Journal of Botany*, 28:1–19, 1979.

[163] S.D. Smith, R.K. Monson, and J.E. Anderson. *Physiological ecology of North American Desert plants.* Springer, Berlin Heidelberg New York, 1997.

[164] A.K. Knapp, P.A. Fay, J.M. Blair, S.L. Collins, M.D. Smith, J.D. Carlisle, C.W. Harper, B.T. Danner, M.S. Lett, and J.K. McCarron. Rainfall variability, carbon cycling and plant species diversity in a mesic grassland. *Science*, 298:2202–2205, 2002.

[165] M. Claussen, V. Brovkin, and A. Ganopolski. Biogeophysical versus Biogeochemical feedbacks of large-scale land cover change. *Geophysical Research Letters*, 28:1011–1014, 2001.

[166] V. Sahin and M.J. Hall. The effects of afforestation and deforestation on water yields. *Journal of Hydrology*, 178:293–309, 1996.

[167] B.R. Scanlon, I. Jolly, M. Sophocleous, and L. Zhang. Global impacts of conversions from natural to agricultural ecosystems on water resources: Quantity versus quality. *Water Resources Research*, 43, 2007.

[168] I. Haddeland, T. Skaugen, and D.P. Lettenmaier. Hydrologic effects of land and water management in North America and Asia: 1700- 1992. *Hydrological Earth System Science*, 11:1035–1045, 2007.

[169] N. Nakicenovic, J. Alcamo, G. Davis, H.J.M. de Vries, J. Fenhann, S. Gaffin, K. Gregory, A. Grubler, T.Y. Jung, T. Kram, E.L. La Rovere, L. Michaelis, S. Mori, T. Morita, W. Papper, H. Pitcher, L. Price, K. Riahi, A. Roehrl, H.H. Rogner, A. Sankovski, M. Schlesinger, P. Shukla, S. Smith, R. Swart, S. van Rooijen, N. Victo, and Z. Dadi. *Special Report on Emissions Scenarios: A Special Report of Working Group III of the Intergovernmental Panel on Climate Change*, 2000.

[170] P. Xie and P. Arkin. Global precipitation: A 17-year monthly analysis based on gauge observations, satellite estimates and numerical model outputs. *Bulletin of American Meteorological Society*, 78:2539–2558, 1997.

[171] G.J. Huffman, R.F. Adler, P. Arkin, A. Chang, R. Ferraro, A. Gruber, J. Janowiak, A. McNab, B. Rudolf, and U. Schneider. The Global Precipitation Climatology Project (GPCP) combined precipitation data set. *Bulletin of American Meteorological Society*, 78:5–20, 1997.